NEW PHYSICS

HIGGS PHYSICS

Conveners: M. Carena and P.M. Zerwas

Working Group: E. Accomando, P. Bagnaia, A. Ballestrero, P. Bambade, D. Bardin, F. Berends, J. van der Bij, T. Binoth, G. Burkart, F. de Campos, R. Contri, G. Crosetti, J. Cuevas Maestro, A. Dabelstein, W. de Boer, C. de StJean, F. Di Lodovico, A. Djouadi, V. Driesen, M. Dubinin, E. Duchovni, O.J.P. Eboli, R. Ehret, U. Ellwanger, J.-P. Ernenwein, J.-R. Espinosa, R. Faccini, M. Felcini, R. Folman, H. Genten, J.–F. Grivaz, E. Gross, J. Guy, H. Haber, Cs. Hajdu, S.W. Ham, R. Hempfling, A. Hoang, W. Hollik, S. Hoorelbeke, K. Hultqvist, P. Igo–Kemenes, P. Janot, S. de Jong, U. Jost, J. Kalinowski, S. Katsanevas, R. Keränen, W. Kilian, B.R. Kim, S.F. King, R. Kleiss, B. A. Kniehl, M. Krämer, A. Leike, E. Lund, V. Lund, P. Lutz, J. Marco, C. Mariotti, J.–P. Martin, C. Martinez–Rivero, G. Mikenberg, M.R. Monge, G. Montagna, O. Nicrosini, S.K. Oh, P. Ohmann, G. Passarino, F. Piccinini, R. Pittau, T. Plehn, M. Quiros, M. Rausch de Traubenberg, T. Riemann, J. Rosiek, V. Ruhlmann-Kleider, C.A. Savoy, P. Sherwood, S. Shichanin, R. Silvestre, A. Sopczak, M. Spira, J.W.F. Valle, D. Vilanova, C.E.M. Wagner, P.L. White, T. Wlodek, G. Wolf, S. Yamashita, and F. Zwirner.

Contents

1 Synopsis

1. The understanding of the mechanism responsible for the breakdown of the electroweak symmetry is one of the central problems in particle physics. If the fundamental particles – leptons, quarks and gauge bosons – remain weakly interacting up to high energies, then the sector in which the electroweak symmetry is broken must contain one or more fundamental scalar Higgs bosons with masses of the order of the symmetry breaking scale $v \sim 174$ GeV. Alternatively, the symmetry breaking could be generated dynamically by novel strong forces at the scale $\Lambda \sim 1$ TeV. However, no compelling model of this kind has yet been formulated which provides a satisfactory description of the fermion sector and reproduces the high precision electroweak measurements.

2. The simplest mechanism for the breaking of the electroweak symmetry is realized in the Standard Model (SM) [1]. To accommodate all observed phenomena, a complex isodoublet scalar field is introduced which, through self-interactions, spontaneously breaks the electroweak symmetry $\mathrm{SU(2)_L \times U(1)_Y}$ down to the electromagnetic $\mathrm{U(1)_{EM}}$ symmetry, by acquiring a non–vanishing vacuum expectation value. After the electroweak symmetry breakdown, the interaction of the gauge bosons and fermions with the isodoublet scalar field generates the masses of these particles [2]. In this process, one scalar field remains in the spectrum, manifesting itself as the physical Higgs particle H.

The mass of the SM Higgs boson is constrained in two ways. Since the quartic self-coupling of the Higgs field grows indefinitely with rising energy, an upper limit on the Higgs mass is obtained by demanding that the SM particles remain weakly interacting up to a scale Λ [3]. On the other hand, stringent lower bounds on the Higgs mass can be derived from the requirement of stability of the electroweak vacuum [3, 4]. Hence, if the Standard Model is valid up to scales near the Planck scale, then the SM Higgs mass is restricted to the range between ~ 130 GeV and ~ 180 GeV, for a top-quark mass $M_t \sim 176$ GeV. Moreover, if the Higgs particle is discovered in the mass range up to the 100 GeV accessible at LEP2, this will imply that new physics beyond the Standard Model should exist at energies below a scale Λ of order 10 TeV. [These bounds become stronger (weaker) for larger (smaller) values of the top quark mass].

The high precision electroweak data give a slight preference to Higgs masses of less than 100 GeV, despite the fact that the electroweak observables depend only logarithmically on the Higgs mass through radiative corrections [5]. They do not, however, exclude values up to ~ 700 GeV at the 2σ level [6], thus sweeping the entire Higgs mass range of the Standard Model. By searching directly for the SM Higgs particle, the LEP experiments [7] have set a lower bound, $m_H > 65.2$ GeV [95% CL], on the Higgs mass.

The dominant production mechanism for the SM Higgs boson within the energy range of LEP2 is the Higgs–strahlung process $e^+e^- \to ZH$ in which the Higgs boson is emitted from a virtual Z boson [8]. The cross section monotonically falls from ~ 1 pb at $m_H \sim 65$ GeV down to very small values for Higgs masses near the kinematical threshold. The cross section for the

production of Higgs bosons via WW fusion [9, 10] is nearly two orders of magnitude smaller at LEP2, except at the edge of the phase space for Higgs–strahlung where both are small. In the mass range between 60 and 120 GeV, the dominant decay mode of the SM Higgs particle is $b\bar{b}$ [12]. Branching ratios for Higgs decays to $\tau^+\tau^-, c\bar{c}$ and gg final states are suppressed by an order of magnitude or more.

The experimental search for the SM Higgs boson at LEP2 will be based primarily on the Higgs–strahlung process. The Z boson can easily be reconstructed in all charged leptonic and hadronic decay channels while the Higgs decay mostly leads to $b\bar{b}$ and, less frequently, to $\tau^+\tau^-$ final states. Moreover, neutrino decays of the Z boson, augmented by W fusion events, can be exploited in the experimental analyses. Higgs events can be searched for with an average efficiency of about 25%. Exploiting micro–vertex detection for tagging b quarks, the Higgs events can be well discriminated from the main background process of ZZ production even for a Higgs mass near the Z mass. When the results of all four LEP experiments are combined, after accumulating an integrated luminosity $\int \mathcal{L} = 150$ pb^{-1} per experiment, the SM Higgs boson can be discovered in the mass range up to $m_H \simeq 95$ GeV at LEP2 for a total center of mass energy of $\sqrt{s} = 192$ GeV.

3. If the Standard Model is embedded in a Grand Unified Theory (GUT) at high energies, then the natural scale of electroweak symmetry breaking would be close to the unification scale $M_{\rm GUT}$, due to the quadratic nature of the radiative corrections to the Higgs mass. Supersymmetry [13] provides a solution to this hierarchy problem through the cancellation of these quadratic divergences via the contributions of fermionic and bosonic loops [14]. Moreover, the Minimal Supersymmetric extension of the Standard Model (MSSM) can be derived as an effective theory from supersymmetric Grand Unified Theories [15], involving not only the strong and electroweak interactions but gravity as well. A strong indication for the realization of this physical picture in nature is the excellent agreement between the value of the weak mixing angle $\sin^2\theta_W$ predicted by the unification of the gauge couplings, and the measured value [15]-[21]. In particular, if the gauge couplings are unified in the minimal supersymmetric theory at a scale $M_{\rm GUT} = \mathcal{O}(10^{16}$ GeV) and if the mass spectrum of the supersymmetric particles is of order m_Z, then the electroweak mixing angle is predicted to be $\sin^2\theta_W = 0.2336 \pm 0.0017$ in the $\overline{\rm MS}$ scheme for $\alpha_s = 0.118 \mp 0.006$, to be compared with the experimental result $\sin^2\theta_W^{exp} = 0.2314 \pm 0.0003$. Threshold effects at both the low scale of the supersymmetric particle spectrum and at the high unification scale may drive the prediction for $\sin^2\theta_W$ even closer to its experimental value.

In the past two decades a detailed picture has been developed of the Minimal Supersymmetric Standard Model. In this extension of the Standard Model the Higgs sector is built up of two doublets, necessary to generate masses for up– and down–type fermions in a supersymmetric theory, and to render the theory anomaly–free [22]. The Higgs particle spectrum consists of a quintet of states: two CP–even scalar (h, H), one CP-odd pseudoscalar neutral (A), and a pair of charged $(H^\pm)$ Higgs bosons [23] .

Since the tree–level quartic Higgs self–couplings in this minimal theory are determined in terms of the gauge couplings, the mass of the lightest CP-even Higgs boson h is constrained very stringently. At tree-level, the mass m_h has been predicted to be less than the Z mass [24, 25]. Radiative corrections to m_h^2 grow as the fourth power of the top mass and the logarithm of the stop masses. They shift the upper limit to about $\lesssim 150$ GeV [26, 27], depending on the MSSM parameters.

The upper limit on m_h depends on $\tan\beta$, the ratio of the vacuum expectation values associated with the two neutral scalar Higgs fields. This parameter can be constrained by additional symmetry concepts. If the theory is embedded into a grand unified theory, the b and τ Yukawa couplings can be expected to unify at $M_{\rm GUT}$. The condition of b-τ Yukawa coupling unification determines the value of the top-quark Yukawa coupling at low energies [28], thus explaining qualitatively the large value of the top quark mass [18],[29]-[32]. For the present experimental range [33], $M_t = 180 \pm 12$ GeV, the condition of b-τ unification implies either low values of $\tan\beta$, $1 \lesssim \tan\beta \lesssim 3$, or very large values of $\tan\beta = \mathcal{O}(m_t/m_b)$ [29]-[32]. In the small $\tan\beta$ regime, the top-quark mass is strongly attracted to its infrared fixed point [34], implying a strong correlation between the top-quark mass and $\tan\beta$. The large $\tan\beta$ regime is more complex because of possible large radiative corrections to the b quark mass associated with supersymmetric particle loops [35, 36]. For small $\tan\beta$ and $M_t \lesssim 176$ GeV, the upper bound on the mass of the lightest neutral Higgs particle is reduced to ~ 100 GeV. This mass bound is just at the edge of the kinematical range accessible at a center of mass energy of 192 GeV [37] – raising the prospects of discovering this Higgs boson at LEP2.

The structure of the Higgs sector in the MSSM at tree level is determined by one Higgs mass parameter, which we choose to be m_A, and $\tan\beta$. The mass of the pseudoscalar Higgs boson m_A may vary between the present experimental lower bound of 45 GeV [7] and ~ 1 TeV, the heavy neutral scalar mass m_H is in general larger than ~ 120 GeV, and the mass of the charged Higgs bosons exceeds ~ 90 GeV. Due to the kinematics the primary focus at LEP2 will be on the light scalar particle h and on the pseudoscalar particle A. In the decoupling limit of large A mass [yielding large $H, H^\pm$ masses], the Higgs sector becomes SM like and the properties of the lightest neutral Higgs boson h coincide with the properties of the Higgs boson H in the Standard Model [38].

The processes for producing the Higgs particles h and A at LEP2 are Higgs–strahlung $e^+e^- \to Zh$, and associated pair production $e^+e^- \to Ah$ [39]. These two processes are complementary. For small values of $\tan\beta$ the h Higgs boson is produced primarily through Higgs–strahlung; if kinematically allowed, associated Ah production becomes increasingly important with rising $\tan\beta$. The typical size of the cross sections is of order 1 pb or slightly below. The dominant decay modes of the h, A Higgs bosons are decays into b and τ pairs, if we consider SM particles in the final state [12]. Only near the maximal h mass for a given value of $\tan\beta$ do $c\bar{c}$ and gg decays occur at a level of several percent, in accordance with the decoupling theorem. However, there are areas in the SUSY $[\mu, M_2]$ parameter space where Higgs particles can decay into invisible $\chi_1^0\chi_1^0$ LSP final states or possibly other neutralino and chargino final states [40, 41]. If the LSP channel is open, the h and A invisible decay branching ratios can be

close to 100% for small to moderate values of $\tan\beta$. However, the Higgs boson h can still be found in the Higgs–strahlung process. The pseudoscalar A, produced only in association with h, would be hard to detect in this case since both particles decay into invisible channels for small $\tan\beta$.

The experimental search for h in the Higgs–strahlung process follows the lines of the Standard Model, while for associated Ah production $b\bar{b}b\bar{b}$ and $b\bar{b}\tau^+\tau^-$ final states can be exploited. Signal events of the Ah type can be searched for with an efficiency of about 30%; the background rejection is somewhat more complicated than for Higgs–strahlung, due to two unknown particles in the signal final state. For small to moderate $\tan\beta$, h particles with masses up to $\sim$ 100 GeV can be discovered in the Higgs–strahlung process. For large $\tan\beta$ the experimentally accessible limits are typically reduced by about 10 GeV. The pseudoscalar Higgs boson A is accessible for masses up to about 80 GeV. [These limits are based on the LEP2 energy of 192 GeV and an integrated luminosity of $\int \mathcal{L} = 150$ pb^{-1} per experiment, with all four experiments pooled.]

The supersymmetric theory may be distinguished from the Standard Model if one of the following conditions occurs: (i) at least two different Higgs bosons are found; (ii) precision measurements of production cross sections and decay branching ratios of h can be performed at a level of a few per cent; and (iii) genuine SUSY decay modes are observed. Near the maximum h mass, the decoupling of the heavy Higgs bosons reduces the MSSM to the SM Higgs boson except for the SUSY decay modes.

4. *In summary.* If a neutral scalar Higgs boson is found at LEP2, new physics beyond the Standard Model should exist at scales of order 10 TeV. In the framework of the Minimal Supersymmetric extension of the Standard Model, there are good prospects of discovering the lightest of the neutral scalar Higgs bosons at LEP2. Even though this discovery cannot be ensured, observation or non–observation will have far reaching consequences on the possible structure of low–energy supersymmetric theories.

In section 2 the theoretical analysis and experimental simulations for the search for the Higgs boson in the Standard Model are presented. In section 3 the Higgs spectrum and the couplings in the MSSM as well as the relevant cross sections and branching ratios are studied. In addition, the results of the experimental simulations are thoroughly discussed. Section 4 investigates opportunities of detecting Higgs particles at LEP2 within non-minimal extensions of the SM and the MSSM. In particular, the next–to–minimal extension of the MSSM with an additional isoscalar Higgs field (NMSSM) is studied.

2 The Standard–Model Higgs Particle

2.1 Mass Bounds

(i) Strong interaction limit and vacuum stability. Within the Standard Model the value of the Higgs mass m_H cannot be predicted. The mass $m_H = \sqrt{2\lambda}v$ is given as a function of the vacuum expectation value of the Higgs field, $v = 174$ GeV, and the quartic coupling λ which is a free parameter. However, since the quartic coupling grows with rising energy indefinitely, an upper bound on m_H follows from the requirement that the theory be valid up to the scale M_{Planck} or up to a given cut-off scale Λ below M_{Planck} [3]. The scale Λ could be identified with the scale at which a Landau pole develops. However, in the following the upper bound on m_H shall be defined by the requirement $\lambda(\Lambda)/4\pi \leq 1$ so that Λ characterizes the energy where the system becomes strongly interacting. [This scale is very close to the scale associated with the Landau pole in practice.] The upper bound on m_H depends mildly on the top-quark mass through the impact of the top-quark Yukawa coupling on the running of the quartic coupling λ,

$$\frac{d\lambda}{dt} = \frac{6}{16\pi^2}\left(\lambda^2 + \lambda h_t^2 - h_t^4\right) + \text{elw. corrections} \qquad (1)$$

with $t = \ln(Q^2/\Lambda^2)$. The first two terms inside the parentheses are crucial in driving the quartic coupling to its perturbative limit. On the other hand, the requirement of vacuum stability in the SM imposes a lower bound on the Higgs boson mass, which depends crucially on the top-quark mass as well as on the cut-off Λ [3, 4]. Again, the dependence of this lower bound on M_t is due to the effect of the top-quark Yukawa coupling on the quartic coupling of the Higgs potential [third term inside the parentheses of eq.(1)], which drives λ to negative values at large scales, thus destabilizing the standard electroweak vacuum.

Fig.1 shows the perturbativity and stability bounds on the Higgs boson mass of the SM for different values of the cut-off Λ at which new physics is expected. From the point of view of LEP physics, the upper bound on the SM Higgs boson mass does not pose any relevant restriction. The lower bound on m_H, instead, needs to be carefully considered. To define the conditions for vacuum stability in the SM and to derive the lower bounds on m_H as a function of M_t, it is necessary to study the Higgs potential for large values of the Higgs field ϕ and to determine under which conditions it develops an additional minimum deeper than the electroweak minimum. The renormalization group improved effective potential of the SM is given by

$$V_{eff.} = V_0 + V_1 \simeq -m^2(t)\phi^2(t) + \frac{\lambda(\phi)}{2}\phi^4(t) \qquad (2)$$

where V_0 and V_1 are the tree–level potential and the one–loop correction, respectively. A rigorous analysis of the structure of the potential has been done in Ref.[4]. Quite generally it follows that the stability bound on m_H is defined, for a given value of M_t, as the lower value of m_H for which $\lambda(\phi) \geq 0$ for any value of ϕ below the scale Λ at which new physics beyond the SM should appear. From eq.(1) it is clear that the stability condition of the effective potential demands new physics at lower scales for larger values of M_t and smaller values of m_H.

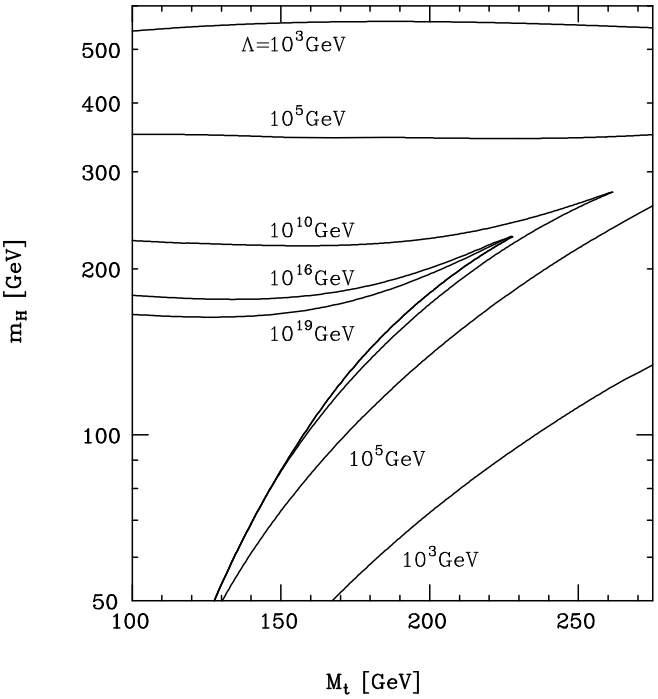

Figure 1: *Strong interaction and stability bounds on the SM Higgs boson mass.* Λ *denotes the energy scale where the particles become strongly interacting.*

From Fig.1 it follows that for $M_t = 175$ GeV and $m_H < 100$ GeV [i.e. in the LEP2 regime] new physics should appear below the scale $\Lambda \sim$ a few to 100 TeV. The dependence on the top-quark mass however is noticeable. A lower value, $M_t \simeq 160$ GeV, would relax the previous requirement to $\Lambda \sim 10^3$ TeV, while a heavier value $M_t \simeq 190$ GeV would demand new physics at an energy scale as low as 2 TeV.

The previous bounds on the scale at which new physics should appear can be relaxed if the possibility of a metastable vacuum is taken into account [42]. In fact, if the effective potential of the SM has a non-standard stable minimum deeper than the standard minimum, the decay of the electroweak minimum by thermal fluctuations or quantum tunnelling to the stable minimum must be suppressed. In this case, the lower bounds on m_H follow from requiring that no transition at any finite temperature occurs, so that all space remains in the metastable electroweak vacuum. In practice, if the metastability arguments are taken into account, the lower bounds on m_H become gradually weaker. They seem to disappear if the cut-off of the theory is at the TeV scale; however, the calculations are technically not reliable in this energy regime. Moreover, the metastability bounds depend on several cosmological assumptions which may be relaxed in several ways.

(ii) Estimate of the Higgs mass from electroweak data. Indirect evidence for a light Higgs boson comes from the high–precision measurements at LEP [6] and elsewhere. Indeed, the fact that the SM is renormalizable only after including the top and Higgs particles in the loop corrections shows that the electroweak observables should be sensitive to these particle masses. Although

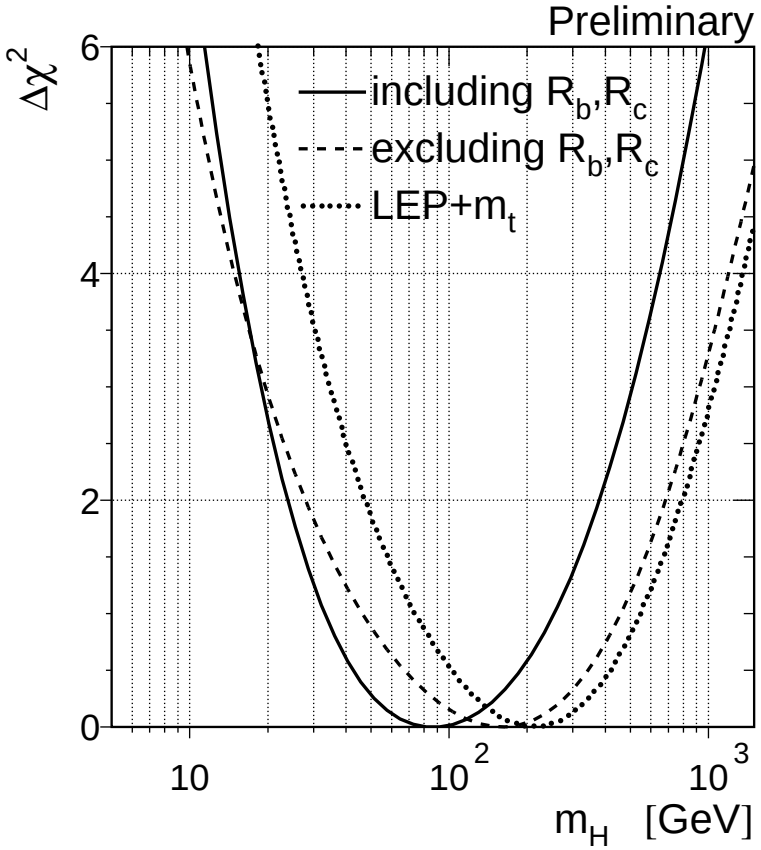

Figure 2: $\Delta\chi^2 = \chi^2 - \chi^2_{min}$ *vs* m_H *curves. Continuous line: based on all LEP, SLD,* $p\bar{p}$ *and* νN *data; dashed line: as before, but excluding the LEP+SLD measurements of* R_b *and* R_c*; dotted line: LEP data including measurements of* R_b *and* R_c*. In all cases, the direct measurement of* M_t *at the TEVATRON is included.*

the sensitivity to the Higgs mass is only logarithmic, while the sensitivity to the top-quark mass is quadratic, the increasing precision of present experiments makes it possible to derive χ^2 curves as a function of m_H. Several groups [6] have performed an analysis of m_H by means of a global fit to the electroweak data, including low and high energy data. In the light of the recent direct determination of M_t, the results favor a light Higgs boson. With all LEP, SLD, $p\bar{p}$ and νN data included, a central value for m_H around 80 GeV and $M_t \sim 170$ GeV is obtained [6]. However, the recently reported LEP values of $R_b \equiv \Gamma_{Z\to b\bar{b}}/\Gamma_{Z\to hadrons}$ and $R_c \equiv \Gamma_{Z\to c\bar{c}}/\Gamma_{Z\to hadrons}$ which are more than 2 standard deviations away from the SM predictions, and the left-right asymmetries of SLD which still lead to a 2σ discrepancy in $\sin^2\theta_W$ compared with LEP analyses, have drastic effects on the SM fits. Fig.2 shows $\Delta\chi^2 = \chi^2 - \chi^2_{min}$ as a function of m_H; the curve is rather flat at the minimum due to the mild logarithmic dependence of the observables on m_H. It should be noticed in this context that the bounds on m_H become very weak if R_b, R_c and/or the left-right asymmetries are excluded from the data.

In summary. It is clear that the indirect bounds on m_H cannot assure the existence of a light Higgs boson at the reach of LEP2. However, the fact that the best fit to the present high-precision data tends to prefer a light SM Higgs boson, indicates that this particle may be found either at LEP or LHC. On the other hand, the stability bounds imply that if the Higgs boson is light, new physics beyond the Standard Model should appear at relatively low energies in the TeV regime.

2.2 Production and Decay Processes

The main mechanism for the production of Higgs particles in e^+e^- collisions at LEP2 energies is the radiation off the virtual Z-boson line [8],

$$\text{Higgs-strahlung}: \quad e^+e^- \to ZH \tag{3}$$

The fusion process [9, 10, 11] in which the Higgs bosons are formed in WW collisions, the virtual W's radiated off the electrons and positrons,

$$\text{WW fusion} \quad : \quad e^+e^- \to \bar{\nu}_e\nu_e H \tag{4}$$

has a considerably smaller cross section at LEP energies. It is suppressed by an additional power of the electroweak coupling with respect to the Higgs-strahlung process, becoming competitive only at the edge of phase space in (3), where the Z boson turns virtual. In this corner, however, both cross sections are small and the experimentally accessible mass parameter space will be extended only slightly by the fusion channel.

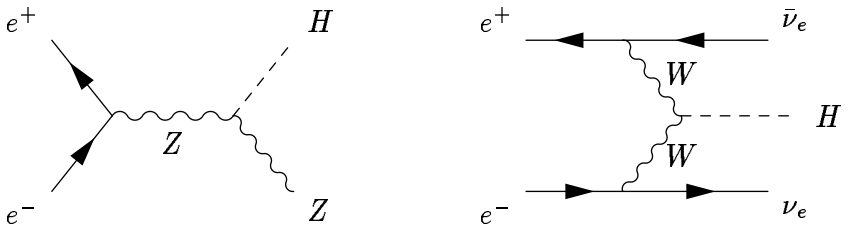

Figure 3: *Higgs-strahlung and WW fusion of the SM Higgs boson.*

2.2.1 Higgs-strahlung

The cross section for the Higgs-strahlung process can be written in the following compact form:

$$\sigma(e^+e^- \to ZH) = \frac{G_F^2 m_Z^4}{96\pi s}\left(v_e^2 + a_e^2\right)\lambda^{\frac{1}{2}}\frac{\lambda + 12m_Z^2/s}{(1 - m_Z^2/s)^2} \tag{5}$$

where $\sqrt{s}$ denotes the center-of-mass energy, and $a_e = -1$, $v_e = -1 + 4\,s_w^2$ are the Z charges of the electron; $\lambda = (1 - m_H^2/s - m_Z^2/s)^2 - 4m_H^2 m_Z^2/s^2$ is the usual two-particle phase space

function. The radiative corrections to the cross section are well under control. The genuine electroweak corrections [43] are small at the LEP energy, less than 1.5% (for a recent review see Ref.[44]). By contrast, photon radiation [45] affects the cross section in a significant way. The bulk of the corrections, real and virtual contributions due to photons and e^+e^- pairs, can be accounted for by convoluting the Born cross section in eq.(5) with the radiator function $G(x)$,

$$\langle\sigma\rangle = \int_{x_H}^1 dx\, G(x)\, \sigma(xs) \tag{6}$$

with $x_H = m_H^2/s$. The radiator function is known to order α^2, including the exponentiation of the infrared sensitive part,

$$G(x) = \beta\,(1-x)^{\beta-1}\,\delta_{V+S} \;+\; \delta_H(x) \tag{7}$$

where δ_{V+S} and δ_H are polynomials in $\log s/m_e^2$ and $\beta = \frac{2\alpha}{\pi}\,[\log s/m_e^2 - 1]$. δ_{V+S} accounts for virtual and soft photon effects, δ_H for hard photon radiation. The δ's are given in Ref.[45].

The cross-section for Higgs-strahlung is shown in Fig.4 for the three representative energy values $\sqrt{s} = 175$, 192 and 205 GeV as a function of the Higgs-mass [46]. The curves include all genuine electroweak and QED corrections introduced above. The Z boson in the final state is allowed to be off-shell, so that the tails of the curves extend beyond the on-shell limit $m_H = \sqrt{s} - m_Z$. [The Higgs boson is so narrow, $\Gamma_H < 3$ MeV for $m_H < 100$ GeV, that the particle need not be taken off-shell.] From a value of order 0.3 to 1 pb at $m_H \sim \sqrt{s} - 110$ GeV, the cross section falls steadily, reaching a level of less than 0.05 pb at the mass $m_H \sim \sqrt{s} - 90$ GeV.

Since the Higgs particle decays predominantly to $b\bar{b}$ and $\tau^+\tau^-$ pairs, the observed final state consists of four fermions. Among the possible final states, the channel $\mu^+\mu^- b\bar{b}$, the μ pair being generated by the Z decay, has a particularly simple structure. Background events of this type are generated by double vector-boson production $e^+e^- \to Z^*Z^*$, $Z^*\gamma^*$ and $\gamma^*\gamma^*$ with the virtual Z^*, γ^* decaying to $\mu^+\mu^-$ and $b\bar{b}$; Z final states generate by far the dominant contribution. Since these processes are suppressed by one and two additional powers of the electroweak coupling compared with the signal [except for $m_H \sim m_Z$], the background can be controlled fairly easily up to the kinematical limit of the Higgs signal. This is demonstrated in Tables 1/2 and Fig. 6 where signal and background cross sections for the process $e^+e^- \to \mu^+\mu^- b\bar{b}$ are compared for three Higgs masses at $\sqrt{s} = 192$ GeV. The invariant $\mu^+\mu^-$ mass is restricted to $m_Z \pm 25$ GeV and the invariant $b\bar{b}$ mass is cut at $m(b\bar{b}) > 50$ GeV. The following conclusions can be drawn from the tables and the figure: (i) The signal-to-background ratio decreases steadily with rising Higgs mass from a value of about three near $m_H = 65$ GeV; (ii) The initial state QED radiative corrections are large, varying between 10 and 20%; (iii) The cross sections are lowered by taking non-zero b quark masses into account, but only marginally at a level of less than 1%. Since massless fermions are coupled to spin-vectors in Z^* decays but to spin-scalars in Higgs decays, signal and background amplitudes do not interfere as long as b quark masses are neglected.

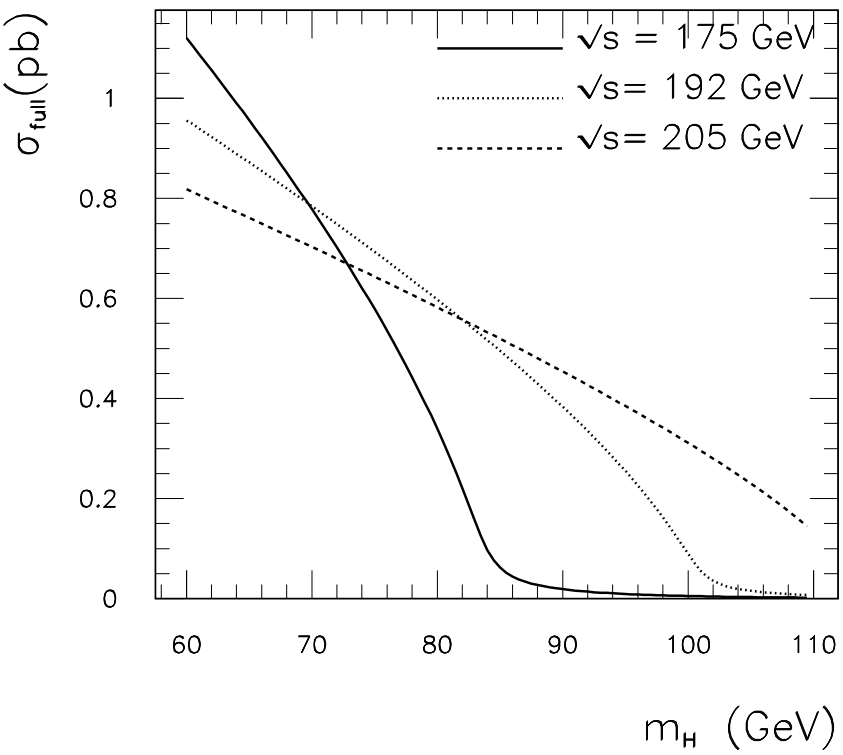

Figure 4: *The cross section for Higgs-strahlung as a function of the Higgs mass for three representative energy values [QED and electroweak radiative corrections included].*

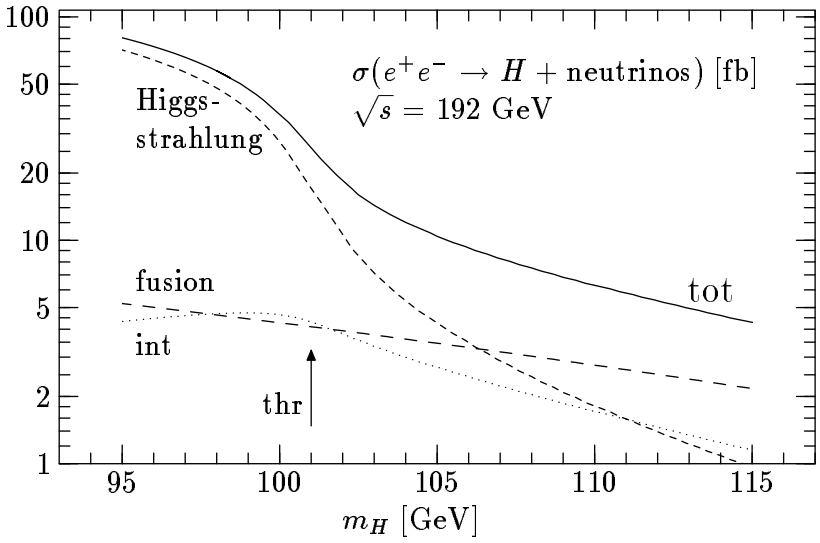

Figure 5: *Higgs-strahlung (dashed) and WW fusion (long-dashed) processes for Higgs production in the cross-over region [without radiative corrections]. The solid line shows the total cross section for both processes including the (dotted line) interference term.*

Table 1: *The process* $e^+e^- \to \mu^+\mu^- b\bar{b}$ *at* $\sqrt{s} = 192$ *GeV. No initial state radiation is included. The cross sections are given in fb.*

m_H [GeV]	65	90	115	∞
CompHEP_0	37.264(58)	24.395(46)	10.696(13)	10.634(13)
$\text{CompHEP}_{4.7}$	37.147(58)	24.279(46)	10.580(13)	10.518(13)
EXCALIBUR	—	—	—	10.6398(15)
FERMISV	—	—	—	9.49(23)
GENTLE_0	37.3975(37)	24.4727(25)	10.7022(11)	10.6401(11)
HIGGSPV	37.393(27)	24.490(21)	10.694(16)	10.65(05)
HZHA/PYTHIA	36.79(13)	23.53(13)	10.28(13)	10.22(13)
$\text{WPHACT}_{4.7}$	—	—	—	10.5243±0.24E-02
WPHACT_0	37.39896±0.64E-02	24.47269±0.40E-02	10.70272±0.24E-02	10.64070±0.24E-02
WTO	37.40994±0.32E-02	24.47653±0.42E-02	10.70360±0.21E-02	10.64157±0.21E-02

Table 2: *The process* $e^+e^- \to \mu^+\mu^- b\bar{b}$ *at* $\sqrt{s} = 192$ *GeV. Initial state radiation included, cross sections in fb.*

m_H [GeV]	65	90	115	∞
EXCALIBUR	—	—	—	8.4306(29)
FERMISV	—	—	—	7.90(27)
GENTLE_0	33.7575(34)	19.4717(19)	8.47729(85)	8.43290(84)
HIGGSPV	33.759(12)	19.480(09)	8.483(05)	8.44(05)
HZHA/PYTHIA	33.48(11)	18.91(11)	8.31(11)	8.27(11)
WPHACT	33.75217±0.16E-01	19.46923±0.91E-02	8.47665±0.57E-02	8.43236±0.57E-02
WTO	33.77741±0.10E-01	19.48562±0.83E-02	8.48511±0.78E-02	8.44090±0.78E-02

The angular distribution of the Z/H bosons in the Higgs-strahlung process is sensitive to the spin-parity quantum numbers $J^P = 0^+$ of the Higgs particle. At high energies the Z boson is produced in a state of longitudinal polarization according to the equivalence theorem so that the angular distribution approaches asymptotically the $\sin^2\theta$ law, where θ is the polar angle between the Z/H flight direction and the e^+e^- beam axis. At non-asymptotic energies the distribution is shoaled [47],

$$\frac{d\sigma}{d\cos\theta} \sim \lambda \, \sin^2\theta \, + \, 8\, m_Z^2/s \tag{8}$$

becoming independent of θ at the threshold. Were a pseudoscalar particle produced in association with the Z, the angular distribution would be given by $\sim (1 + \cos^2\theta)$, independent of the energy; the Z polarization would be transverse in this case. Thus, the angular distribution is sensitive to the assignment of spin-parity quantum numbers to the Higgs particle. The coefficients of the $\sin^2\theta$ term and the constant term are independent and could be modified separately by additional effective ZZH, γZH couplings or $eeZH$ contact terms induced by interactions outside the Standard Model [48].

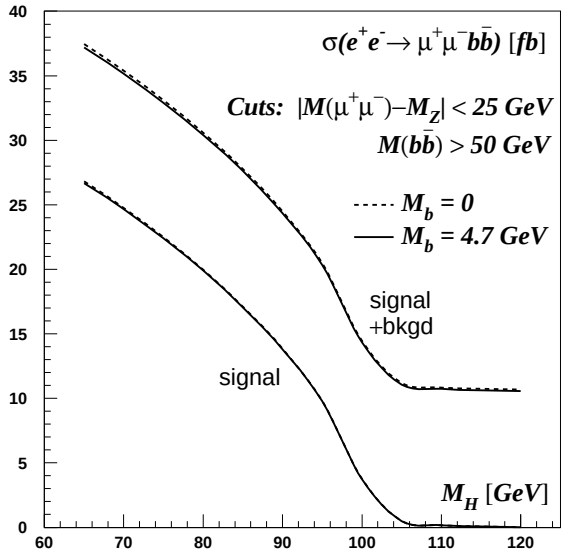

Figure 6: *Comparison of the Higgs signal with the background in the $\mu^+\mu^- b\bar{b}$ final state for zero and non-zero quark mass.*

2.2.2 The WW Fusion Process

The final state in which the Higgs particle is produced in association with neutrinos

$$e^+e^- \to H + \nu\bar{\nu} \tag{9}$$

is built up by two different mechanisms, Higgs-strahlung with Z decays to the three types of neutrinos and WW fusion [9, 10, 11, 49, 50]. For $\nu_e\bar{\nu}_e$ final states the two amplitudes interfere. At e^+e^- energies above the HZ threshold for on-shell Z, Higgs-strahlung is by far the dominant process, while below the HZ threshold the fusion process becomes dominant. Correspondingly, the interference term is most important near the threshold where the cross-over between the two mechanisms occurs. The cross section for Higgs-strahlung above the HZ threshold is of order g_W^4 while below the threshold it is suppressed by the additional electroweak vertex as well as by the off-shell Z propagator. The fusion cross-section is of order g_W^6 and therefore small at LEP energies where no $\log s/m_H^2$ enhancement factors are effective.[1] The cross section for WW fusion can be expressed in a compact form [49]:

$$\sigma(e^+e^- \to \nu_e\bar{\nu}_e H) = \frac{G_F^3 m_W^4}{4\sqrt{2}\pi^3} \int_{x_H}^1 dx \int_x^1 \frac{dy\, F(x,y)}{[1+(y-x)/x_W]^2} \tag{10}$$

$$F(x,y) = \left[\frac{2x}{y^3} - \frac{1+3x}{y^2} + \frac{2+x}{y} - 1\right]\left[\frac{z}{1+z} - \log(1+z)\right] + \frac{x}{y^3}\frac{z^2(1-y)}{1+z} \tag{11}$$

with $x_H = m_H^2/s$, $x_W = m_W^2/s$ and $z = y(x-x_H)/(xx_W)$. The more involved analytic form of the interference term between fusion and Higgs-strahlung [11] is given in the Appendix 5.1.

[1] The cross-section for ZZ fusion is reduced by another order of magnitude since the leptonic NC couplings are considerably smaller than the CC couplings.

The size of the various contributions to the cross section for the final state $e^+e^- \rightarrow H$ + neutrinos is shown in Fig.5 at $\sqrt{s} = 192$ GeV. The Higgs-strahlung includes all three neutrinos in the final state. The nominal threshold value of the Higgs mass for on-shell Z production in Higgs-strahlung is $m_H = 101$ GeV at $\sqrt{s} = 192$ GeV. A few GeV above this mass value the fusion mechanism becomes dominant while the Higgs-strahlung becomes rapidly more important for smaller Higgs masses. In the cross-over range, the cross-sections for fusion, Higgs-strahlung and the interference term are of the same size. With a cross section of the order of 0.01 pb only a few events can be generated in the cross-over region for the integrated luminosity at LEP. Dedicated efforts are therefore needed to explore this domain experimentally and to extract the signal from the event sample $e^+e^- \rightarrow b\bar{b}$ + neutrinos, which includes several background channels. Nevertheless, WW fusion can extend the Higgs mass range that can be explored at LEP2 by a few (perhaps very valuable) GeV.

2.2.3 Higgs Decays

The Higgs decay width is predicted in the Standard Model to be very narrow, being less than 3 MeV for m_H less than 100 GeV. The width of the particle can therefore not be resolved experimentally. The main decay modes (Fig.7), relevant in the LEP2 Higgs mass range, are in the following channels [12, 46]:

$$\begin{array}{lcl} \text{quark decays} & : & H \rightarrow b\bar{b} \text{ and } c\bar{c} \\ \text{lepton decay} & : & H \rightarrow \tau^+\tau^- \\ \text{gluon decay} & : & H \rightarrow gg \\ W \text{ boson decay} & : & H \rightarrow WW^* \end{array} \qquad (12)$$

The $b\bar{b}$ decays are by far the leading decay mode, followed by τ, charm, and gluon decays at a level of less than 10%. Only at the upper end of the mass range do decays of the Higgs particle to W pairs start playing an increasingly important role.

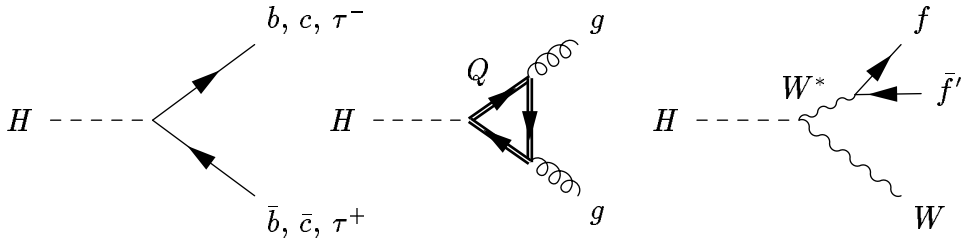

Figure 7: *The main decay modes of Higgs particles in the LEP2 mass range.*

The theoretical analysis of the Higgs decay branching ratios is not only important for the prediction of signatures to define the experimental search techniques. In addition, once the Higgs boson is discovered, the measurement of the branching ratios will be necessary to determine its couplings to other particles. This will allow us to explore the physical nature of the Higgs particle and to encircle the Higgs mechanism as the mechanism for generating the

masses of the fundamental particles. In fact, the strength of the Yukawa coupling of the Higgs boson to fermions, $g_{ffH} = [\sqrt{2}\,G_F]^{1/2} m_f$, and the couplings to the electroweak $V = W, Z$ gauge bosons, $g_{VVH} = 2\,[\sqrt{2}\,G_F]^{1/2} m_V^2$, both grow with the masses of the particles. While the latter can be measured through the production of Higgs particles in the Higgs-strahlung and WW fusion processes, fermionic couplings can be measured at LEP only through decay branching ratios.

Higgs decay to fermions. The partial width of the Higgs decay to $\tau^+\tau^-$ pairs is given by [51]

$$\Gamma(H \to \tau^+\tau^-) = \frac{G_F m_\tau^2}{4\sqrt{2}\pi} m_H \tag{13}$$

For the decay into $b\bar{b}$ and $c\bar{c}$ quark pairs, QCD radiative corrections [52] must be included which are known up to order α_s^2 [in the δ_t' term up to order α_s^3],

$$\Gamma(H \to q\bar{q}) = \frac{3G_F}{4\sqrt{2}\pi}\, m_q^2(m_H)\, m_H \left[1 + 5.67\left(\frac{\alpha_s}{\pi}\right) + (35.94 - 1.36N_F + \delta_t + \delta_t')\left(\frac{\alpha_s}{\pi}\right)^2\right] \tag{14}$$

δ_t accounts for the top-quark triangle coupled to the $q\bar{q}$ final state in second order by 2-gluon s-channel exchange [53], $\delta_t = 1.57 - \frac{2}{3}\log(m_H^2/M_t^2) + \frac{1}{9}\log^2(m_q^2(m_H)/m_H^2)$, while δ_t' accounts for Higgs decays to two gluons with one gluon split into a $q\bar{q}$ pair [12], discussed in detail below. The strong coupling α_s is to be evaluated at the scale m_H, and $N_F = 5$ is the number of active flavors [all quantities defined in the $\overline{\rm MS}$ scheme]. The bulk of the QCD corrections can be absorbed into the running quark masses evaluated at the scale m_H,

$$m_q(m_H) = m_q(M_q)\left[\frac{\alpha_s(m_H)}{\alpha_s(M_q)}\right]^{\frac{12}{33-2N_F}} \frac{1 + c_1\,[\alpha_s(m_H)/\pi] \;+\; c_2[\alpha_s(m_H)/\pi]^2}{1 + c_1\,[\alpha_s(M_q)/\pi] \;+\; c_2[\alpha_s(M_q)/\pi]^2} \tag{15}$$

In the case of bottom (charm) quarks, the coefficients c_1 and c_2 are 1.17 (1.01) and 1.50 (1.39), respectively. Since the relation between the pole mass M_c of the charm quark and the $\overline{\rm MS}$ mass $m_c\,(M_c)$ evaluated at the pole mass is badly convergent, the running quark masses $m_q(M_q)$ lend themselves as the basic mass parameters in practice. They have been extracted directly from QCD sum rules evaluated in a consistent $\mathcal{O}(\alpha_s)$ expansion [54]. Typical values of the running b, c masses at the scale $\mu = 100$ GeV, which is of the order of the Higgs mass, are displayed in Table 3. The evolution has been performed for the QCD coupling $\alpha_s(m_Z) = 0.118 \pm 0.006$. The large uncertainty in the running charm mass is a consequence of the small scale at which the evolution starts and where the errors of the QCD coupling are very large. In any case the value of the c mass, relevant for the prediction of the c branching ratio of the Higgs particle, is reduced to about 600 MeV.

An additional mechanism for b, c quark decays of the Higgs particle [12] is provided by the gluon decay mechanism where virtual gluons split into $b\bar{b}$, $c\bar{c}$ pairs, $H \to gg^* \to gb\bar{b}$, $gc\bar{c}$. These contributions add to the QCD corrected partial widths (14) in which the b, c quarks are coupled to the Higgs boson directly. As long as quark masses are neglected in the final states, the two amplitudes do not interfere. In this approximation, the contributions of the

Table 3: *The running b, c quark masses in the $\overline{\rm MS}$ scheme at the scale $\mu = 100$ GeV. The initial values $m_Q(M_Q)$ of the evolution are extracted from QCD sum rules; the pole masses M_Q^{pt2} are defined by the $\mathcal{O}(\alpha_s)$ relation with the running masses $m_Q(M_Q^{pt2}) = M_Q^{pt2}/[1 + 4\alpha_s/3\pi]$.*

	$\alpha_s(m_Z)$	$m_Q(M_Q)$	$M_Q = M_Q^{pt2}$	$m_Q\,(\mu = 100\ \text{GeV})$
b	0.112	(4.26 ± 0.02) GeV	(4.62 ± 0.02) GeV	(3.04 ± 0.02) GeV
	0.118	(4.23 ± 0.02) GeV	(4.62 ± 0.02) GeV	(2.92 ± 0.02) GeV
	0.124	(4.19 ± 0.02) GeV	(4.62 ± 0.02) GeV	(2.80 ± 0.02) GeV
c	0.112	(1.25 ± 0.03) GeV	(1.42 ± 0.03) GeV	(0.69 ± 0.02) GeV
	0.118	(1.23 ± 0.03) GeV	(1.42 ± 0.03) GeV	(0.62 ± 0.02) GeV
	0.124	(1.19 ± 0.03) GeV	(1.42 ± 0.03) GeV	(0.53 ± 0.02) GeV

splitting channels are obtained by taking the differences of the widths $H \to gg(g), q\bar{q}g$ between $N_F = 5$ and 4 for b, and $N_F = 4$ and 3 for c final states, given below in eq.(16). The $b/\bar{b}$ and the $c/\bar{c}$ quarks are in general emitted into two different parts of the phase space for the two mechanisms; for the direct process the flight directions tend to be opposite, while by contrast for gluon splitting they are parallel.

The electroweak radiative corrections to fermionic Higgs decays are well under control [55, 44]. If the Born formulae are parametrized in terms of the Fermi coupling G_F, the corrections are free of large logarithms associated with light fermion loops. For b, c, τ decays the electroweak corrections are of the order of one percent.

Higgs decays to gluons and light quarks. In the Standard Model, gluonic Higgs decays $H \to gg$ are primarily mediated by top-quark loops [56]. Since in the LEP2 range Higgs masses are much below the top threshold, the gluonic width can be cast into the approximate form [57]

$$\Gamma(H \to gg(g), q\bar{q}g) = \frac{G_F\,\alpha_s^2(m_H)}{36\sqrt{2}\,\pi^3} m_H^3 \left[1 + \left(\frac{95}{4} - \frac{7}{6}N_F\right)\frac{\alpha_s(m_H)}{\pi}\right] \tag{16}$$

The QCD corrections, which include the splitting of virtual gluons into gg and $q\bar{q}$ final states, are very important; they nearly double the partial width.

It is physically meaningful to separate the gluon and light-quark decays of the Higgs boson [12] from the b, c decays which add to the b, c decays through direct coupling to the Higgs boson. In this case, the partial width $\Gamma(H \to \text{gluons} + \text{light quarks})$ is obtained from (16) by choosing $N_F = 3$ for the light u, d, s quarks and by evaluating the running QCD coupling at m_H for three flavors only [corresponding to $\Lambda^{(3)}_{\overline{\rm MS}} = 378^{+105}_{-92}$ MeV for $\alpha_s^{(5)}(m_Z) = 0.118 \pm 0.006$].

Higgs decay to virtual W bosons. The channel $H \to WW^* \to 4$ fermions becomes relevant for Higgs masses $m_H > m_W$ when one of the W bosons can be produced on-shell. The partial width for this final state is given by

$$\Gamma(H \to WW^*) = \frac{3\,G_F^2\,m_W^4}{16\,\pi^3} m_H\,R(x) \tag{17}$$

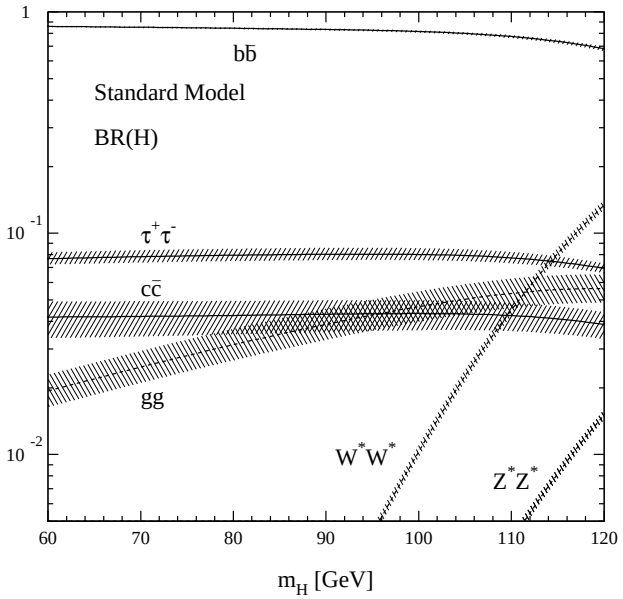

Figure 8: *Branching ratios for the Higgs decays in the Standard Model. The bands include the uncertainties due to the errors in the quark masses and the QCD coupling.*

$$R(x) = \frac{3(1-8x+20x^2)}{(4x-1)^{1/2}}\arccos\left(\frac{3x-1}{2x^{3/2}}\right) - \frac{1-x}{2x}(2-13x+47x^2) - \frac{3}{2}(1-6x+4x^2)\log x$$

with $x = m_W^2/m_H^2$. Due to the larger Z mass and the reduced NC couplings compared with W mass and the CC couplings, respectively, decays to ZZ^* final states are suppressed by one order of magnitude.

Summary of the branching ratios. The numerical results for the branching ratios are displayed in Fig.8, taking into account all QCD and electroweak corrections available so far. Separately shown are the branching ratios for τ's, c, b quarks, gluons plus light quarks, and electroweak gauge bosons. The analyses have been performed for the following set of parameters: $\alpha_s^{(5)}(m_Z) = 0.118 \pm 0.006$, t pole mass $M_t = 176 \pm 11$ GeV, and the $\overline{\rm MS}$ masses $m_b(M_b)$ and $m_c(M_c)$ as listed in Table 3. The dominant error in the predictions is due to the uncertainty in α_s which migrates to the running quark masses at the high energy scales.

Despite the uncertainties, the hierarchy of the Higgs decay modes is clearly preserved. The $\tau^+\tau^-$ branching ratio is more than an order of magnitude smaller than the $b\bar{b}$ branching ratio, following from the ratio of the two masses squared and the color factor. Since the charm quark mass is small at the scale of the Higgs mass, the ratio of BR_c to BR_b is reduced to about 0.04, i.e. more than would have been expected naïvely.

Thus, the measurements of the production cross sections and of the decay branching ratios enable us to explore experimentally the physical nature of the Higgs boson and the origin of mass through the Higgs mechanism.

2.3 The Experimental Search for the SM Higgs Particle

Selection algorithms were developed by the four LEP experiments [58] towards the Higgs production *via* the Higgs-strahlung process, for the following event topologies:

(i) the four-jet channel, ($Z \to q\bar{q}$) ($H_{SM} \to b\bar{b}$);

(ii) the missing energy channel, ($Z \to \nu\bar{\nu}$) ($H_{SM} \to b\bar{b}$);

(iii) the leptonic channel, ($Z \to e^+e^-, \mu^+\mu^-$) ($H_{SM} \to$ anything);

(iv) the $\tau^+\tau^- q\bar{q}$ channel, ($Z \to \tau^+\tau^-$) ($H_{SM} \to$ hadrons) and vice-versa;

altogether amounting to more than 90% of the possible final states in the LEP2 mass range.

All important background processes were included in the simulations. Whenever possible, the corresponding cross-sections were computed and events were generated using PYTHIA 5.7 [59]. The $Z\nu\bar{\nu}$ process being not simulated in PYTHIA, the corresponding results were derived from a Monte Carlo generator based on Ref.[60]. The most relevant cross-sections are indicated in Table 4 for the three different center-of-mass energies at which the studies were carried out. Events from the Higgs-strahlung process were generated using either PYTHIA (DELPHI, L3, OPAL), the HZGEN generator [61] (DELPHI, for the $HZ \to b\bar{b}\nu_e\bar{\nu}_e$ final state) or the HZHA generator [62] (ALEPH, for all signal final states), and the signal cross-section and Higgs boson decay branching ratios were determined from Ref.[46], or directly from the HZHA program in the case of ALEPH.

Table 4: *The cross-sections for the most relevant background processes, in pb. Whenever a Z is indicated, the cross-section also includes the γ^* contribution. The $\gamma\gamma \to f\bar{f}$ cross-section is given for a fermion pair mass in excess of 30 GeV/c^2.*

	175 GeV	192 GeV	205 GeV
$e^+e^- \to f\bar{f}$	173.4	135.5	116.5
$e^+e^- \to WW$	14.63	17.74	18.07
$e^+e^- \to ZZ$	0.45	1.20	1.43
$e^+e^- \to Ze^+e^-$	2.75	2.93	3.05
$e^+e^- \to We\nu$	0.68	0.90	1.10
$e^+e^- \to Z\nu\bar{\nu}$	0.011	0.015	0.020
$\gamma\gamma \to f\bar{f}$	22.3	24.9	26.3

The selection efficiencies and the background rejection capabilities were evaluated after a simulation of each of the four LEP detectors. Fully simulated events were produced by DELPHI [63, 64], L3 [65] and OPAL [66] for all the background processes and for the signal at several

Higgs boson masses, including all the detector upgrades foreseen for the LEP2 running. A fast, but reasonably detailed simulation was used in ALEPH [67] instead, with the current detector design (in particular, the gain expected from the installation of a new vertex detector was conservatively ignored), but it was checked in the four-jet topology and in the missing energy channel, at $\sqrt{s} = 175$ GeV and with $m_{\rm H} = 70$ GeV, that this fast simulation faithfully reproduces the predictions of the full simulation chain both for the background rejection and for the signal selection, up to an accuracy at the percent level.

a) Search in the Four-jet Topology

The four-jet topology arises when the Z decays into a pair of quarks, in 70% of the cases, and the Higgs boson decays into hadrons, in more than 90% of the cases. This topology represents therefore by far the most abundant final state (occurring in $\sim$ 65% of the cases) produced by the Higgs-strahlung process. However, the search in this channel is affected by a large background consisting of multijet events from $e^+e^- \rightarrow q\bar{q}$, WW and ZZ production. For instance, at $\sqrt{s} = 192$ GeV, and for an integrated luminosity of 150 pb^{-1}, approximately 1500 $q\bar{q}$, 1000 WW and 80 ZZ events have at least four jets with all jet-jet invariant masses in excess of 10 GeV/c^2, while only 40 $H_{SM}Z$ events are expected if $m_{\rm H} = 90$ GeV/c^2.

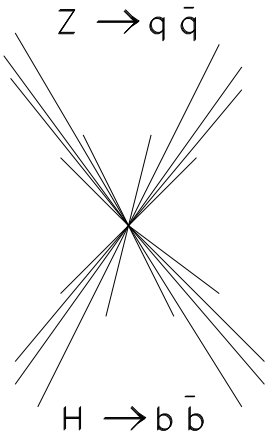

The selection procedures developed by the four collaborations to improve the signal-to-noise ratio are very close to each other. After a preselection aimed at selecting four-jets events, either from global events properties or directly from a jet algorithm such as the DURHAM or JADE algorithms, the four-jet energies and momenta are subjected to a kinematical fit with the four constraints resulting from the energy-momentum conservation, in order to improve the Higgs boson mass resolution beyond the detector resolution. Events consistent with the $e^+e^- \rightarrow$ WW hypothesis, *i.e.* events in which two pairs of jets have an invariant mass close to $m_{\rm W}$, are rejected. Only events in which the mass of one pair of jets is consistent with $m_{\rm Z}$ are kept, and they are fitted again with the Z mass constraint in addition. This last step improves again the Higgs boson mass resolution, which is found to be between 2.5 and 3.5 GeV/c^2 by the four LEP experiments.

However, these requirements do not suffice to reduce the background contamination to an adequate level. This is illustrated in Fig.9a where the distribution of the fitted Higgs boson mass (*i.e.* the mass of the pair of jets recoiling against the pair consistent with a Z) is shown, for the signal ($m_{\rm H} = 90$ GeV/c^2) and for the backgrounds, at $\sqrt{s} = 192$ GeV and for a luminosity of 500 pb^{-1} as obtained from the ALEPH simulation at this level of the analysis.

The high branching of the Higgs boson into $b\bar{b}$ must then be taken advantage of to further reduce the background, by requiring that the jets associated to the Higgs boson be identified as b-jets. This is done by means of a microvertex detector, either by counting the charged particle tracks with large impact parameters, or by evaluating the probability $\mathcal{P}$ that these tracks come from the main interaction point [68], or by directly reconstructing secondary decay vertices [69]. Shown in Fig.9b is the resulting Higgs boson mass distribution after such a b-tagging requirement is applied. The same distribution as seen by DELPHI is shown in Fig.10, together with the efficiency of the DELPHI lifetime b-tagging requirement applied to four-jet events, in which four b-jets, two b-jets or no b-jets are present, as a function of the logarithm of the probability $\mathcal{P}$. The OPAL result in this topology is shown in Fig.11a. Due to the recent vertex detector installation, the L3 b-tagging algorithm is not yet fully optimized and its performance is thus expected to improve in the future.

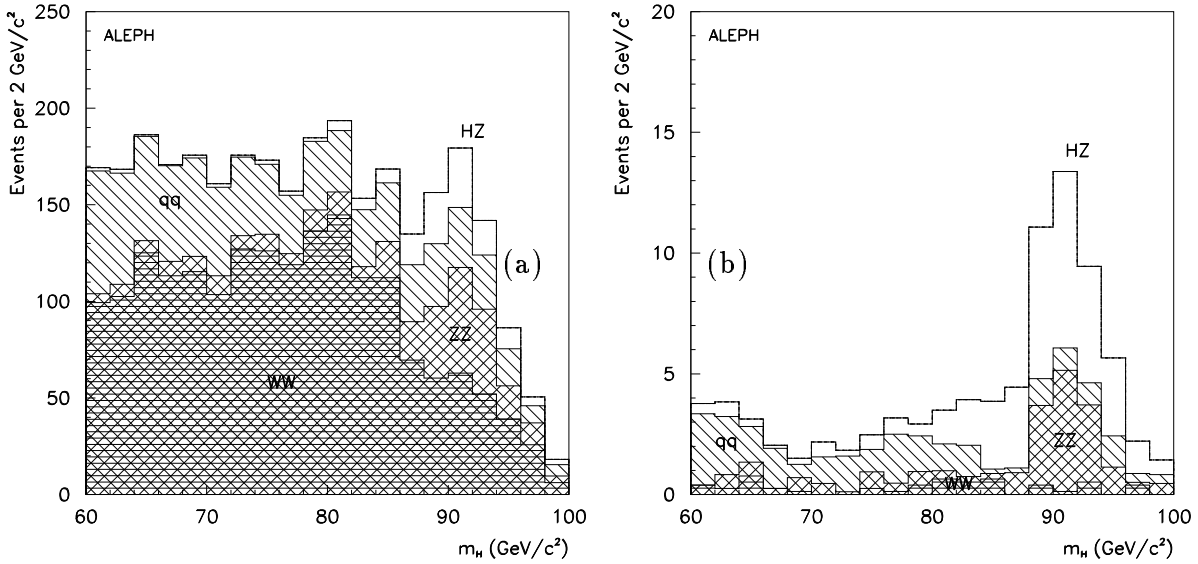

Figure 9: *Distribution of the fitted Higgs boson mass as obtained from the ALEPH simulation, in the four-jet topology before (a) and after (b) a b-tagging requirement is applied, at 192 GeV, with 500 pb^{-1} and for $m_H = 90$ GeV/c^2.*

Table 5: *Accepted cross-sections (in fb) for the signal and the backgrounds, as expected by ALEPH, DELPHI, L3, OPAL, for $m_H = 90$ GeV/c^2 at 192 GeV, in the four-jet topology.*

Experiment	ALEPH	DELPHI	L3	OPAL
Signal	58	43	43	46
Background	33	33	47	26

The numbers of background and signal events expected to be selected by ALEPH, DELPHI, L3, and OPAL in a window of $\pm 2\sigma$ around the reconstructed Higgs boson mass are shown in Table 5 for a Higgs boson mass of 90 GeV/c^2 and at a center-of mass energy of 192 GeV.

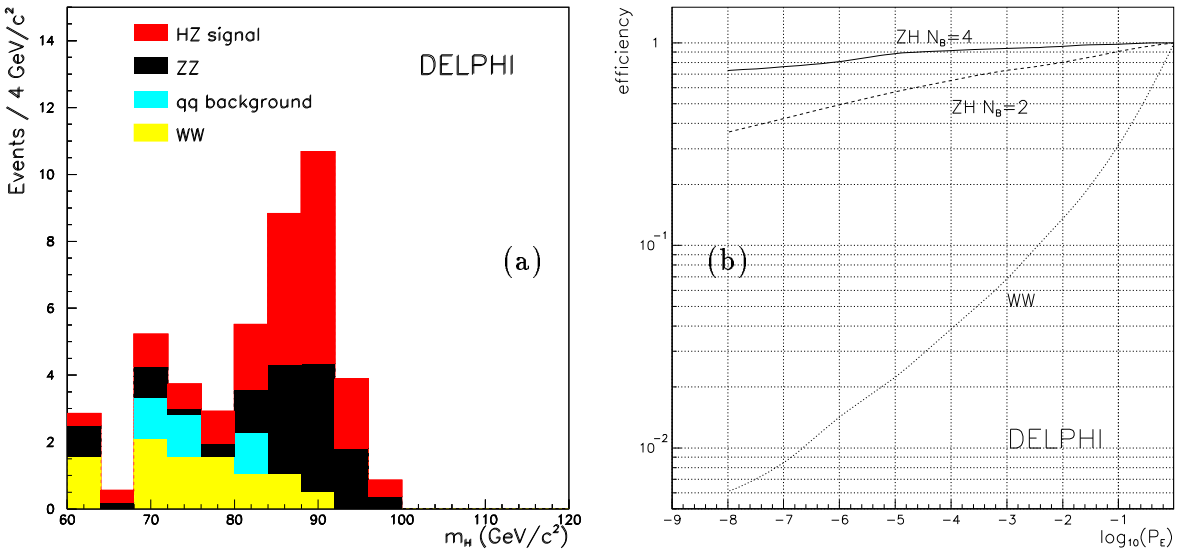

Figure 10: *(a) Distribution of the fitted Higgs boson mass as obtained from the DELPHI experiment, after a b-tagging requirement is applied, at 192 GeV, with 300 pb^{-1} and for $m_H = 90$ GeV/c^2, and (b) Evolution of the b-tagging efficiency as a function of the cut on $\mathcal{P}$ when applied to four jet events, with four, two or zero b-jets.*

b) Search in the Missing Energy Channel

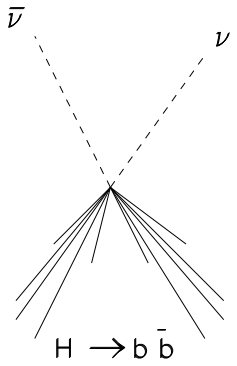

The topology of interest here, arising in 18% of the cases, is an acoplanar pair of b-quark jets with mass m_H, accompanied by large missing energy and large missing mass, close to the Z mass. The background, with the exception of the $ZZ \to b\bar{b}\nu\bar{\nu}$ or the $Z\nu\bar{\nu}$ with $Z \to b\bar{b}$ processes, either has no missing energy ($e^+e^- \to q\bar{q}$ with no initial state radiation, $WW, ZZ \to$ four-jets), or no missing mass and isolated particles ($e^+e^- \to q\bar{q}(\gamma)$, $WW \to \ell\nu +$ two jets, Ze^+e^-), or no missing transverse momentum and small acoplanarity angle ($e^+e^- \to q\bar{q}(\gamma\gamma)$, $\gamma\gamma \to q\bar{q}$), or light quark jets ($e^+e^- \to (e)\nu W$, $WW \to \tau\nu +$ two jets, $ZZ \to q\bar{q}\nu\bar{\nu}$).

The four collaborations developed a selection procedure with a sequence of criteria, based on these differences between signal and background, including a b-tagging requirement. The mass of the Higgs boson can be either rescaled or fitted by constraining the missing mass to equal the Z mass, allowing mass resolutions from 3.5 to 5 GeV/c^2 to be achieved. The mass distribution obtained by OPAL in this channel, for a Higgs boson mass of 90 GeV/c^2 and at a center-of mass energy of 192 GeV, is shown in Fig.11b.

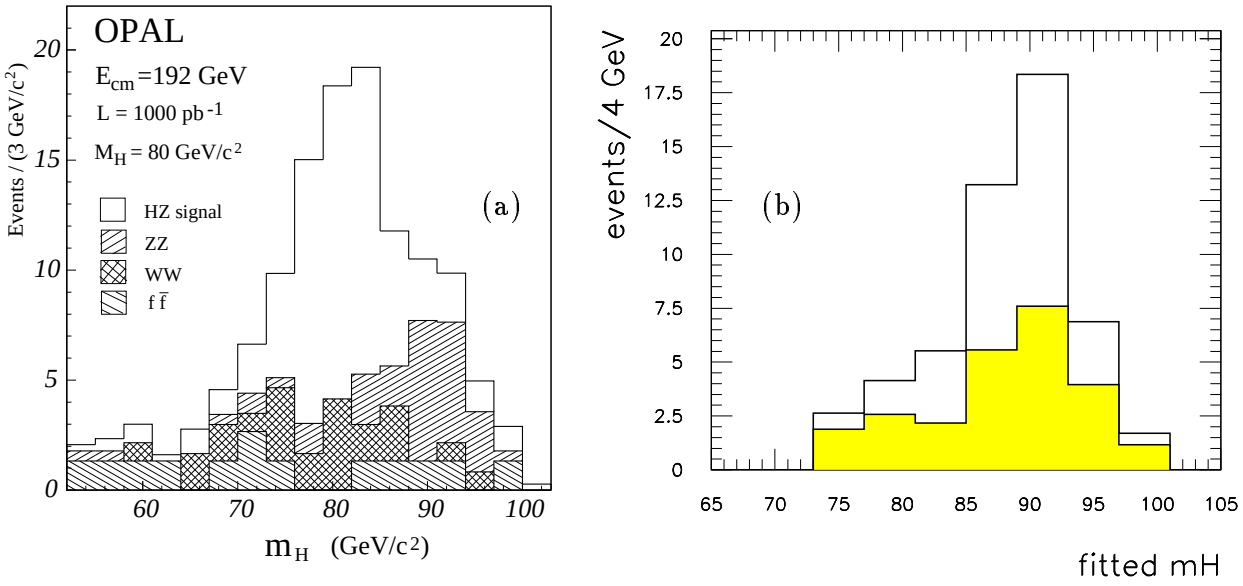

Figure 11: *Distribution of the fitted Higgs boson mass as obtained from the OPAL experiment, in the four-jet channel (a) and in the missing energy channel (b), at a centre-of mass energy of 192 GeV, normalized to a luminosity of 1000 pb^{-1} and for $m_{\rm H} = 80$ and 90 GeV/c^2, respectively. The signal (in white) is shown on top of the background (shaded histogram).*

This selection procedure was supplemented in DELPHI by an alternative multi-variate probabilistic method, confirming (or slightly improving) the first analysis results. The contribution of the t-channel WW fusion to the H$\nu\bar{\nu}$ final topology was also estimated by DELPHI with the recently released HZGEN event generator which includes both the Higgs-strahlung and the WW fusion diagrams together with their interference. As can be naively expected, the relative gain is only sizeable above the HZ kinematical threshold, and amounts to 28% for a 100 GeV/c^2 Higgs boson at 192 GeV, corresponding to 0.25 additional events expected for an integrated luminosity of 300 pb^{-1}.

Table 6: *Accepted cross-sections (in fb) for the signal and the backgrounds, as expected by ALEPH, DELPHI, L3, OPAL, for $m_{\rm H} = 90$ GeV/c^2 at 192 GeV, in the missing energy channel.*

Experiment	ALEPH	DELPHI	L3	OPAL
Signal	24	24	9	25
Background	13	17	11	20

The numbers of background and signal events expected to be selected by ALEPH, DELPHI, L3, and OPAL in a window of $\pm 2\sigma$ around the reconstructed Higgs boson mass are shown in Table 6 for a Higgs boson mass of 90 GeV/c^2 and at a center-of mass energy of 192 GeV.

c) Search in the Leptonic Channel

Although occurring in only 6.7% of the cases, this topology can be selected in a simple way by requiring the presence of a high mass pair of energetic, isolated, and thus well identifiable leptons (e or μ) in association with a high multiplicity hadronic system. The process $e^+e^- \rightarrow ZZ$ where one of the Z bosons decays into a lepton pair and the other into $q\bar{q}$ and, to a much lesser extent, the $e^+e^- \rightarrow Ze^+e^-$ process, constitute the only irreducible background sources. A mild b-tagging requirement can also be applied, especially when $m_H \sim m_Z$, to improve the signal-to-noise ratio. Selection efficiencies varying from 50 to 80% were achieved by the four LEP experiments.

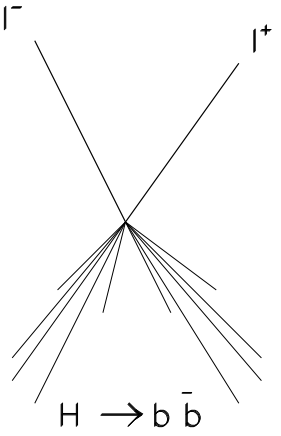

In addition to these high efficiencies, the mass of the Higgs boson can be determined with a very good resolution (typically better than 2 GeV/c^2) either as the mass recoiling to the lepton pair with the mass of the pair constrained to the Z mass, or with a full fitting procedure using the energies and the directions of the leptons and of the Higgs decay products, the energy-momentum conservation and the Z mass constraint. As shown in Fig.12 from L3, this drastically reduces the ZZ background contamination, except if $m_H \sim m_Z$ when the two mass peaks merge together.

The numbers of background and signal events expected to be selected by ALEPH, DELPHI, L3, and OPAL in a window of $\pm 2\sigma$ around the reconstructed Higgs boson mass are shown in Table 7 for a Higgs boson mass of 90 GeV/c^2 and at a centre-of mass energy of 192 GeV.

d) Search in the $\tau^+\tau^-q\bar{q}$ Channel

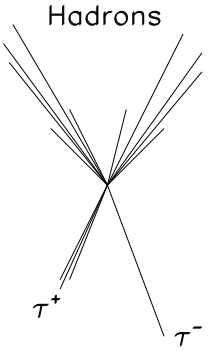

At present, only ALEPH [67] and DELPHI [70] have investigated this topology, occurring in 9% of the cases when ($Z \rightarrow \tau^+\tau^-$) ($H_{SM} \rightarrow$ hadrons) (3%) or when ($H_{SM} \rightarrow \tau^+\tau^-$) ($Z \rightarrow$ hadrons) (6%). It is characterized by two energetic, isolated *taus*, defined as 1- or 3-prong slim jets, with masses compatible with m_τ, not identified as an electron or a muon pair, and associated to a high multiplicity hadronic system. After a selection of this topology either by successive topological cuts (ALEPH) or by a single multi-dimensional cut (DELPHI), a fit to the four-body final state hypothesis with the energy-momentum conservation constraint is performed to reject most of the backgrounds.

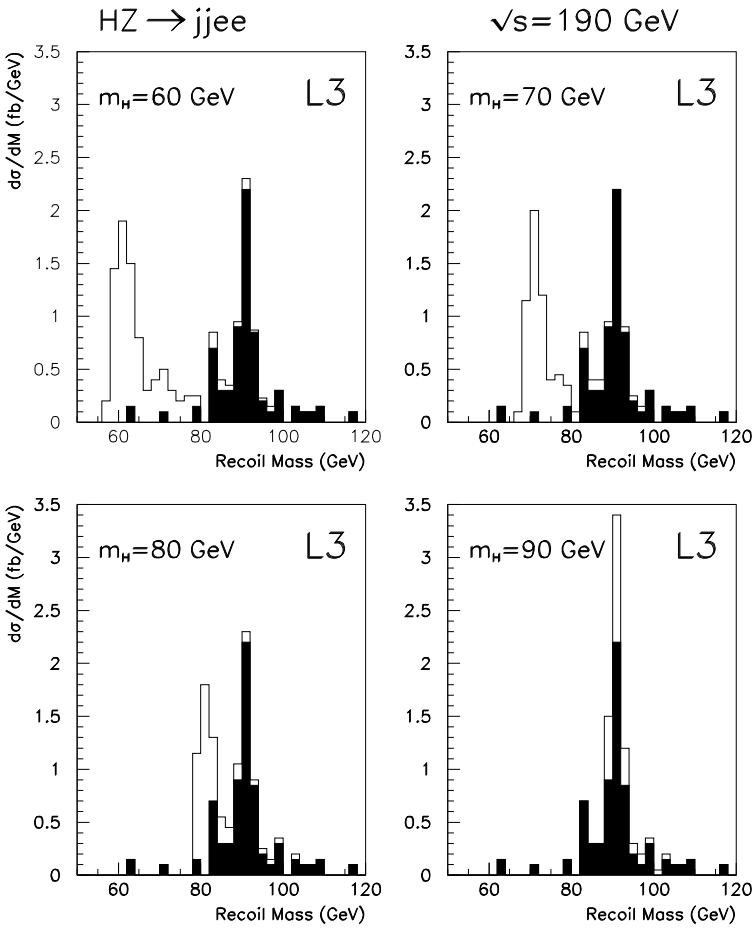

Figure 12: *Distribution of mass recoiling to the lepton pair as obtained from the L3 experiment, in the He^+e^- channel, at a center-of mass energy of 192 GeV, normalized to a luminosity of 1000 pb^{-1} and for $m_H = 60, 70, 80, 90$ GeV/c^2. The signal (in white) is shown on top of the ZZ background (in black).*

Table 7: *Accepted cross-sections (in fb) for the signal and the backgrounds, as expected by ALEPH, DELPHI, L3 and OPAL, for $m_H = 90$ GeV/c^2 at 192 GeV, in the leptonic channel.*

Experiment	ALEPH	DELPHI	L3	OPAL
Signal	12	11	7	6.5
Background	12	24	10	9.4

The typical efficiency for such an analysis is 20 to 30%, corresponding to 6 to 8 signal events expected for a 90 GeV/c^2 Higgs boson with 1 fb^{-1} at 192 GeV, and the $\tau^+\tau^-$ and the hadronic mass resolutions amount to approximately 3 GeV/c^2. These resolutions can be further improved by fitting the final state to the HZ hypothesis, with $m_{\rm H}$ free and $m_{\rm Z}$ constrained. As in the leptonic channel, the only really irreducible background source is the process $e^+e^- \to ZZ$ when one of the Zs decays into a τ pair and the other hadronically. The existence of the Higgs boson would then be observed as an accumulation around ($m_{\rm H}$, $m_{\rm Z}$) in the folded two-dimensional distribution of these masses. A signal-to-noise ratio between 1 and 2 can be achieved when $m_{\rm H} \sim m_{\rm Z}$. It could be further improved by a factor of two with a b-tagging requirement, at the expense of a drastic efficiency loss, since two thirds of these events (when $H \to \tau^+\tau^-$) do not contain b-quarks.

Summary: Numbers of Events Expected

Tables 8, 9 and 10 summarize the results of the standard model Higgs boson search, with the total numbers of signal and background events expected by each experiment given for several Higgs boson masses, at $\sqrt{s}$ = 175, 192 and 205 GeV, respectively. The uncertainties are due to the limited Monte Carlo statistics. No systematic uncertainties (due for instance to the simulation of the b-tagging efficiency) are included.

Table 8: *Accepted cross-sections (in fb) expected for the signal and the background, for various Higgs boson masses, at a center-of-mass energy of 175 GeV.*

$m_{\rm H}$ (GeV/c^2)	60	65	70	75	80	85
ALEPH						
Signal	275 ± 5	234 ± 4	168 ± 4	115 ± 3	61 ± 2	7 ± 1
Background	51 ± 7	45 ± 7	38 ± 6	31 ± 6	24 ± 5	24 ± 5
DELPHI						
Signal	210 ± 13	180 ± 11	147 ± 9	109 ± 7	64 ± 4	7 ± 1
Background	25 ± 4	25 ± 4	28 ± 5	28 ± 5	28 ± 5	15 ± 3
L3						
Signal	167 ± 10	142 ± 9	119 ± 7	88 ± 5	49 ± 3	7 ± 3
Background	79 ± 11	83 ± 10	87 ± 9	65 ± 7	44 ± 5	44 ± 5
OPAL						
Signal	188 ± 9	160 ± 8	128 ± 6	98 ± 7	56 ± 4	6 ± 1
Background	27 ± 5	27 ± 5	26 ± 4	27 ± 5	17 ± 4	7 ± 3
ALL						
Signal	840 ± 20	715 ± 17	561 ± 13	410 ± 12	229 ± 6	27 ± 3
Background	182 ± 14	180 ± 13	179 ± 13	151 ± 11	112 ± 9	89 ± 8

Table 9: *Accepted cross-sections (in fb) expected for the signal and the background, for various Higgs boson masses, at a center-of-mass energy of 192 GeV.*

	m_{H} (GeV/c^2)	80	85	90	95	100
ALEPH	Signal	125 ± 3	115 ± 3	103 ± 3	64 ± 2	13 ± 2
	Background	33 ± 6	48 ± 7	63 ± 8	57 ± 7	51 ± 7
DELPHI	Signal	99 ± 4	108 ± 5	85 ± 4	60 ± 4	13 ± 2
	Background	42 ± 5	68 ± 5	79 ± 5	50 ± 3	25 ± 2
L3	Signal	93 ± 5	77 ± 4	64 ± 3	45 ± 3	9 ± 1
	Background	66 ± 6	67 ± 5	68 ± 5	44 ± 5	19 ± 3
OPAL	Signal	98 ± 4	81 ± 3	72 ± 3	40 ± 2	13 ± 2
	Background	28 ± 4	37 ± 4	46 ± 5	36 ± 5	26 ± 5
ALL	Signal	414 ± 8	381 ± 8	323 ± 6	209 ± 6	47 ± 4
	Background	169 ± 10	220 ± 1	255 ± 12	187 ± 11	121 ± 9

Table 10: *Accepted cross-sections (in fb) expected for the signal and the background, for various Higgs boson masses, at a center-of-mass energy of 205 GeV.*

m_{H} (GeV/c^2)	80	90	100	105	110	115
ALEPH						
Signal	118 ± 3	90 ± 3	63 ± 2	46 ± 2	32 ± 3	5 ± 1
Background	48 ± 7	82 ± 9	28 ± 5	24 ± 5	20 ± 5	20 ± 5
DELPHI						
Signal	78 ± 4	84 ± 4	66 ± 4	48 ± 3	23 ± 2	3 ± 1
Background	56 ± 6	66 ± 6	52 ± 6	26 ± 4	13 ± 3	8 ± 2
L3						
Signal	88 ± 6	68 ± 4	51 ± 3	38 ± 3	22 ± 3	4 ± 1
Background	70 ± 6	94 ± 7	59 ± 6	30 ± 6	20 ± 6	20 ± 6
OPAL						
Signal	55 ± 2	48 ± 2	39 ± 2	26 ± 2	13 ± 1	4 ± 0.3
Background	25 ± 4	45 ± 4	26 ± 4	20 ± 4	15 ± 4	15 ± 4
ALL						
Signal	339 ± 8	287 ± 7	220 ± 6	158 ± 5	89 ± 4	16 ± 1
Background	198 ± 12	288 ± 13	166 ± 11	101 ± 10	68 ± 9	62 ± 9

2.4 Discovery and Exclusion Limits

Based on the simulations described in Section 2.3, it is possible to derive the exclusion and discovery limits of the standard model Higgs boson as a function of the luminosity for the three center-of-mass energies specified earlier. The contours are defined at 5σ for the discovery in the case of the existence of the Higgs boson and at 95% C.L. for the exclusion limits in the case of negative searches, with the specifications described in Appendix 5.3.

In Table 11, the minimum integrated luminosities needed to exclude or discover a given Higgs boson mass at the center-of-mass energies $\sqrt{s} = 175$, 192 and 205 GeV are given for the combination of all channels for each of the four experiments separately, as well as for the combination of all channels for the four LEP experiments together. The results of the combination of the four experiments are graphically shown in Fig.13, and summarized in Table 12.

Combining the four LEP experiments, the required minimal integrated luminosity per experiment to discover or exclude a certain Higgs boson mass at a given center-of-mass energy is reduced to approximately a fourth of the average minimal integrated luminosity of each individual experiment. This implies that the maximal value of the Higgs boson mass will be reached at a given energy for luminosities which can be naturally expected at LEP2. The following conclusions can be drawn from detailed analyses of the figures and tables.

(i) At a center-of-mass energy of 175 GeV, the maximum integrated luminosity needed is of the order of 150 pb^{-1} and this allows the discovery of a Higgs boson with a maximum mass of about 82 GeV/c^2. Indeed, combining the four experiments it follows that raising the luminosity leads only to a marginal increase of the exclusion and discovery limits, which are very close to each other.

(ii) At 192 GeV it is again sufficient to have an integrated luminosity of about 150 pb^{-1}, in this case to discover a Higgs boson with mass up to 95 GeV/c^2. Increasing the center-of-mass energy from 175 to 192 GeV leads to a significant extension in the discovery range of the Higgs boson mass. It is of great interest to observe that at $\sqrt{s} = 192$ GeV a 95 GeV/c^2 Higgs boson mass can be excluded at the 95% confidence level with an integrated luminosity as low as 33 pb^{-1} while with 150 pb^{-1} a Higgs boson mass close to 100 GeV/c^2 can be excluded.

(iii) This development continues up to 205 GeV, where a luminosity as low as 70 pb^{-1} is sufficient to exclude Higgs boson masses up to about 110 GeV/c^2, and a 5σ discovery of a Higgs boson with a mass of order 105 GeV/c^2 requires an integrated luminosity of $\sim$ 160 pb^{-1}. More luminosity is needed in this case, since the cross section of the irreducible ZZ background increases. With an integrated luminosity of $\sim$ 300 pb^{-1} a Higgs boson mass close to 110 GeV can be discovered.

If each experiment is considered separately, the 5σ discovery limit for an integrated luminosity of 500 pb^{-1} is, on average, approximately given by $m_{\mathrm{H}} = 82$ (95) (103) GeV/c^2 for $\sqrt{s}=$

Table 11: *Minimum luminosity needed, in pb^{-1}, by ALEPH, DELPHI, L3, OPAL, and for a simple combination of the four experiments, at the three center-of-mass energies and for various Higgs boson masses. The first number holds for the 95% C.L. exclusion, the second one for the 5σ discovery.*

$\sqrt{s}$ = 175 GeV

Experiment	m_H = 60	65	70	75	80
ALEPH	12:34	18:49	25:76	36:126	80:316
DELPHI	16:48	18:51	31:87	40:140	78:335
L3	29:127	39:180	56:244	75:334	152:727
OPAL	17:56	20:75	34:96	44:161	74:294
All	6:15	6:19	8:28	10:41	21:90

$\sqrt{s}$ = 192 GeV

Experiment	m_H= 80	85	90	95
ALEPH	33:117	42:166	59:238	103: 510
DELPHI	50:195	50:231	80:388	118: 529
L3	64:306	90:426	118:596	172: 832
OPAL	43:157	60:251	85:360	182: 825
All	12:44	15:60	20:87	33:149

$\sqrt{s}$ = 205 GeV

Experiment	m_H= 80	90	100	105	110
ALEPH	41:157	80:369	76:327	119: 504	186: 870
DELPHI	75:356	78:372	97:462	114: 507	283:1296
L3	74:342	142:704	162:817	164: 897	409:2103
OPAL	87:372	149:735	151:719	267:1284	680:3500
All	16:66	25:119	30:125	38:158	72:339

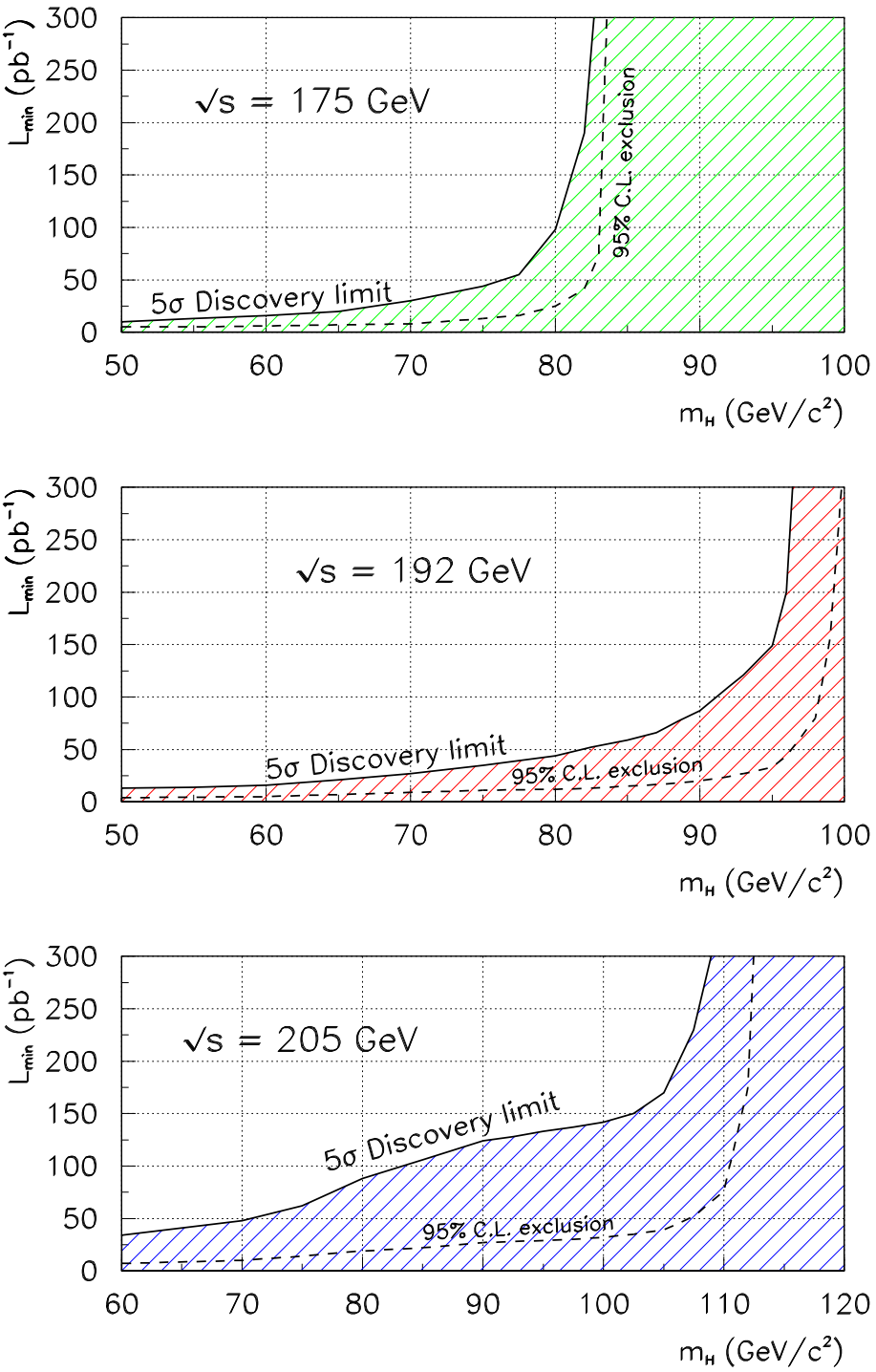

Figure 13: *Minimum luminosity needed per experiment, in pb^{-1}, for a combined 5σ discovery (full line) or a 95% C.L. exclusion (dashed line) as a function of the Higgs boson mass, at the three center-of-mass energies.*

Table 12: *Maximal Higgs boson masses that can be excluded or discovered with a given integrated luminosity L_{min} per experiment at the three representative energy values of 175, 192 and 205 GeV, when the four LEP experiments are combined.*

	Exclusion:		Discovery:	
$\sqrt{s}$ (GeV)	$m_{\rm H}$ (GeV/c^2)	L_{min} (pb^{-1})	$m_{\rm H}$ (GeV/c^2)	L_{min} (pb^{-1})
175	83	75	82	150
192	98	150	95	150
205	112	200	108	300

175 (192) (205) GeV. Similar results may be obtained by combining the four experiments for an integrated luminosity per experiment of about 150 pb^{-1}. For the combined exclusion limits, the maximum value of $m_{\rm H}$ at $\sqrt{s}$= 175, 192, 205 GeV is reached for a luminosity per experiment of about 75, 150, 200 pb^{-1}. A further increase in luminosity is not very useful in case of negative searches. Clearly, energy rather than luminosity is the crucial parameter to improve the range of masses which can be reached at LEP2.

2.5 The LHC Connection

It has been shown in section 2.4 that LEP2 can cover the SM Higgs mass range up to 82 GeV at a total energy of $\sqrt{s} = 175$ GeV while the Higgs mass discovery limit increases to ~ 95 GeV for a total energy of 192 GeV. Since this mass range contains the lower limit at which the SM Higgs particle can be searched for at the LHC, the upper limit of the LEP2 energy is quite crucial for the overlap in the discovery regions of the two accelerators.

Low–mass Higgs particles are produced at the LHC predominantly in gluon–gluon collisions [71, 72] or in Higgs–strahlung processes [73, 74],

$$\begin{aligned} pp &\rightarrow H \rightarrow \gamma\gamma \\ pp &\rightarrow WH, ZH, t\bar{t}H \rightarrow \ell + \gamma\gamma \quad \text{and} \quad \ell + b\bar{b} \end{aligned}$$

with the Higgs boson emitted from a virtual W boson or from a top quark. In the gluon–fusion process the Higgs particle is searched for as a resonance in the $\gamma\gamma$ decay channel which comes with a branching ratio of order 10^{-3}. Even though large samples of Higgs particles can be generated in this mass range, the signal–to–background ratio is only a few percent and the rejection of jet background events which are eight orders of magnitude more frequent, is a very difficult experimental task. Excellent energy resolution and particle identification is needed [75] to tackle this problem. It has been shown in detailed experimental simulations that the

significance $S/\sqrt{B}$ of the Higgs signal is expected to rise in this channel from a value ~ 2.5 at $m_H = 80$ GeV to a value ~ 4.5 at $m_H = 100$ GeV for $\int \mathcal{L} = 3 \times 10^4$ pb^{-1} if ATLAS and CMS analyses are combined.

In the Higgs–strahlung process, the events can be tagged by leptonic decays of the W/Z bosons or the t quark to trigger the experiment and to reduce the jet background. In these subsamples the Higgs boson can be searched for in the $b\bar{b}$ decay mode with a branching ratio close to unity. This method is based on b tagging by micro–vertex detection which is anticipated to be an excellent tool of the LHC detectors. After suitable cuts in the transverse momenta of the isolated lepton and the b jets, a peak is looked for in the invariant $M(b\bar{b})$ mass. The experimental significance $S/\sqrt{B}$ of this method is biggest for small Higgs masses. For $\int \mathcal{L} = 3\times 10^4$ pb^{-1} and ATLAS/CMS combined, experimental simulations of the $[W]_l b\bar{b}$ sample suggest that $S/\sqrt{B}$ falls from ~ 8 at $m_H = 80$ GeV down to ~ 6 at $m_H = 100$ GeV. It is not yet clear how the search can be extended to higher luminosities where the layers in the micro–vertex detectors closest to the beams may not survive, thus reducing significantly the b–tagging performance of the experiments.

Combining the prospective signals from the $\gamma\gamma$ and the $[W]_l b\bar{b}$ analyses, an overall significance of 7 to 8 may be reached for Higgs masses below 100 GeV, based on a low integrated luminosity of $\int \mathcal{L} = 3 \times 10^4$ pb^{-1} within three years. Raising the integrated luminosity to $\int \mathcal{L} = 10^5$ pb^{-1} increases the discovery significance to almost 9 for $80 < m_H < 100$ GeV [76].

3 The Higgs Particles in the Minimal Supersymmetric Standard Model

The Minimal Supersymmetric Standard Model leads to clear and distinct experimental signatures in the Higgs sector. Two Higgs doublets, H_1 and H_2, must be present, in order to give masses to the up and down quarks and leptons, and to cancel the gauge anomalies induced through the Higgs superpartners. In the supersymmetric limit, the Higgs potential is fully determined as a function of the gauge couplings and the supersymmetric mass parameter μ. The breakdown of supersymmetry is associated with the introduction of soft supersymmetry breaking parameters, which are essential to yield a proper electroweak symmetry breaking. In the broken phase, the ratio of the Higgs vacuum expectation values, $\tan\beta = v_2/v_1$, appears as a new parameter, which can be related to the other parameters of the theory by minimizing the Higgs potential.

The physical Higgs spectrum of the MSSM contains two CP-even and one CP-odd neutral Higgs bosons, h/H and A, respectively, and a charged Higgs boson pair $H^\pm$ [23]. The tree–level Higgs spectrum is determined by the weak gauge boson masses, the CP–odd Higgs mass, m_A, and $\tan\beta$. It is only through radiative corrections that the other parameters of the model affect the Higgs mass spectrum. The dominant radiative corrections to the Higgs masses grow as the fourth power of the top-quark mass and they are logarithmically dependent on the sparticle spectrum. The mass of the heavy Higgs doublet is controlled by the CP-odd Higgs mass and, for large values of m_A, the effective low energy theory contains only one Higgs doublet, which couples to fermions in the standard way. In a first approximation, the Higgs masses may be calculated by assuming that all sparticles acquire masses of order of the characteristic supersymmetry breaking scale M_S which, based on naturalness arguments, should be below a few TeV. The low–energy effective theory below M_S is a general two–Higgs doublet model, with couplings which can be calculated as a function of the other parameters of the theory. Under these conditions, a general upper bound on the lightest CP-even Higgs boson mass is derived for values of the CP-odd Higgs mass of order M_S. For smaller values of m_A, a more stringent upper bound is obtained. In the following, we shall discuss in detail the different methods to compute the Higgs spectrum in the MSSM and the bounds which can be derived in each case.

3.1 Higgs Mass Spectrum and Couplings

3.1.1 Tree–level Mass Bounds

The masses of the Higgs bosons at tree level are determined as a function of m_A, $\tan\beta$ and the gauge boson masses as follows,

$$m^2_{h,H} = \frac{1}{2}\left[m^2_A + m^2_Z \mp \sqrt{(m^2_A + m^2_Z)^2 - 4m^2_Z m^2_A \cos^2 2\beta}\right], \qquad (18)$$

$$m^2_{H^\pm} = m^2_A + m^2_W. \tag{19}$$

The mass of the lightest MSSM neutral Higgs particle is bounded to be smaller than the Z mass [24, 25],

$$m_h^{\rm tree} \leq m_Z |\cos 2\beta|, \tag{20}$$

and it approaches this upper bound for large values of m_A. The bound is modified by radiative corrections, which raise the upper limit on the lightest CP-even Higgs mass to values close to 150 GeV.

3.1.2 Radiative Corrections to the Higgs Masses

The one- and partial two-loop radiative corrections to the Higgs mass spectrum in the MSSM have been calculated. Computations implying a variety of different approximations, which may be distinguished according to their level of refinement, exist. In general, the radiative corrections to the Higgs masses are large and positive, being dominated by the contributions of the third-generation quark superfields. Since the upper bound on m_h determines the limit for the detectability of the Higgs boson at LEP2, it is interesting to discuss the different methods in some detail.

a) Diagrammatic Approach. Order by order, a precise method of computation of the radiative corrections to the Higgs masses is the full diagrammatic approach. At the one-loop level such calculations have been pursued by several authors [24, 26, 80]. Complete expressions, including all supersymmetric particle contributions are available [81]. The resulting Higgs masses are defined as the location of the pole in the Higgs propagator. In order to obtain a more accurate estimate of the Higgs spectrum in the diagrammatic approach, the two-loop effects must be evaluated. A first step in this direction was performed in Ref.[82] for the case of large values of the CP-odd Higgs boson mass, large $\tan\beta$, and degenerate squark masses. It was shown that these corrections may be quite significant, of order 10–15 GeV, underlining the need for a careful treatment of the two-loop effects on the Higgs mass spectrum.

b) Effective Potential Methods. The leading corrections to the Higgs mass spectrum in the MSSM can be computed in a very simple way by means of effective potential methods [27, 78]. If all the contributions from the MSSM particles are included, the results within this scheme differ from those of the full diagrammatic approach in that the Higgs masses are evaluated at zero momentum. In order to simplify the calculations, it is possible to consider only the contributions of the third-generation quark superfields, neglecting all weak gauge coupling effects in the one-loop expressions [27]. This treatment of the effective potential has the virtue of displaying, in a compact way, the full dependence of the one-loop radiative corrections on the stop/sbottom masses and mixing angles. For a given squark spectrum, the numerical results obtained in this case differ by only a few GeV from the results obtained within the full one–loop diagrammatic approach. This reflects the smallness of the one-loop contributions from superfields other than

top and bottom. Moreover, it shows that the one-loop vacuum polarization effects relating the Higgs pole masses to the running masses calculated through the effective potential approach are in general small. The effective potential computation can be improved by including the dependence of the stop and sbottom spectrum on the weak gauge couplings [79]. In the limit $m_{\tilde{t}_1},\ m_{\tilde{t}_2},\ m_A \gg m_Z$, where $m_{\tilde{t}_{1,2}}$ are the two stop mass eigenvalues, the expression of the lightest Higgs mass takes a simple form,

$$m_h^2 = m_Z^2 \cos^2 2\beta + (\Delta m_h^2)_{\rm 1LL} + (\Delta m_h^2)_{\rm mix} \tag{21}$$

where

$$(\Delta m_h^2)_{\rm 1LL} = \frac{3 m_t^4}{4\pi^2 v^2} \ln\left(\frac{m_{\tilde{t}_1} m_{\tilde{t}_2}}{m_t^2}\right)\left[1 + \mathcal{O}\left(\frac{m_W^2}{m_t^2}\right)\right] \tag{22}$$

and

$$(\Delta m_h^2)_{\rm mix} = \frac{3 m_t^4 \tilde{A}_t^2}{8\pi^2 v^2}\left[2h(m_{\tilde{t}_1}^2, m_{\tilde{t}_2}^2) + \tilde{A}_t^2 f(m_{\tilde{t}_1}^2, m_{\tilde{t}_2}^2)\right]\left[1 + \mathcal{O}\left(\frac{m_W^2}{m_t^2}\right)\right] \tag{23}$$

In eq.(23), $\tilde{A}_t = A_t - \mu \cot\beta$ and the functions h and f are given by

$$h(a,b) = \frac{1}{a-b}\ln\left(\frac{a}{b}\right) \qquad \text{and} \qquad f(a,b) \equiv \frac{1}{(a-b)^2}\left[2 - \frac{a+b}{a-b}\ln\left(\frac{a}{b}\right)\right] \tag{24}$$

The above expression is particularly interesting since it provides the upper bound on m_h for a given stop spectrum. Including two–loop effects remains, however, a necessary further step to obtain a correct quantitative estimate of the Higgs mass.

c) Renormalization Group Improvement of the Radiatively Corrected Higgs Sector. The most important two–loop effects may be included by performing a renormalization group improvement of the effective potential, while taking into account, in a proper way, the effect of the decoupling of the heavy third–generation squarks. This program can be easily carried out in the case of a large CP-odd Higgs boson mass and degenerate squarks [77]. Since only one Higgs doublet survives at low energies, the lightest CP–even Higgs mass may be calculated through the renormalization group evolution of the effective quartic coupling, assuming that the heavy sparticles decouple at a common scale M_S. The one-loop renormalization group evolution of the quartic couplings includes two-loop effects through the resummation of the one-loop result. The general result is, however, scale dependent but this dependence is reduced by taking into account the two-loop renormalization group improvement of the one–loop effective potential [84, 85]. The vacuum expectation value of the Higgs field and the renormalized Higgs mass scale (approximately) with the appropriate one–loop anomalous dimension factors within this approximation. The scale dependence of the Higgs mass is cancelled by adding the one-loop vacuum polarization effects, necessary to define the Higgs pole mass. For the case of small stop mixing and large values of $\tan\beta$, the Higgs spectrum evaluated through this method agrees with the diagrammatic computation at the two–loop level [82, 85].

Analytical Expression for the Lightest CP-even Higgs Mass. The two-loop RG improvement of the one–loop effective potential includes two–loop effects in two different ways: through the

resummation of one–loop effects and through genuine two–loop effects. Numerically, the latter are small compared to the resummation effects [83]. Once an appropriate scale of order of the top-quark mass is adopted, the results of the one–loop RG improvement of the tree–level effective potential including the proper threshold effects of squark decoupling, are in excellent agreement with the pole Higgs masses computed by the two-loop RG improvement of the one-loop effective potential [85, 89]. This holds, for large values of the CP-odd Higgs mass, for any value of $\tan\beta$ and the squark mixing angles. Based on this result, an analytical approximation may be obtained [89] which reproduces the dominant two-loop results [85] within an error of less than 2 GeV. Fig.14 shows the agreement of the one–loop and two–loop results for m_h evaluated at the appropriate scale M_t, and the accuracy of the analytical approximation. In the $\overline{MS}$ scheme, the pole top-quark mass M_t must be related to the on-shell running mass $m_t \equiv m_t(M_t)$ by taking into account the corresponding one-loop QCD correction factor

$$m_t = \frac{M_t}{1 + \frac{4}{3\pi}\alpha_s(M_t)} \tag{25}$$

Top Yukawa effects have been neglected in eq.(25), since they are essentially cancelled by the two–loop QCD effects. Observe that eq.(25) gives the correct relation between the running and the pole top-quark masses only if the leading-log contributions to the running mass, associated with the decoupling of the heavy sparticles, are properly taken into account and the sparticles are sufficiently heavy so that the finite corrections become small [90]. The analytical approximation to the one-loop renormalization-group improved result, including two-loop leading-log effects, is given by [89]

$$\begin{aligned} m_h^2 &= m_Z^2 \cos^2 2\beta \left(1 - \frac{3}{8\pi^2}\frac{m_t^2}{v^2}\, t\right) \\ &\quad + \frac{3}{4\pi^2}\frac{m_t^4}{v^2}\left[\frac{1}{2}\tilde{X}_t + t + \frac{1}{16\pi^2}\left(\frac{3}{2}\frac{m_t^2}{v^2} - 32\pi\alpha_s\right)\left(\tilde{X}_t t + t^2\right)\right] \end{aligned} \tag{26}$$

where the angle β is defined at the scale $m_A = M_S$ and $t = \log(M_S^2/M_t^2)$. $\tilde{A}_t$ is defined above and

$$\tilde{X}_t = \frac{2\tilde{A}_t^2}{M_S^2}\left(1 - \frac{\tilde{A}_t^2}{12 M_S^2}\right) \tag{27}$$

Furthermore, $\alpha_s(M_t) = \alpha_s(m_Z)/\left(1 + \frac{b_3}{4\pi}\alpha_s(m_Z)\log(M_t^2/m_Z^2)\right)$ with $b_3 = 11 - 2N_F/3$ being the one-loop QCD beta function and N_F the number of quark flavours [$N_F = 5$ at scales below M_t]. The supersymmetric scale M_S is defined as $M_S = \sqrt{(m_{\tilde{t}_1}^2 + m_{\tilde{t}_2}^2)/2}$. For simplicity, all supersymmetric particle masses are assumed to be of order M_S. Notice that eq.(26) includes the leading D-term correction $\mathcal{O}(m_Z^2 m_t^2)$ [79].

A similar analytical result to eq.(26) has been obtained in Ref.[92]. In this approximation the two-loop leading-logarithmic contributions to m_h^2 are incorporated by replacing m_t in eq.(21) by the running top quark mass evaluated at appropriately chosen scales. For $m_{\tilde{t}_1} \approx m_{\tilde{t}_2} \equiv M_S$ the result is:

$$m_h^2 = m_Z^2 \cos^2 2\beta + (\Delta m_h^2)_{1\,\mathrm{LL}}(m_t(\mu_t)) + (\Delta m_h^2)_{\mathrm{mix}}(m_t(M_S)) \tag{28}$$

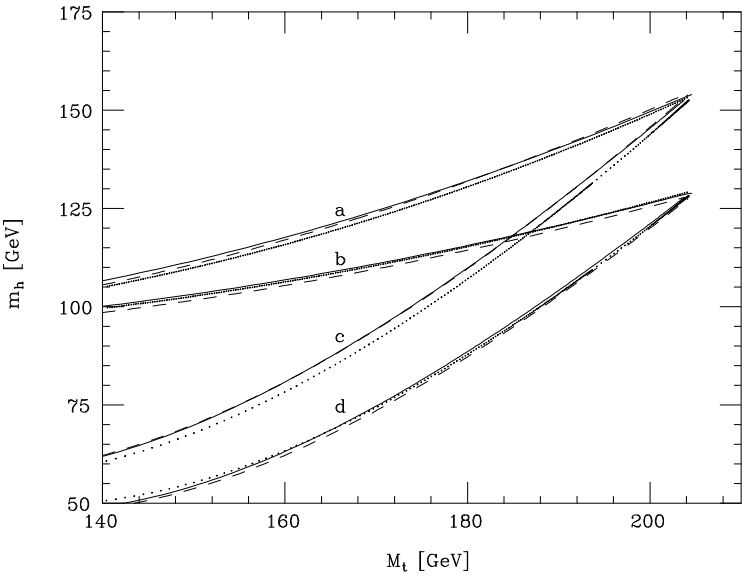

Figure 14: *The lightest Higgs mass as a function of the physical top-quark mass, for $M_S = 1$ TeV, evaluated in the limit of large m_A, as obtained from the two–loop RG improved effective potential (solid lines), the one–loop improved RG evolution (dashed lines) and the analytical approximation, eq.(26) (dotted-lines). The four sets of lines correspond to a) $\tan\beta = 15$ with maximal squark mixing, b) $\tan\beta = 15$ with zero-squark mixing, c) the minimal value of $\tan\beta$ allowed by perturbativity constraints for the given value of M_t (IR fixed point) for maximal mixing and d) $\tan\beta$ the same as in c) for zero mixing.*

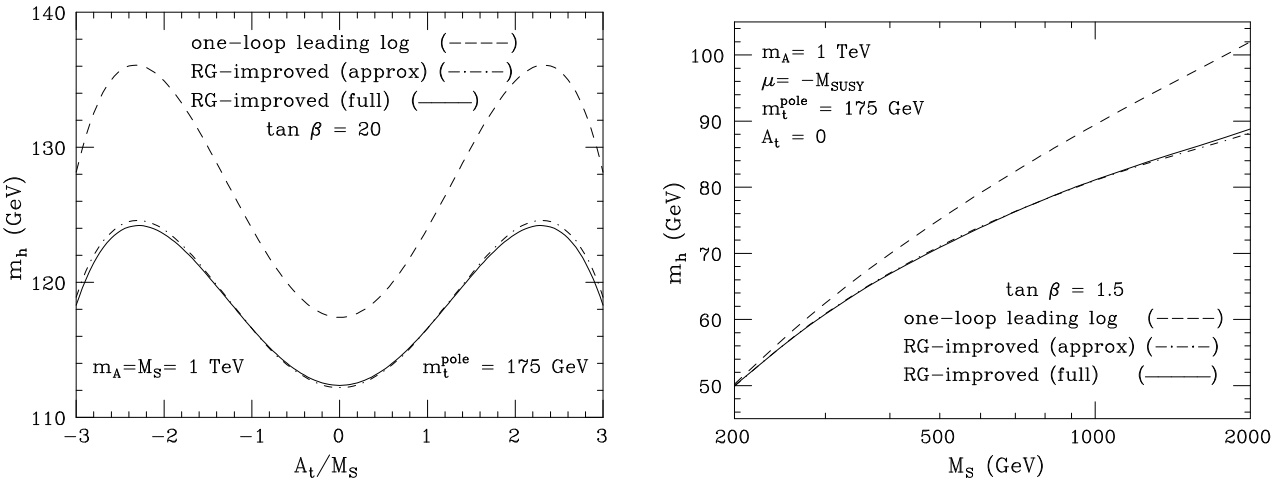

Figure 15: *The radiatively corrected light CP-even Higgs mass is plotted as a function of the MSSM parameters. The one-loop leading-log computation is compared with the RG-improved result which was obtained by numerical analysis and by using the simple analytic result given in eq.(28).*

where $\mu_t \equiv \sqrt{M_t M_S}$; the running top-quark mass is given by

$$m_t(\mu) = m_t \left[1 - \left(\frac{\alpha_s}{\pi} - \frac{3\alpha_t}{16\pi} \right) \ln \left(\frac{\mu^2}{M_t^2} \right) \right] \tag{29}$$

with $\alpha_t = h_t^2/4\pi$. All couplings on the right hand side of eq.(29) are evaluated at M_t. The requirement that the two stop mass eigenstates be close to each other allows an expansion of the functions h and f, eq.(24), in powers of $m_t \tilde{A}_t / M_S^2$. The resulting expression for the Higgs mass is equivalent to the one obtained by performing an expansion of the effective potential in powers of the Higgs field ϕ. Keeping only operators up to order four in the effective potential, eq.(28) reproduces the expression of eq.(26). This comparison holds up to small differences associated with the treatment of the effects due to the weak gauge couplings in the one-loop effective potential, and with the inclusion of the top Yukawa effects in the relation between the pole and running top-quark mass [89, 92]. A more detailed treatment of the dependence of the Higgs mass on the weak gauge couplings may be also found in Ref.[91].

Fig.15 shows the comparison between the results of the analytical approximation, eq.(29), and the one-loop RG improvement to the full one–loop leading–log diagrammatic calculation. In general, the prescription given in eq.(29) reproduces the full one-loop RG-improved Higgs masses to within 2 GeV for top-squark masses of 2 TeV or below. The dashed line in the figure shows the result that would be obtained by ignoring the RG-improvement; it reflects the relevance of the two-loop effects in the evaluation of the Higgs mass.

The Case $m_A \lesssim M_S$. A similar RG improvement of the effective potential method to the one already discussed can be applied to calculate all the masses and couplings in the more general case of a light CP-odd Higgs boson $m_A \lesssim M_S$. As above, the finite one-loop threshold corrections to the quartic couplings at the scale M_S at which the heavy squarks decouple [87] are also taken into account. The effective theory below the scale M_S [86, 87] is a two-Higgs doublet model where the tree–level quartic couplings can be written in terms of dimensionless parameters λ_i, $i = 1, \ldots, 7$, whose tree–level values are functions of the gauge couplings. The one-loop threshold corrections $\Delta\lambda_i$, $i = 1, \ldots, 7$, are expressed as functions of the supersymmetric Higgs mass μ and the soft supersymmetry breaking parameters A_t, A_b and M_S [87]. An analytical approximation, which reproduces the previous one–loop RG improved results for all values of $\tan\beta$ and m_A, can also be derived. For example, generalizations of Eq. (21) can be found in Refs.[89, 92]. The CP-even light and heavy Higgs masses and the charged Higgs mass are given as functions of $\tan\beta$, M_S, A_t, A_b, μ, the CP-odd Higgs mass m_A and the physical top-quark mass M_t related to the on-shell running mass m_t through eq.(25). The analytical expressions for the masses and mixing angle of the Higgs sector as a function of the parameters λ_i are presented in Appendix 5.2. These expressions are the analogue of eq.(26) for the case in which two-Higgs doublets survive at low energies. Effects of the bottom Yukawa coupling, which may become large for values $\tan\beta \simeq m_t/m_b$ (m_b being the running bottom mass at the scale M_t), are also included. A subroutine implementing this method is available [93].

Table 13: *MSSM Higgs couplings relevant at LEP2.*

Vertex	Coupling
$\{h,H\}W_\mu W_\nu$	$i2(G_F\sqrt{2})^{1/2}m_W^2 g_{\mu\nu}\{\sin(\beta-\alpha),\cos(\alpha-\beta)\}$
$\{h,H\}Z_\mu Z_\nu$	$i2(G_F\sqrt{2})^{1/2}\frac{m_W^2}{\cos^2\theta_W}g_{\mu\nu}\{\sin(\beta-\alpha),\cos(\alpha-\beta)\}$
$\{h,H,A\}u\overline{u}$	$-i\frac{(\sqrt{2}G_F)^{1/2}m_u}{\sin\beta}\{\cos\alpha,\sin\alpha,-i\gamma_5\cos\beta\}$
$\{h,H,A\}d\overline{d}$	$-i\frac{(\sqrt{2}G_F)^{1/2}m_d}{\cos\beta}\{-\sin\alpha,\cos\alpha,-i\gamma_5\sin\beta\}$
$\{h,H\}AZ_\mu$	$-(\sqrt{2}G_F)^{1/2}m_Z(p+k)_\mu\{\cos(\beta-\alpha),-\sin(\beta-\alpha)\}$

Couplings. Notice that the radiatively corrected quartic couplings λ_i, $i=1,\ldots,7$, and hence the corresponding value of the Higgs mixing angle α as given in Appendix 5.2, permit us to evaluate all radiatively corrected Higgs couplings. For instance, the Yukawa and gauge Higgs couplings relevant for LEP2 energies are listed in Table 13 [p_μ (k_μ) is the incoming (outgoing) CP-odd (CP-even) Higgs momentum]. The size of the couplings of the two scalar Higgs bosons to fermions and a gauge boson are shown in Fig.16 [95]. For fermions the charged Higgs particles couple to mixtures of scalar and pseudoscalar currents, with components proportional to $m_u\cot\beta$ and $m_d\tan\beta$ for the two $\pm$ chiralities. The couplings to left(right)-handed ingoing u quarks are given by $g_{H^+\bar{d}u_{L(R)}}=[\sqrt{2}G_F]^{1/2}m_u\cot\beta\,(m_d\tan\beta)$. For large $\tan\beta$ the down–type mass defines the size of the coupling; for small to moderate $\tan\beta$ it is defined by the up–type mass. Furthermore, the trilinear Higgs couplings can be explicitly written as functions of λ_i, α and β [87, 88].

d) Renormalization Group Improvement of the Effective Potential: General Third–Generation Squark Mass Parameters. The above one–loop RG improved treatment of the effective potential relies on the definition of an effective supersymmetric threshold scale, $M_S^2=(m_{\tilde{t}_1}^2+m_{\tilde{t}_2}^2)/2$. Its validity is therefore restricted to the case of small differences between the squark mass eigenvalues. Quantitatively, the method is valid if $(m_{\tilde{t}_1}^2-m_{\tilde{t}_2}^2)/(m_{\tilde{t}_1}^2+m_{\tilde{t}_2}^2)\leq 0.5$. Furthermore, all the RG Higgs analyses performed in the literature, besides Ref.[91], rely on the expansion of the effective potential up to operators of dimension four. However, to safely neglect higher dimensional operators, the conditions $2|M_tA_t|\leq M_S^2$ and $2|M_t\mu|\leq M_S^2$ must be fulfilled.

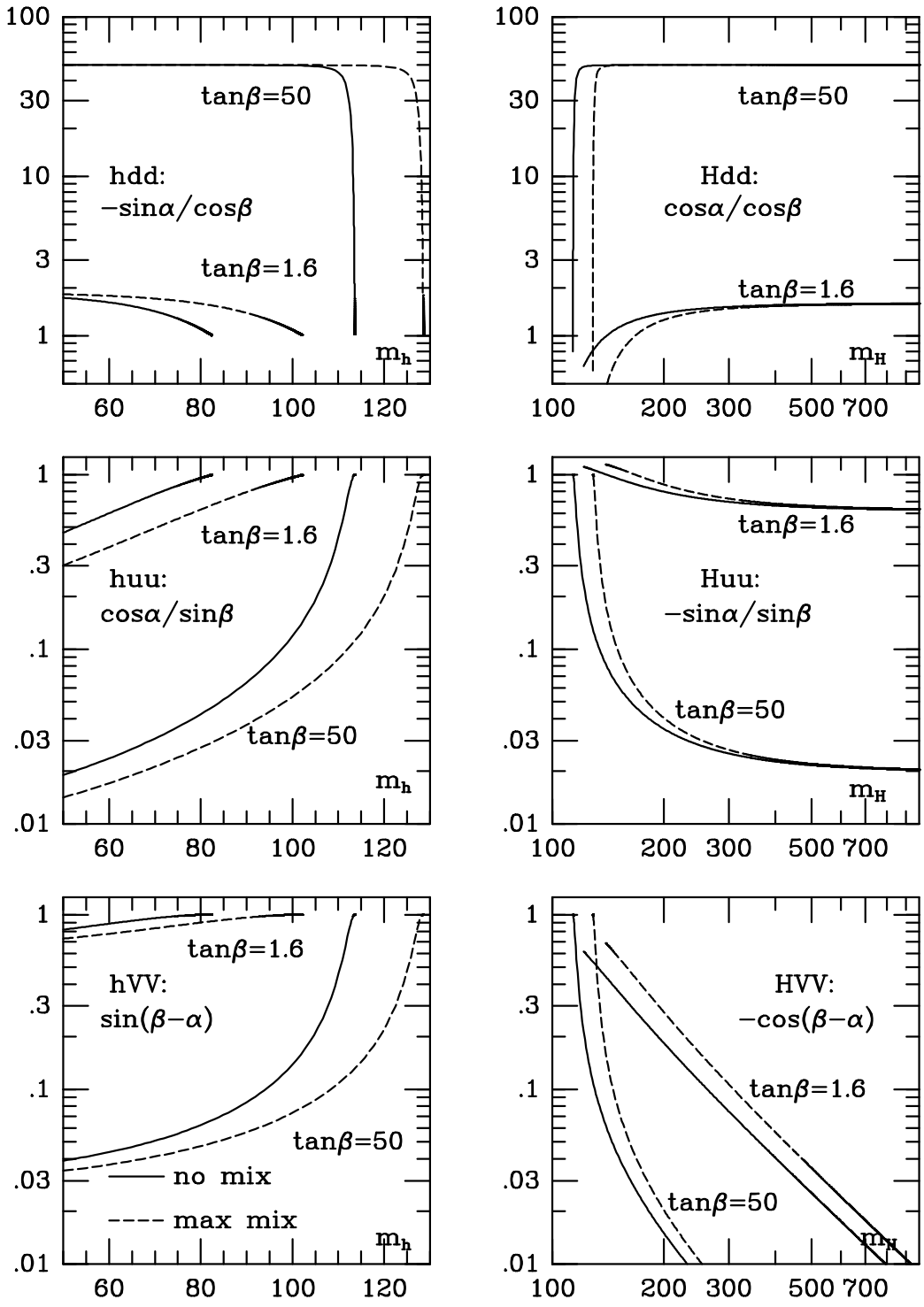

Figure 16: *MSSM Higgs couplings normalized to the SM couplings* $g^{SM}_{Hff} = [\sqrt{2}G_F]^{1/2} m_f$ *and* $g^{SM}_{HVV} = 2[\sqrt{2}G_F]^{1/2} m_V^2$.

The case of large splitting in the stop sector is particularly interesting in the light of recent measurements of $R_b \equiv \Gamma(Z \to b\bar{b})/\Gamma(Z \to \text{hadrons})$, whose discrepancy of more than 3 standard deviations with the SM prediction can be ameliorated in the presence of a light higgsino together with a light right–handed stop (see the discussion in the chapter on New Particles) [101]-[104]. The left–handed stop must instead remain reasonably heavy to avoid undesirable contributions to the W mass and the Z leptonic width. It is hence important to generalize the results previously obtained by using the renormalization group improved one-loop effective potential, to the case of general values of the left– and right–handed squark masses and mixing parameters, m_Q, m_U, m_D, A_t and A_b, respectively. In this case the contribution of higher dimensional operators to the effective potential must be properly taken into account; hence, the naive treatment in terms of quartic couplings is no longer appropriate.

In Ref.[91], a method has been developed for the neutral Higgs sector of the theory, in which each stop and sbottom particle is decoupled at its corresponding mass scale. Threshold effects, associated with the decoupling of the heavy sparticles, are frozen at the decoupling scales; they evolve, in the squared mass matrix, with the anomalous dimensions of the Higgs fields. The threshold effects achieve a complete matching of the effective potential for scales above and below the decoupling scales, and include all higher order (non–renormalizable) terms arising from the whole MSSM effective potential. The dominant leading–log contributions in the expressions of the renormalized Higgs quartic couplings involve the scale dependent contributions to the effective potential and are treated in the same way as in the RG improved approach described above. The way to proceed in evaluating the CP-even Higgs mass values and mixing angle α is explained in detail in Ref.[91]. A subroutine implementing the method is available [94]. This approach makes contact with the computation of the Higgs masses by means of the effective potential performed in Ref.[27]. Moreover, it reproduces the results of Ref.[89] for small mass splitting of the squark masses. This comparison holds up to a tiny difference coming from the inclusion of the small dependence of the one-loop radiative corrections on the weak couplings and the vacuum polarization effects. Indeed, in Ref.[91] the definition of pole Higgs masses is introduced by including the most relevant vacuum polarization effects. The gaugino corrections, which are relatively small, have been also included by incorporating (only) the one-loop leading logarithmic contributions.

3.1.3 Results

The lightest CP–even Higgs mass is a monotonically increasing function of m_A, which in the low $\tan\beta$ regime converges to its maximal value for $m_A \gtrsim 300$ GeV. In Fig.17 the upper limits on the lightest CP-even Higgs mass m_h [realized in the large m_A limit] are shown as a function of $\tan\beta$. Since the radiative corrections to the Higgs mass depend on the fourth power of the top mass, the maximal top-quark mass compatible with perturbation theory up to the GUT scale has been adopted for each value of $\tan\beta$. Apart from the natural choice of the mixing mass–parameters and the scale M_S, this result is the most general upper limit on m_h for a given value of $\tan\beta$ in the MSSM. The variation of the upper bound on m_h as a function of M_t is

shown by the solid line (a) of Fig.14. In Fig.18 the mass m_h is plotted for different values of the mixing parameters $A = A_t$ and μ. In fact, $A \simeq |\mu| \ll M_S$ yields the case of negligible squark mixing, while $A = \sqrt{6} M_S$, $|\mu| \ll M_S$ characterizes the case of large mixing [i.e. the impact of stop mixing in the radiative corrections is maximized]; $A = -\mu = M_S$ yields moderate mixing for large $\tan\beta$ while the mixing effect is close to maximal for low $\tan\beta$. In Fig.19 we show the masses of the two CP–even Higgs bosons and of the charged Higgs boson as a function of m_A for the case $A = -\mu = M_S = 1$ TeV, $M_t = 175$ GeV and different values of $\tan\beta$. The peculiar behavior of m_h and m_H for large $\tan\beta$ will be explained in the following.

In general, for very *large values of* $\tan\beta$ and values of μ, A_t and A_b of order or smaller than M_S, the mixing in the Higgs sector is negligible and the CP-even Higgs mass eigenstates are approximately given by H_1 and H_2. As a result, the properties of h and H mainly depend on the value of m_A. For $m_A^2 > 2v^2\lambda_2 \equiv m_Z^2 + \text{rad.corr.}$, one approaches the decoupling limit and the relations $\sin\alpha \simeq -\cos\beta$ and $\cos\alpha \simeq \sin\beta$ hold. Hence, the CP-even Higgs mass eigenstates are given by $h \simeq \sin\beta H_2 + \cos\beta H_1 \simeq H_2$ and $H \simeq \sin\beta H_1 - \cos\beta H_2 \simeq H_1$. In this case the lightest CP-even Higgs couples to up (down) fermions as

$$h u\bar{u} \to h_u \sin\beta \quad \text{and} \quad h d\bar{d} \to h_d \cos\beta \tag{30}$$

where $h_u \sin\beta$ ($h_d \cos\beta$) is the SM coupling h_u^{SM} (h_d^{SM}) [Observe that $h_f^{SM} = g_{Hff}^{SM}\sqrt{2}$, with $f = u, d$]. The heaviest CP-even Higgs boson, instead, couples in highly non-standard way to fermions,

$$H u\bar{u} \to h_u \cos\beta = h_u^{SM} \cot\beta \quad \text{and} \quad H d\bar{d} \to h_d \sin\beta = h_d^{SM} \tan\beta \tag{31}$$

so that the coupling to up (down) quarks is highly suppressed (enhanced) with respect to the coupling in the Standard Model. For $m_A^2 < 2v^2\lambda_2$ instead, $\sin\alpha \simeq -\sin\beta$ and $\cos\alpha \simeq \cos\beta$. Hence, the CP-even Higgs mass eigenstates are given by $h \simeq \cos\beta H_2 + \sin\beta H_1 \simeq H_1$ and $H \simeq -\sin\beta H_2 + \cos\beta H_1 \simeq -H_2$. In this case the situation is interchanged; h has the non-standard type of couplings to fermions, eq.(31), and H has the SM couplings, eq.(30).

The values of the CP-even Higgs masses depend on the size of the H_2 or H_1 component. When the Higgs is predominantly H_2, its mass is given by eq.(26) for $|\cos 2\beta| = 1$, neglecting the small bottom–quark Yukawa effects. When the Higgs is predominantly H_1, instead, its mass is given by m_A. Hence, the mass of the lightest Higgs boson is given by $m_h^2 \simeq m_A^2$ (and non-standard couplings to fermions) if $m_A^2 \leq 2v^2\lambda_2$, and it is given by eq.(26) for larger m_A, for which the couplings to fermions are SM-like. The complementary situation occurs for H and this can clearly be observed in Fig.19.

The effects of the bottom quark are only relevant in the limit of large μ parameters. For values of μ larger than M_S relevant corrections, which are dependent on the bottom mass, enter the Higgs mass formulae. This can be easily understood in the case $m_Q = m_U = m_D = M_S$, by studying the dependence of λ_2 on the supersymmetric Yukawa coupling h_b [see appendix 5.2]. For values of h_b of order of h_t, or equivalently for $\tan\beta \simeq m_t/m_b$, λ_2 depends significantly on the fourth power of the μ parameter. These radiative corrections are negative, lowering the mass of the CP-even Higgs associated with the H_2 doublet. Fig.20 shows the case of large m_A.

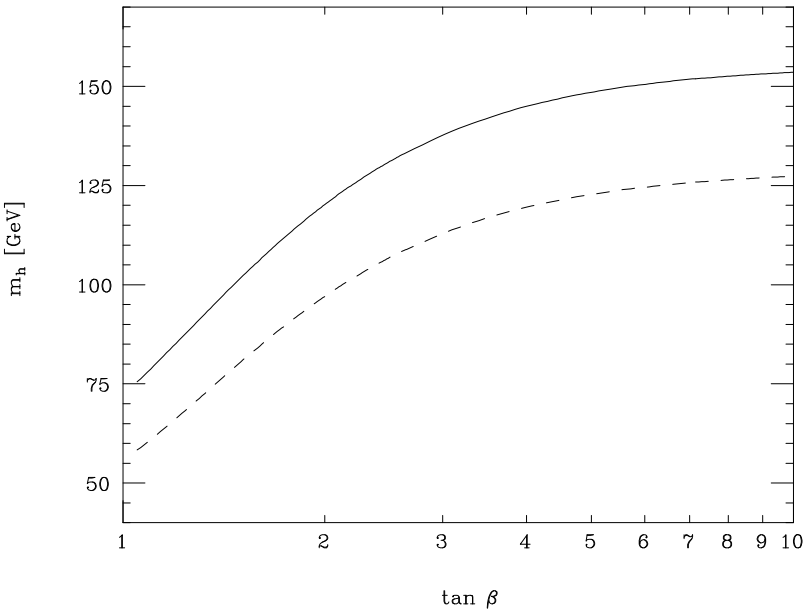

Figure 17: *Upper limit on the mass of the lightest neutral Higgs boson mass m_h as a function of* $\tan\beta$ *for zero mixing (dashed line) and for the maximal impact of mixing in the stop sector (solid line); $M_S = 1$ TeV.*

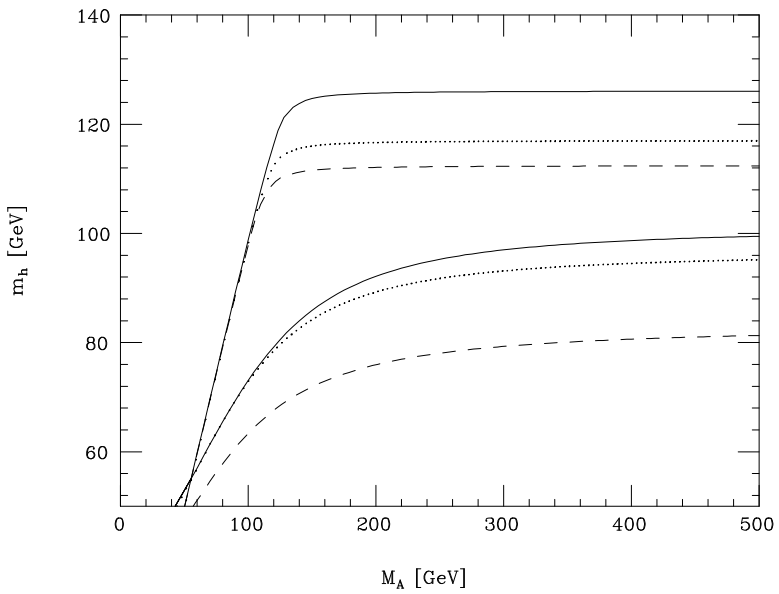

Figure 18: *Lightest neutral Higgs boson h in the MSSM as a function of m_A for zero mixing (dashed line), for intermediate mixing (dotted line) and for the maximal impact of mixing in the stop sector (solid line); for two values of* $\tan\beta = 1.6$ *(lower set), 15 (upper set): $M_S = 1$ TeV and $M_t = 175$ GeV.*

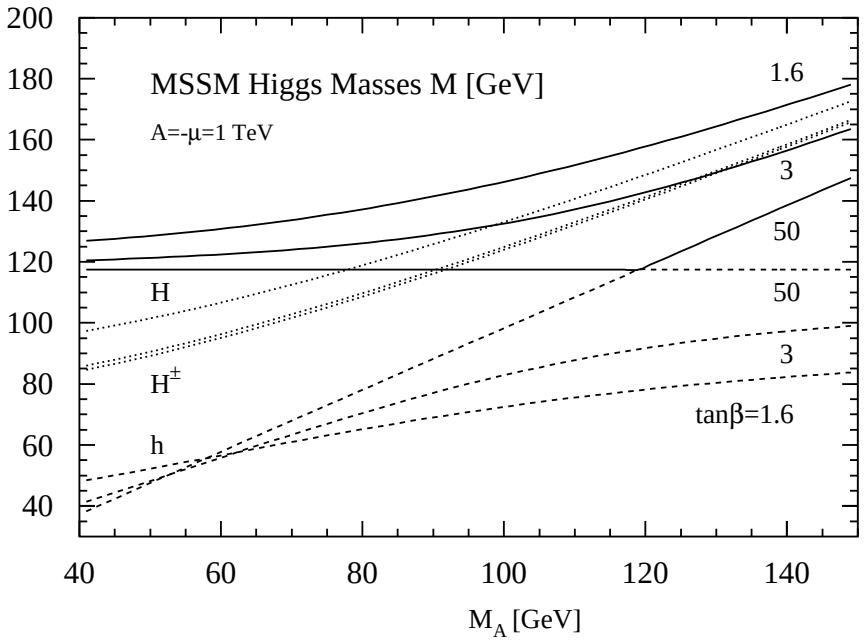

Figure 19: *Lightest CP–even Higgs boson mass (dashed line), heaviest CP–even Higgs mass (solid) and charged Higgs mass (dotted line) in the MSSM as a function of m_A for $A = -\mu = M_S = 1$ TeV, $M_t = 175$ GeV and different values of* $\tan\beta$

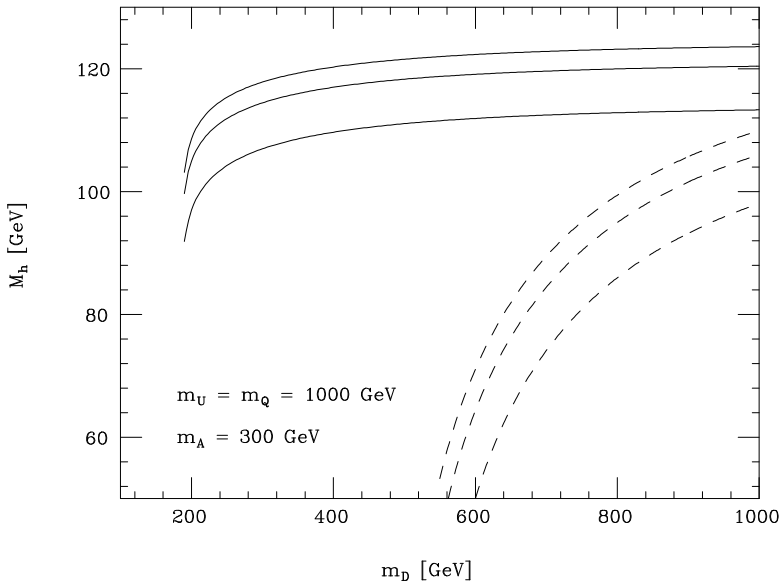

Figure 20: *Plot of the pole Higgs mass M_h as a function of m_D, for $M_t = 175$ GeV,* $\tan\beta = 60$, $A_b = 0$, $m_U = m_Q = 1$ TeV, $A_t = 0.$ *1.5, 2.4 TeV (from bottom to top) and $\mu = 1$ TeV (solid curves), $\mu = 2$ TeV (dashed curves).*

For large values of μ and small values of m_A, the charged Higgs mass also receives large negative radiative corrections, which grow as the fourth power of the μ parameter. Hence, large negative corrections to the charged Higgs mass may be obtained. Such large values of μ, however, may be in conflict with the stability of the ordinary vacuum state.

3.1.4 Additional Constraints: b-τ Unification and Infrared Fixed Point Structure

The MSSM can be derived as an effective theory in the framework of supersymmetric grand unified theories. In addition to the unification of gauge couplings, the unification of the b and τ Yukawa couplings, $h_b(M_{GUT}) = h_\tau(M_{GUT})$, appears naturally in most grand unified scenarios. Given this additional constraint, the experimental values of the b and τ masses at low energies determine the value of M_t as a function of $\tan\beta$ [18, 29, 30]. In fact, for the present experimental range of the top-quark mass $M_t = 180 \pm 12$ GeV [33], the condition of b-τ unification implies either low values of $\tan\beta$, $1 \leq \tan\beta \leq 3$, or very large values of $\tan\beta = \mathcal{O}(m_t/m_b) \simeq 50$ [18, 29]-[32]. To accommodate b-τ unification, large values of the top Yukawa coupling are necessary in order to compensate for the effects of the renormalization by strong interactions in the running of the bottom Yukawa coupling. Large values of $h_t^2(M_{GUT})/4\pi \simeq 0.1$–$1$ ensure the attraction towards the infrared (IR) fixed point solution for the top quark mass [34]. The strength of the strong gauge coupling as well as the experimentally allowed range of the bottom mass play a decisive role in this behavior [30]-[32]. In the low $\tan\beta$ case, for the presently allowed values of the electroweak parameters and of the bottom mass and for values of $\alpha_s(m_Z) \gtrsim 0.115$, b-τ unification implies that the top-quark mass must be within ten percent of its infrared fixed point values. A mild relaxation of exact unification [0.85-0.9 $\leq h_b/h_\tau|_{M_{GUT}} \leq 1.15$] still preserves this feature, especially for values of $M_b \leq 4.95$ GeV. In the large $\tan\beta$ region, h_b is $\mathcal{O}(h_t)$ and the infrared fixed point attraction, within the context of b-τ Yukawa coupling unification, is much weaker.

The top-quark mass is also predicted to be close to its infrared-fixed point value in string scenarios, in which the top-quark Yukawa coupling is determined by minimizing the effective potential with respect to moduli fields [99]. Quite generally, the fixed point solution, $h_t = h_t^{IR}$, is obtained for large values of the top Yukawa coupling at high energy scales, which however remain in the perturbative regime. Within the framework of grand unification, one obtains $(h_t^{IR})^2/4\pi \simeq (8/9)\alpha_s(m_Z)$ for $M_{GUT} \simeq 10^{16}$ GeV, and the running top-quark mass tends to its infrared fixed point value $m_t^{IR} = h_t^{IR} v \sin\beta$. Hence, relating the running top-quark mass m_t with the pole top-quark mass M_t by taking into account the appropriate QCD corrections we arrive in the low $\tan\beta$ regime at [100],

$$M_t^{IR} \simeq \sin\beta\,[1 + 2\,(\alpha_s(m_Z) - 0.12)]\left[1 + \frac{4\alpha_s(m_Z)}{3\pi} + \mathcal{O}(\alpha_s^2)\right] \times 196 \text{ GeV} \qquad (32)$$

The strong M_t–$\tan\beta$ correlation associates with each value of M_t at the infrared fixed point the lowest value of $\tan\beta$ consistent with the validity of perturbation theory up to scales of order M_{GUT}. If the physical top-quark mass is in the range 160–190 GeV, the values of $\tan\beta$

are restricted to the interval between 1 and 3. This is in agreement with the results from b-τ Yukawa unification.

The infrared fixed point solution can also be analysed in the large $\tan\beta$ case, where the effects of the bottom Yukawa coupling need to be taken into account in the RG evolution as well. For instance, if the values of the supersymmetric Yukawa couplings of the bottom and top quarks are very close to each other, $m_t(M_t) \simeq m_b(M_t)\tan\beta$, the infrared fixed point prediction for the top-quark mass is reduced by a factor $\sqrt{6/7}$ with respect to eq.(32) [98, 105]. Still, the values of M_t predicted in this regime are about 190 GeV.

After the above general discussions we shall describe their consequences for the Higgs sector:

(i) The infrared fixed point structure in the low $\tan\beta$ region have far-reaching consequences for the lightest CP-even Higgs mass in the MSSM [96]-[98]. Indeed, for $\tan\beta$ larger than one, the lowest tree–level Higgs mass is obtained at the lowest value of $\tan\beta$. Hence, in any theory consistent with perturbative unification, the fixed point solution is associated with the lowest value of the tree–level mass consistent with the theory. Even after including radiative corrections, the upper bound on the Higgs mass is considerably reduced at the fixed point solution: for a top mass of 175 GeV, the upper limit of the Higgs mass is less than 100 GeV, while for $M_t = 160$ GeV, it is even less than 80 GeV (see Fig.14). Hence, if the infrared fixed point solution for the top-quark with $M_t \lesssim 175$ GeV is realized in nature, the lightest CP-even Higgs mass must be accessible at LEP2 for $\sqrt{s} = 192$ GeV [37, 89]. Fig.14 shows also that for M_t= 175 GeV the upper bound on the lightest Higgs mass in the case of b-τ Yukawa coupling unification is nearly 25 GeV smaller than the unrestricted MSSM limit.

The present data indicate that the value of $R_b = \Gamma_b/\Gamma_h$ is more than 3σ above the SM prediction for this quantity. Large positive radiative corrections to R_b are always associated with large values of the Yukawa couplings; they are therefore maximized at the infrared fixed point solution [102, 100]. Moreover, presicion measurements also provide information about the structure of the soft supersymmetry breaking terms: Low values of the right–handed SUSY breaking stop mass m_U and of the SUSY mass parameter μ are preferred, while the left–handed stop mass parameter m_Q must be larger than m_U. For a fixed large value of m_Q, the upper bound on the Higgs mass is significantly lower in the case $m_U \ll m_Q$ than in the case $m_U \simeq m_Q$. Fig21 shows the Higgs mass as a function of m_Q for $m_U = 100$ GeV, $m_A = 300$ GeV and $\tan\beta$ consistent with the fixed point solution for $M_t = 175$ GeV, for different values of the mixing mass parameter A_t. Even for the largest value of A_t physically acceptable [i.e. $m_{\tilde{t}}$ above the experimental lower bound], the Higgs mass remains below 85 GeV. Hence, for the values of the supersymmetry breaking mass terms preferred by the precision electroweak data, associated with a light right-handed stop, lower values of m_h than naïvely expected are obtained.

Furthermore, the most general upper bounds on m_h at the infrared fixed point are valid for very large values of the mixing parameters in the squark sector [A_t, A_b and μ] which in general are hard to realize. Requiring radiative breaking of the electroweak symmetry [yet no colour breaking], and imposing the boundary conditions from experimental SUSY mass limits, the

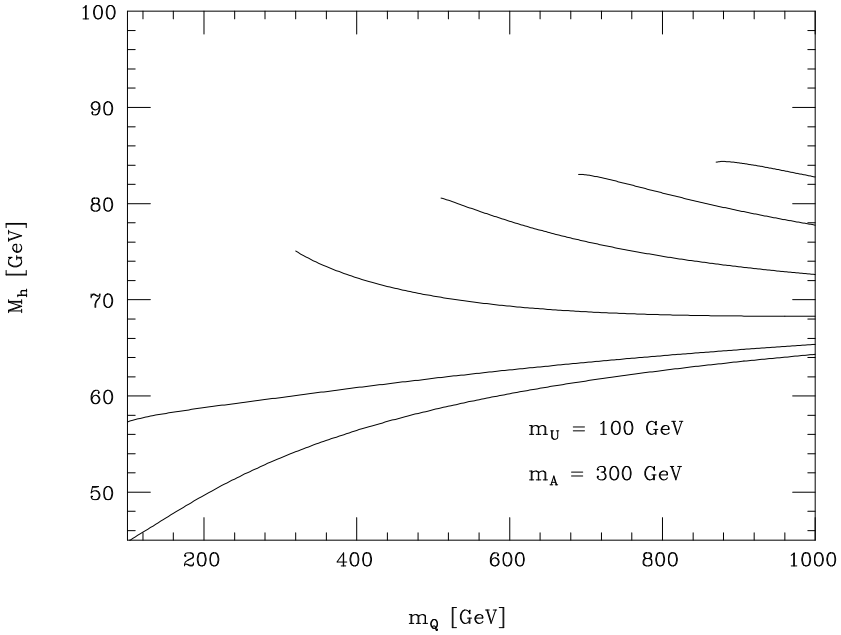

Figure 21: *Plot of the pole Higgs mass M_h as a function of m_Q, for M_t = 175 GeV,* $\tan\beta$ = *1.6, $\mu = A_b = 0$, $m_U = m_D$ = 1 TeV and m_A = 300 GeV. The lines denote different values of the A_t parameter. Starting from below at m_Q = 1 TeV, A_t = 0, 0.2, 0.4, 0.6, 0.8, 1 TeV, respectively.*

range of upper values of m_h is reduced further [100]. In the general framework of supergravity models, various analyses have been performed in the literature to study the spectrum of a constrained MSSM at different levels of refinement [106].

(ii) The condition of b-τ Yukawa coupling unification is also consistent with the values of the top-quark mass measured at the Tevatron for very large values of $\tan\beta \simeq m_t/m_b$. There are, however, large uncertainties in this sector associated with one–loop supersymmetric corrections to the bottom mass. These radiative corrections are strongly dependent on the structure of the supersymmetric spectrum and induce strong variations in the predictions for the top-quark mass and $\tan\beta$, once the unification of the b and τ Yukawa couplings is implemented. Nevertheless, the large $\tan\beta$ regime with unification of the b-τ Yukawa couplings, although more model dependent, provides an interesting framework for Higgs particle searches at LEP2.

Large positive radiative corrections to R_b can also be obtained for large values of $\tan\beta$, since the supersymmetric bottom–quark Yukawa coupling is enhanced in this regime. Indeed, the value of R_b can be significantly increased if the CP-odd Higgs mass is below 70 GeV [101]-[103]. This is a result of the large positive one-loop corrections associated with the neutral CP-odd Higgs scalar sector of the theory. Low values of the CP-odd Higgs mass, $m_A \simeq m_Z$, imply that both the lightest CP-even and the CP-odd Higgs masses would be at the reach of LEP2. The charged Higgs mass is approximately determined through the CP-odd Higgs mass value, $m^2_{H^\pm} \simeq m^2_A + m^2_W$, and hence, strong constraints on m_A are obtained from the charged Higgs contributions to BR($b \to s\gamma$). Even conservatively taking into account the QCD uncertainties

associated with the branching ratio BR($b \to s\gamma$) [i.e. assuming e.g. 40% QCD uncertainties], the $b \to s\gamma$ decay rate becomes larger than the presently allowed experimental values [107] for $m_{H^\pm} \lesssim 130$ GeV, unless the supersymmetric particle contributions suppress the charged Higgs enhancement of the decay rate. The most important supersymmetric contributions to this rare bottom decay come from the chargino-stop one-loop diagram [108]. The chargino contribution to the $b \to s\gamma$ decay amplitude depends on the soft supersymmetry breaking mass parameter A_t and on the supersymmetric mass parameter μ. For very large values of $\tan\beta$, it is given by

$$A_{\tilde{\chi}^+} \simeq \frac{m_t^2}{m_{\tilde{t}}^2} \frac{A_t \mu}{m_{\tilde{t}}^2} \tan\beta \; G\left(\frac{m_{\tilde{t}}^2}{\mu^2}\right) \tag{33}$$

where $G(x)$ is a function with values of order unity when the characteristic stop mass $m_{\tilde{t}}$ is of order μ, and it grows as μ decreases. For positive (negative) values of $A_t \times \mu$ the chargino contributions are of the same (opposite) sign as the charged–Higgs contributions. Hence, to partially cancel the light charged–Higgs contributions and render the $b \to s\gamma$ decay rate acceptable, negative values for $A_t \times \mu$ are required. This requirement has direct implications on the corrections to the bottom mass mentioned above and puts strong constraints on models with unification of the Yukawa couplings [36, 109].

3.1.5 MSSM Parameters

In the experimental simulations, we have chosen as the two basic parameters of the Higgs sector the mass m_A of the pseudoscalar Higgs boson within the limits 40 GeV $\leq m_A \leq$ 400 GeV, and the angle β within the bounds $1 \leq \tan\beta \leq m_t(M_t)/m_b(M_t) \simeq 60$. The upper limit on m_A is introduced merely for convenience, since the variation of m_h with m_A becomes negligible for values of $m_A \geq$ 200–250 GeV. The upper value of $\tan\beta$ is chosen such that the bottom Yukawa coupling remains in the perturbative regime for scales below the grand unification scale. A given value of $\tan\beta$ implies an upper limit on the top mass for which the theory can be extended perturbatively up to the GUT scale. For $\tan\beta = 1$ this upper limit is already close to 150 GeV so that lower values of $\tan\beta$ would be inconsistent with values of the top quark mass in the experimental range. In the examples we shall discuss, we have chosen:

(i) Top mass, $M_t = 175 \pm 25$ GeV;

(ii) SUSY scale, $M_S = 10^3$ GeV;

(iii) SUSY Higgs mass parameter μ and soft SUSY breaking parameter $A_t = A_b = A$:
$A = 0$ and $|\mu| \ll M_S$ [no mixing];
$A = \sqrt{6} M_S$ and $|\mu| \ll M_S$ [maximal mixing];
$A = M_S = -\mu$ ["typical" mixing].

We have taken M_S of order 1 TeV to include the effects of possibly large radiative corrections to the lightest CP-even Higgs mass. In the same way the choice of the soft SUSY breaking parameter A and of the SUSY mass parameter μ is motivated. The central top mass value is close to the central value measured at the Tevatron [33]. The upper and lower bounds are extreme, roughly corresponding to the $\pm 2\sigma$ limits of the CDF measurement. Although the central value for M_t extracted from the LEP precision measurements in the MSSM for large masses of the SUSY particles would be somewhat lower than the central value observed in the Tevatron events, the lower values are still consistent at the 2σ level.

3.2 Production and Decay Modes of MSSM Higgs Particles

3.2.1 Higgs Production

The main production mechanisms of the neutral Higgs bosons h and A in the MSSM at LEP2 energies are through the following processes [110]:

$$\begin{array}{ll} \text{Higgs–strahlung:} & e^+e^- \to Z\,h \\ \text{Associated pair production:} & e^+e^- \to A\,h \end{array} \tag{34}$$

The fusion processes, similar to the Standard Model, play only a marginal role at the kinematical limit of the Higgs-strahlung process for the production of the CP-even Higgs boson h. The CP-odd Higgs boson A cannot be produced in Higgs-strahlung and in fusion processes to leading order.

The production of the heavy CP-even Higgs particle H is very difficult at LEP energies. In the tiny corner of parameter space, for moderate to large $\tan\beta$, where associated AH production would be allowed kinematically, the production cross section is suppressed by the small coefficient $\sin^2(\beta-\alpha)$, due to the ZAH coupling discussed earlier, and the threshold P-wave factor. For $\tan\beta = 3\,(50)$, $m_A = 60$ GeV, $m_H = 123\,(117)$ GeV, it is $4\,(0.001)$ fb.

The cross sections (34) may be expressed in terms of the cross section $\sigma_{\rm SM}$ for Higgs-strahlung in the Standard Model in the following way [110, 41]:

$$\sigma(e^+e^- \to Z\,h) = \sin^2(\beta-\alpha)\,\sigma_{\rm SM} \tag{35}$$

$$\sigma(e^+e^- \to A\,h) = \cos^2(\beta-\alpha)\,\bar{\lambda}\,\sigma_{\rm SM} \tag{36}$$

The factor $\bar{\lambda} = \lambda_{Ah}^{3/2}/\{\lambda_{Zh}^{1/2}\,[12m_Z^2/s + \lambda_{Zh}]\}$ accounts for the correct suppression of the P-wave cross section near the thresholds. [$\lambda_{ij} = (1-(m_i+m_j)^2/s)(1-(m_i-m_j)^2/s)$ is the usual momentum factor of the two particle phase space.] The cross section for WW fusion of h is reduced by the same factor $\sin^2(\beta-\alpha)$ as is the cross section for Higgs–strahlung.

The cross sections for Higgs–strahlung Zh and associated pair production Ah are complementary to each other, coming either with the coefficient $\sin^2(\beta-\alpha)$ or $\cos^2(\beta-\alpha)$. The cross

sections are shown for two representative values of $\tan\beta = 1.6$ and 50 in Fig.22. The top-quark mass is varied, as usual, between 175 ± 25 GeV. Since the upper limit on m_h depends strongly on M_t for small values of $\tan\beta$ where the tree-level mass is small, the endpoints of the curves are shifted upwards significantly with increasing top mass. For large values of $\tan\beta$, on the other hand, the dependence of the upper bound of m_h on the radiative corrections is weaker for rising top mass due to the large value of m_h at the tree level. The supersymmetric coefficient $\cos^2(\beta-\alpha)$ is nearly independent of the top mass and it is very close to unity, so that the spread between the curves is negligible; the coefficient $\sin^2(\beta-\alpha)$ is correspondingly small. In this large $\tan\beta$ case, the curves terminate at the kinematical limit before $m_h^{\rm max}$ can be reached, in contrast to the small $\tan\beta$ case. For large $\tan\beta$ the non-zero widths of the particles are taken into account.

For small $\tan\beta$, Higgs–strahlung Zh provides the largest production cross section while the cross section for Ah associated pair production is much smaller. With $\sigma_{Zh} \sim \mathcal{O}(0.5$ pb) at $\sqrt{s} = 192$ GeV, this mechanism gives rise to a large sample of Higgs particles. For large $\tan\beta$, associated Ah production is the dominant mechanism with rates similar to the previous case.

The predictions for the cross sections $e^+e^- \to Zh$ and Ah presented above have been based on the improved effective potential approximation which takes into account heavy (s)quark effects on Higgs masses, mixings and couplings. It turns out *a posteriori* that this scheme is quite accurate. Indeed, the box contributions to the cross sections are fairly small [111]. This is demonstrated in Fig.23 where the box contributions are compared with the Born term, defined for the effective value $\tan 2\alpha = -(m_Z^2+m_A^2)\tan\beta/(m_Z^2+m_A^2\tan^2\beta - m_h^2/\cos^2\beta)$. The leading part of the box contributions is generated by the two-Higgs doublet diagrams while the contributions of the genuine SUSY particles are very small.

The angular distributions are of the standard form [47] for Higgs–strahlung and spin–zero pair production,

$$\frac{d\sigma}{d\cos\theta} \sim \begin{cases} \lambda \sin^2\theta + 8m_Z^2/s & \text{for } e^+e^- \to Zh \\ \sin^2\theta & \text{for } e^+e^- \to Ah \end{cases} \tag{37}$$

Since the main decay mode of scalar and pseudoscalar Higgs particles are $b\bar{b}$ decays in the MSSM, it is interesting to study the 4–fermion process $e^+e^- \to b\bar{b}b\bar{b}$ in greater detail. The final state includes the signal $Zh \to (b\bar{b})_Z(b\bar{b})_h$ in the Higgs–strahlung process, and the signal $Ah \to (b\bar{b})_A(b\bar{b})_h$ for associated pair production. The main component of the background is $e^+e^- \to Z^*Z^*$ production followed by $Z^* \to b\bar{b}$ decays. These cross sections have been evaluated for a cut on the invariant $b\bar{b}$ mass of $m(b\bar{b}) > 20$ GeV. The results are shown for a variety of combinations $(m_A, \tan\beta)$ in Table 14 for $\sqrt{s} = 192$ GeV.

The cross section for the production of charged Higgs bosons

$$e^+e^- \to H^+H^- \tag{38}$$

is built up by s-channel γ and Z exchanges [41, 112]. It depends only on the charged Higgs

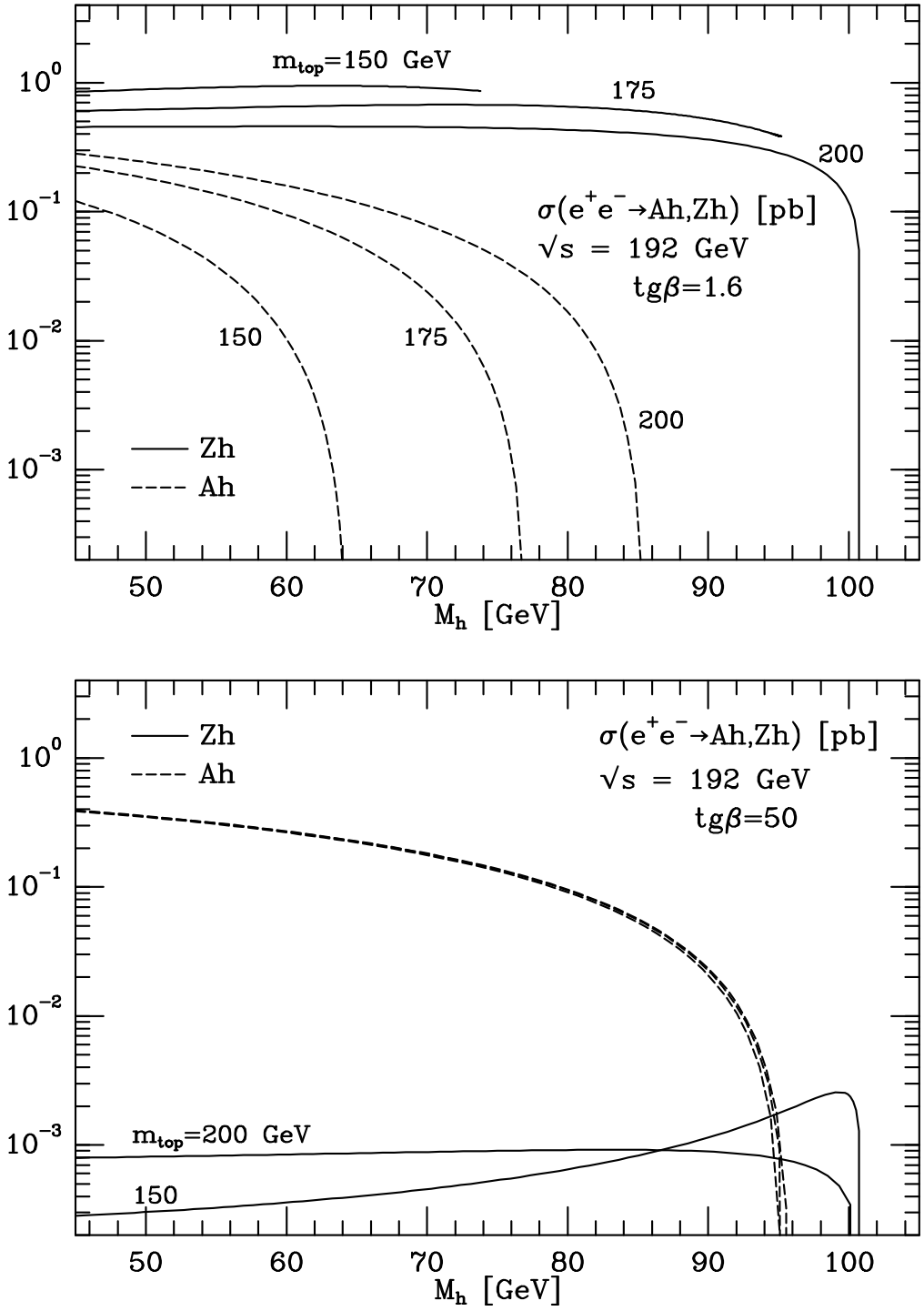

Figure 22: *The cross sections for Higgs-strahlung Zh and associated pair production Ah in the MSSM for two values of* $\tan\beta = 1.6$ *and* 50 *and the top mass* $M_t = 175 \pm 25$ *GeV.*

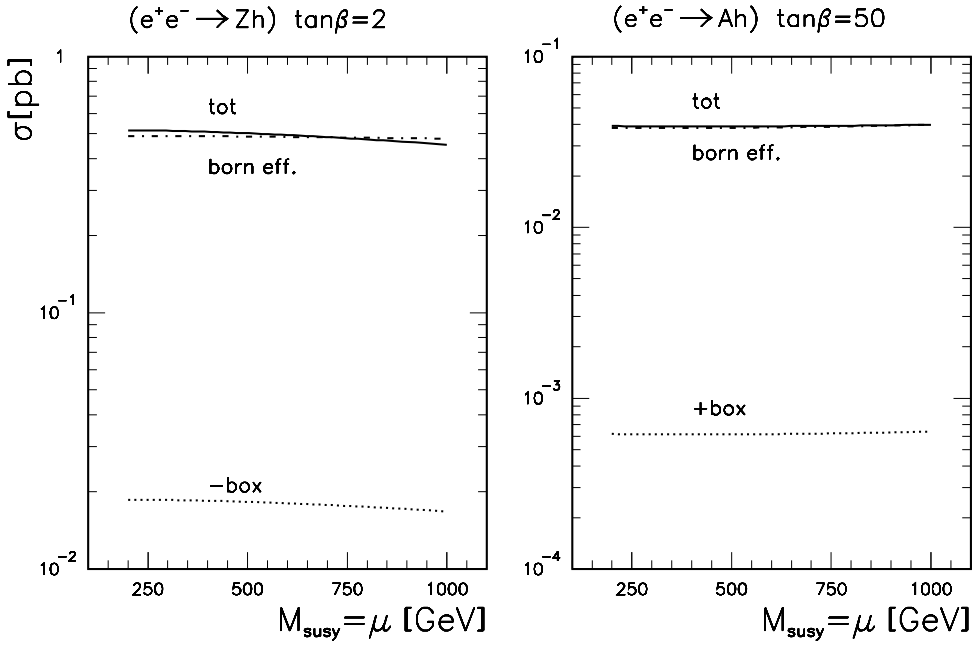

Figure 23: *The box contributions to the cross sections for Higgs-strahlung Zh and associated pair production Ah for $\sqrt{s} = 192$ GeV; $m_A = 90$ GeV and a slepton mass $m_{\tilde{\ell}} = 100$ GeV.*

mass and no extra parameter,

$$\sigma(e^+e^- \to H^+H^-) = \frac{2G_F^2 m_W^4 s_W^4}{3\pi s}\left[1 + \frac{2\hat{v}_e\hat{v}_H}{1-m_Z^2/s} + \frac{(\hat{a}_e^2+\hat{v}_e^2)\,\hat{v}_H^2}{(1-m_Z^2/s)^2}\right]\beta_H^3 \qquad (39)$$

where the rescaled Z charges are defined by $\hat{a}_e = -1/4c_W s_W$ and $\hat{v}_e = (-1+4s_W^2)/4c_W s_W$ and $\hat{v}_H = (-1+2s_W^2)/2c_W s_W$ [note that $s_W^2 = \sin^2\theta_W$]; $\beta_H = (1-4m_{H^\pm}^2/s)^{1/2}$ is the velocity of the Higgs particles. The cross section is shown in Fig.24 as a function of the charged Higgs mass for the three representative LEP2 energy values $\sqrt{s} = 175$, 192 and 205 GeV. Within the MSSM the present lower limit of the charged Higgs boson mass is about 85 GeV so that only a small window is left for LEP2. Even though the cross section is not particularly small for

Table 14: *The process $e^+e^- \to b\bar{b}b\bar{b}$ at $\sqrt{s} = 192$ GeV. Cross sections in fb.*

	$(m_A$ [GeV], $\tan\beta)$	(75,30)	(400,30)	(75,1.75)	(400,1.75)	∞
no	EXCALIBUR	—	—	—	—	25.933(10)
ISR	HZHA/PYTHIA	135.17(61)	23.286(58)	163.36(75)	74.04(31)	22.816(50)
with	EXCALIBUR	—	—	—	—	23.045(23)
ISR	HZHA/PYTHIA	118.60(58)	18.761(87)	151.75(75)	57.74(28)	18.384(80)

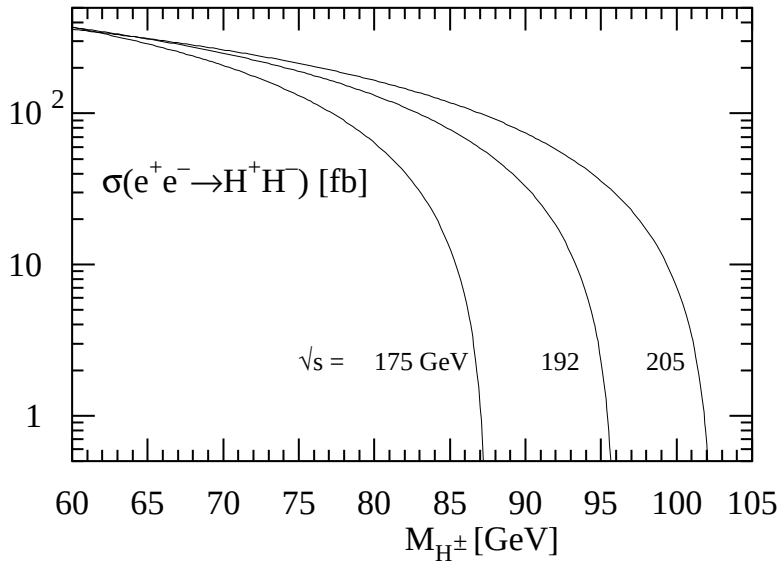

Figure 24: *The cross section for charged Higgs boson production.*

$m_{H^\pm} \sim 80$ to 90 GeV, the signal is very hard to extract from the overwhelming background of WW pair production in this mass range. The analysis of cascade decays $H^\pm \to W^* h, W^* A$ [95] can ameliorate the prospects of detecting the charged Higgs boson in this mass range for small $\tan\beta$.

3.2.2 Decay Modes of the MSSM Higgs Particles

Decays to SM particles. For $\tan\beta > 1$ the lightest CP-even neutral Higgs boson h decays almost exclusively to fermion pairs if the mass m_h is less than 100 GeV. Near the upper limit of m_h for a given $\tan\beta$, i.e. in the decoupling region, the decay pattern becomes SM–like. Fermion pairs are also the dominant decay mode of the pseudoscalar Higgs boson A. The partial decay widths of all the neutral Higgs bosons Φ into fermions are given by

$$\Gamma(\Phi \to f\bar{f}) = N_c \frac{G_F m_f^2}{4\sqrt{2}\pi} g^2_{\Phi ff} m_\Phi \left[1 + \frac{17}{3}\frac{\alpha_s}{\pi}\right] \tag{40}$$

in the limit $m_\Phi^2 \gg m_f^2$. The couplings $g_{\Phi ff}$ have been defined in Table 13. The small additional $\mathcal{O}(\alpha_s^2)$ contributions have been summarized in Ref.[12]. As anticipated from chirality arguments, the widths, including the QCD radiative corrections, do not depend on the parity of the state apart from the overall coupling $g_{\Phi ff}$ in the limit of large Higgs masses. For quark decays, m_f has to be chosen as the running quark mass evaluated at the scale m_Φ. The electroweak corrections are incorporated at a sufficient level of accuracy by adopting the effective potential approximation for the couplings [113].

The partial width for charged Higgs decays to quark pairs is obtained from

$$\Gamma(H^\pm \to U\bar{D}) = \frac{3G_F m_{H^\pm}}{4\sqrt{2}\pi} |V_{UD}|^2 \left[\cot^2\beta\, m_U^2 + \tan^2\beta\, m_D^2\right]\left[1 + \frac{17}{3}\frac{\alpha_s}{\pi}\right] \tag{41}$$

This formula is valid if either the first or the second term is dominant. The up and down quark masses $m_{U,D}$ are defined again at the mass scale of the charged Higgs boson.

Since the b quark couplings to the Higgs bosons are in general strongly enhanced and the t quark couplings suppressed in the MSSM [cf. Fig.16], b loops may contribute significantly to the gg coupling so that the approximation $m_Q^2 \gg m_\Phi^2$ cannot be applied any more in general. Nevertheless, it turns out *a posteriori* that this remains an excellent approximation for the QCD corrections. The CP-even and CP-odd Higgs decays to gluons and light quarks [12] are given by the expressions

$$\Gamma(\Phi \to gg(g), q\bar{q}g) = \frac{G_F \alpha_s^2 m_\Phi^3}{16\sqrt{2}\pi^3}\Big|\sum_{t,b} A_Q^\Phi\Big|^2 \left\{1 + \left[\frac{95}{4}\left(\frac{97}{4}\right) - \frac{7}{6}N_F\right]\frac{\alpha_s}{\pi}\right\} \tag{42}$$

where the parentheses refer to the pseudoscalar particle. The form factors are defined by

$$A_Q^{h,A} = g_Q^{h,A} \times \tau\,[1 + (1-\tau)\,f(\tau)] \quad \text{and} \quad A_Q^A = g_Q^A \tau f(\tau) \tag{43}$$

with $f(\tau) = \arcsin^2(1/\sqrt{\tau})$ for $\tau \geq 1$ and $-\frac{1}{4}[\log(1+\sqrt{1-\tau})/(1-\sqrt{1-\tau}) - i\pi]^2$ for $\tau < 1$. The parameter $\tau = 4m_Q^2/m_\Phi^2$ is defined by the pole mass of the heavy loop quark Q. In the same way as $\alpha_s(m_\Phi)$, the coefficient of the QCD corrections must be evaluated for $N_F = 3$ if gluons and only light quarks are considered in the final state [cf. the SM section for details].

At the edge of the mass range accessible at LEP2, the CP-even Higgs boson h can decay into virtual gauge boson pairs W^*W/Z^*Z. The widths are the same as in the Standard Model, yet suppressed by the MSSM coefficient $\sin^2(\beta-\alpha)$.

(ii) Cascade decays. A variety of cascade decays could in principle play a role in some ranges of the MSSM parameter space accessible at LEP2, if sufficiently large samples of heavy Higgs bosons were generated. However, for the typical set of parameters discussed in this report, these decay modes are not very important in general and details may be traced back from [95, 114]. The only exception are the cascade decays of the charged Higgs bosons [95] for small to moderate $\tan\beta$,

$$\Gamma(H^+ \to hW^{+*} \to hf\bar{f}') = \frac{9G_F^2 m_W^4}{8\pi^3}\cos^2(\beta-\alpha)\, m_{H^\pm} G_{hW} \tag{44}$$

$$\Gamma(H^+ \to AW^{+*} \to Af\bar{f}') = \frac{9G_F^2 m_W^4}{8\pi^3} m_{H^\pm} G_{AW} \tag{45}$$

The coefficients G depend on the mass ratios of the particles involved,

$$\begin{aligned} G_{ij} = \frac{1}{4}\Bigg\{ & 2(-1+\kappa_j-\kappa_i)\sqrt{\lambda_{ij}}\left[\frac{\pi}{2} + \arctan\left(\frac{\kappa_j(1-\kappa_j+\kappa_i)-\lambda_{ij}}{(1-\kappa_i)\sqrt{\lambda_{ij}}}\right)\right] \\ & + (\lambda_{ij}-2\kappa_i)\log(\kappa_i) + \frac{1}{3}(1-\kappa_i)\left[5(1+\kappa_i) - 4\kappa_j - \frac{2}{\kappa_j}\lambda_{ij}\right]\Bigg\} \end{aligned} \tag{46}$$

with $\kappa_i = m_i^2/m_{H^\pm}^2$ and $\lambda_{ij} = -1 + 2\kappa_i + 2\kappa_j - (\kappa_i - \kappa_j)^2$. These decay modes are important for sufficiently light h/A Higgs bosons. If they are allowed, in particular $H^\pm \to AW^*$, they reduce the $\tau\nu_\tau$ branching ratio considerably, and they overrule cs decays as the second most important decay channel of the charged Higgs bosons.

Summary of the branching ratios. The branching ratios for the standard quark/lepton/gauge boson and the cascade decay modes discussed above, are shown for "typical mixing" and two representative values $\tan\beta = 1.6$ and 50 in Fig.25. Unless otherwise specified the top mass in Fig.25 has been fixed to $M_t = 176$ GeV. Increasing the top mass shifts the upper end of the b and τ curves upwards while the cc and gg curves are transferred nearly parallel, a consequence of the larger Higgs mass values. The effect of varying $\alpha_s = 0.118 \pm 0.006$ is indicated by the hatched bands. The curves labeled bb and cc correspond to all mechanisms generating inclusive b, c quarks in the final states, while the curve labeled gg includes gluons and light quarks. At $\tan\beta = 1.6$, interesting cascade decays are predicted for moderately small charged Higgs masses, $H^\pm \to AW^*$ and hW^*; they affect the experimental search techniques also in the $\tau\nu_\tau$ channel by reducing this important decay branching ratio. For large $\tan\beta$, $b\bar{b}$ and $\tau^+\tau^-$ decays are overwhelming except in the decoupling regime near the upper limit of the h mass.

Predictions for decays of the heavy CP–even Higgs boson H are discussed in great detail in Ref.[12].

Neutralino decays. For h, A Higgs masses up to ~ 120 GeV, there are still windows open for decays into pairs of light neutralinos [41, 115]. These windows have been left by LEP1 and they cannot be closed by LEP1.5 either. The decay channels of interest are

$$h,\, A \to \chi_1^0\chi_1^0 \tag{47}$$

for small to moderate $\tan\beta$.

Masses and couplings of the states χ_i depend on $\tan\beta$, the SU_2 gaugino mass parameter M_2, and the Higgs mass parameter μ. [We assume the relation $M_1 = \frac{5}{3}\tan^2\theta_W M_2 \simeq \frac{1}{2}M_2$.] For large M_2 and small (positive) μ values, the lightest neutralino χ_1^0 is predominantly built up by the higgsino component while for large values of μ the light χ_1^0 state is predominantly gaugino-like. The couplings of χ_1^0 to h and A are given in terms of the neutralino mixing matrix Z by

$$\begin{aligned} \kappa_h &= (Z_{12} - \tan\theta_W Z_{11})(\sin\alpha\, Z_{13} + \cos\alpha\, Z_{14}) \\ \kappa_A &= (Z_{12} - \tan\theta_W Z_{11})(-\sin\beta\, Z_{13} + \cos\beta\, Z_{14}) \end{aligned}$$

[see e.g. [116]]. Since Z_{11}/Z_{12} correspond to the gaugino components of χ_1^0 while Z_{13}/Z_{14} correspond to the higgsino components, the couplings $h\chi_1^0\chi_1^0$ and $A\chi_1^0\chi_1^0$ can only be non-negligible if the state χ_1^0 incorporates both components at a significant level. Moderate values of M_2, μ are therefore the favorable domain for LSP decays. The widths for the h, A decays into $\chi_1^0\chi_1^0$ pairs can be written as

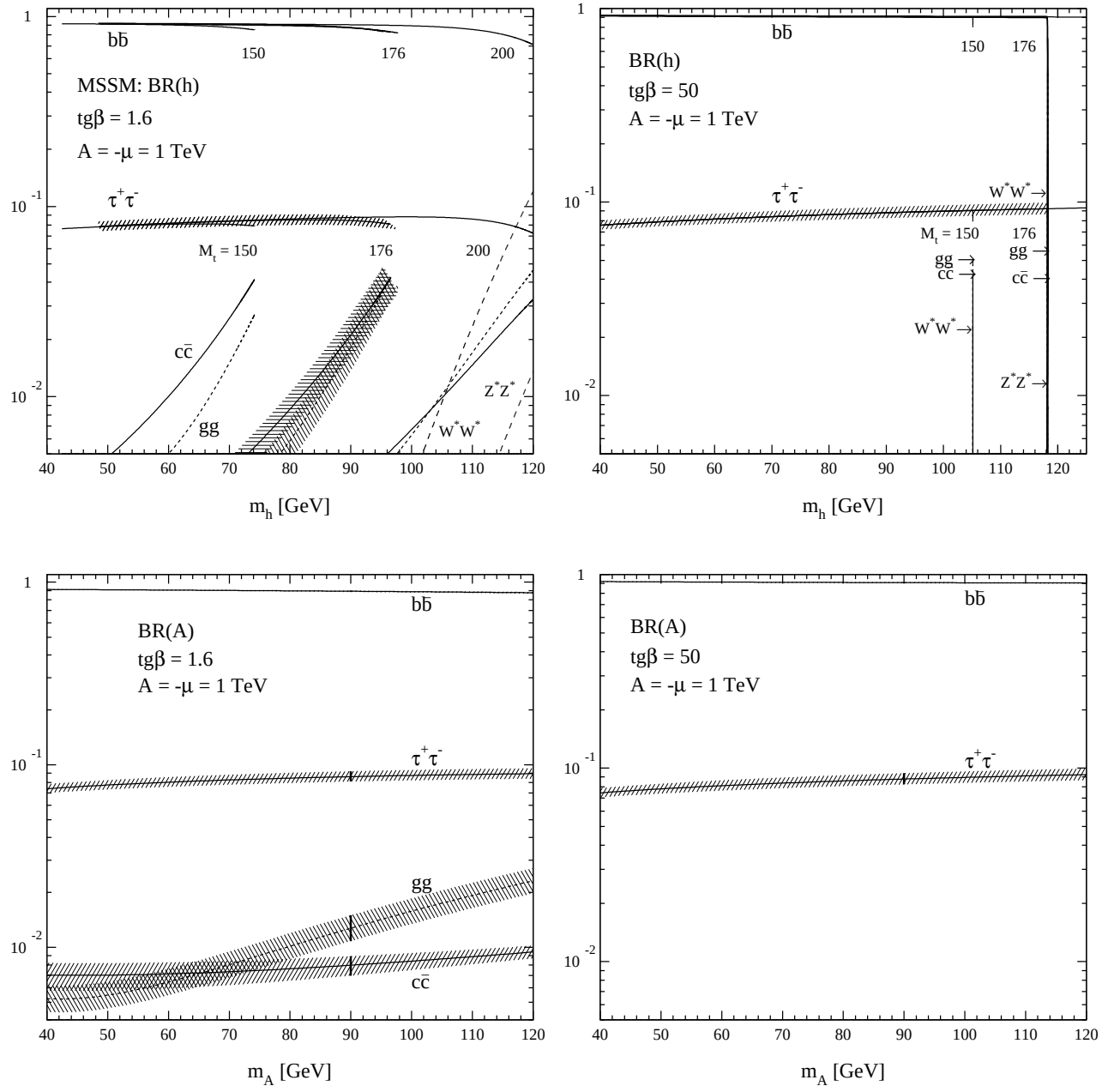

Figure 25: *Decay branching ratios of the MSSM Higgs bosons $h, A, H^{\pm}$ into SM particles and cascade decays. The bands characterize the uncertainties in the predictions, except those due to the top mass, which are indicated by bars.*

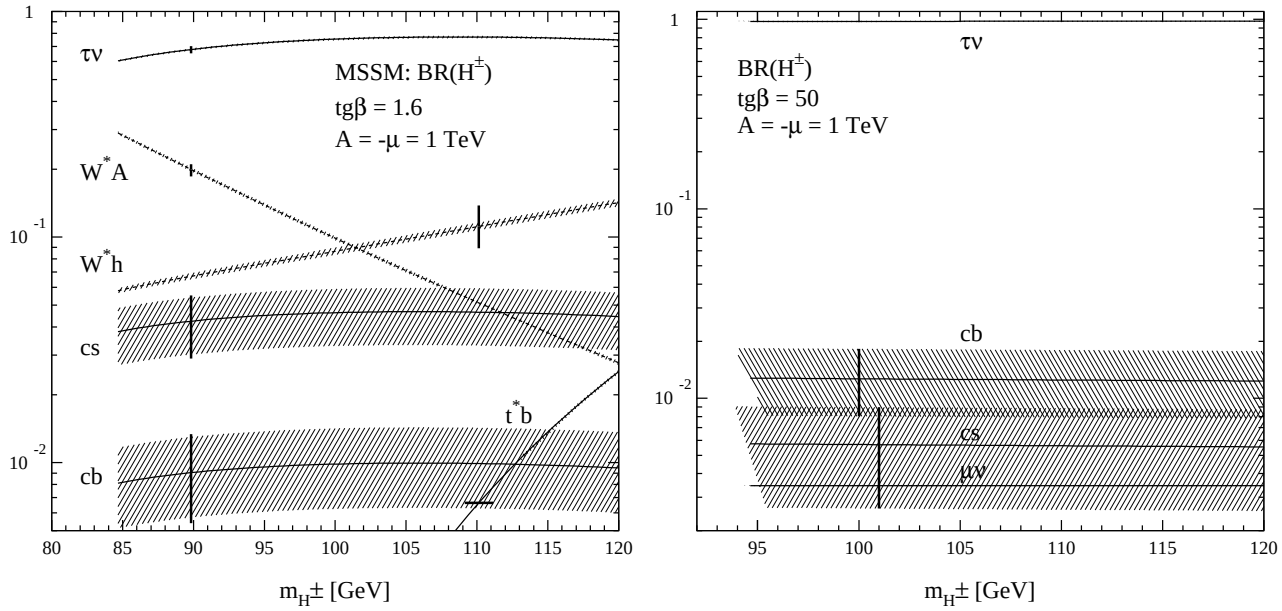

Figure 25: *(cont'd).*

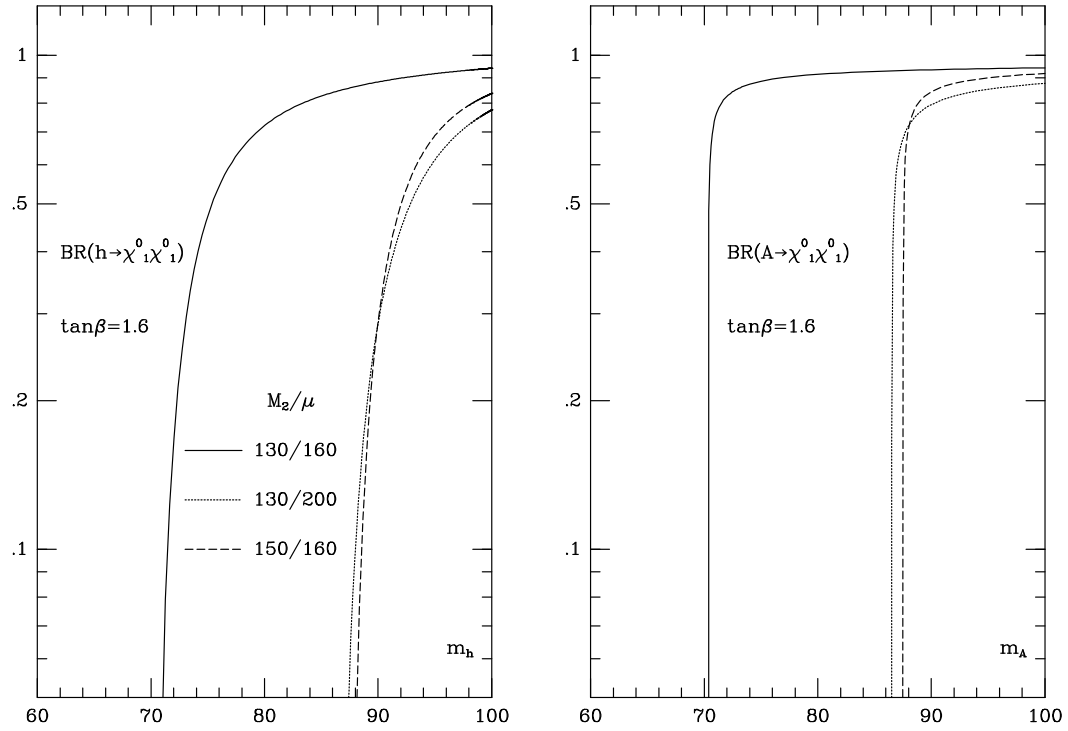

Figure 26: *Branching ratios for h, A decays into pairs of the lightest neutralino for a set of SU_2 gaugino and higgsino mass parameters not excluded by LEP1/1.5. If χ_1^0 is the LSP and if R parity is unbroken, these decays lead to invisible final states.*

$$\Gamma(h \to \chi_1^0 \chi_1^0) = \frac{G_F m_W^2}{2\sqrt{2}\pi} \kappa_h^2 m_h \beta_\chi^3 \quad (48)$$

$$\Gamma(A \to \chi_1^0 \chi_1^0) = \frac{G_F m_W^2}{2\sqrt{2}\pi} \kappa_A^2 m_A \beta_\chi \quad (49)$$

These decays of the Higgs particles are invisible if χ_1^0 is stable. The Higgs particle h can still be observed in the Higgs-strahlung process through the recoiling Z at small to moderate $\tan\beta$ where this production channel is dominant. However, the pseudoscalar Higgs boson A cannot be detected if, produced in associated Ah production, both particles decay into invisible $\chi_1^0\chi_1^0$ channels for small to moderate values of $\tan\beta$.

Since for large $\tan\beta$ the $b\bar{b}$ decays of the h and A Higgs bosons are overwhelming, $\tan\beta$ needs to be small to moderate for χ_1^0 decays to be relevant. Typical examples of large branching ratios for h, A Higgs decays to LSP pairs are shown in Fig.26 for a set of SU_2 gaugino and higgsino mass parameters M_2 and μ. The LSP masses can be read off the threshold values. The branching ratios are large whenever the LSP decay channels are open for $\mu > 0$. For $\mu < 0$ the LSP decays play a less prominent role; only in a small window close to $\mu \sim -M_2/2$ are the couplings large enough to allow for invisible h and A decays [115].

3.3 The Experimental Search for the Neutral Higgs Bosons

3.3.1 Searches in the Higgs-strahlung Process

For the $e^+e^- \to hZ$ process, as well as for $e^+e^- \to HZ$ when kinematically allowed, all the analyses [58] developed for the standard model Higgs boson and presented in Section 2.3 can be used with no modifications and with a similar efficiency, provided that the Higgs boson decays into supersymmetric particles, such as charginos and neutralinos, are not open. As soon as the decay into a pair of LSPs (Lightest Supersymmetric Particle) $h \to \chi\chi$ is allowed, it may even become dominant therefore rendering the existing analyses ineffective.

Two new selection algorithms were developed by ALEPH to take care of this particular situation where the Higgs boson would decay invisibly, for the following events topologies:

(i) the acoplanar lepton pair topology, $(Z \to e^+e^-, \mu^+\mu^-)$ $(h \to \chi\chi)$;

(ii) the acoplanar jet topology, $(Z \to q\bar{q})$ $(h \to \chi\chi)$.

Only minor modifications to the selection procedure would be needed to extend the validity of these analyses to "almost invisible" Higgs boson decays, such as $h \to \chi'\chi$ or $\chi^+\chi^-$ when the mass difference between the LSP and the next-to-LSP is small.

a) Search in the Acoplanar Lepton Pair Topology

The acoplanar lepton pair topology arises when the Z decays into a pair of leptons and the Higgs boson h decays invisibly into a pair of neutralinos. Events can be selected by requiring a high mass e^+e^- or $\mu^+\mu^-$ pair, compatible with the Z hypothesis and with large missing energy and missing mass. Events from $e^+e^- \to \ell^+\ell^-(\gamma)$, Ze^+e^- or $\gamma\gamma \to \ell^+\ell^-$ are characterized by a large missing momentum along the beam direction and a small acoplanarity angle, and can therefore easily be rejected. The only irreducible background sources are $e^+e^- \to WW \to e\nu e\nu, \mu\nu\mu\nu$, $e^+e^- \to ZZ \to e^+e^-\nu\bar{\nu}, \mu^+\mu^-\nu\bar{\nu}$, and to a lesser extent $e^+e^- \to Z\nu\bar{\nu}$.

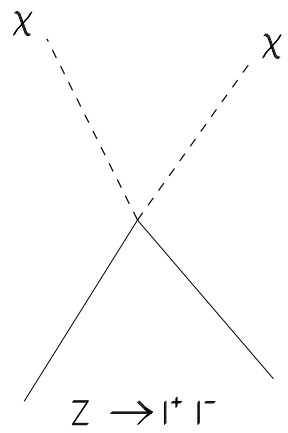

An efficiency of 45 to 50% was achieved independently of m_h. The lepton momenta were subsequently fitted to the Z mass hypothesis, and the missing mass calculated from the energy-momentum conservation as recoiling against the lepton pair, with a typical resolution of 2 GeV/c^2. Shown in Fig.27 are the mass distributions obtained with 500 pb^{-1} at 175 and 192 GeV, for several Higgs boson masses. At 192 GeV, and for $m_h = 90$ GeV/c^2, the numbers of signal and background events expected in a window of $\pm 2\sigma$ around the reconstructed Higgs

boson mass are 6.2 and 6.1 respectively, assuming a 100% branching fraction into invisible final states.

b) Search in the Acoplanar Jet Topology

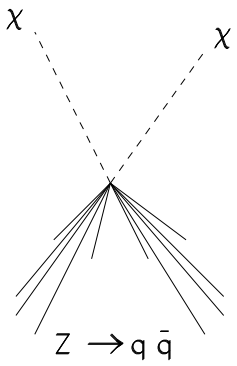

In order to add to the numbers of signal events expected from the acoplanar lepton pair topology, the hadronic decays of the Z were also investigated. A very similar selection procedure as in Section 3.3.1a) was developed, in which the two hadronic jets played the role of the leptons. A similar selection efficiency was achieved, but with a much higher background from $e^+e^- \rightarrow WW$ and $(e)\nu W$ in particular, due to the much worse jet-jet invariant mass resolution. A b-tagging requirement may or may not be applied to reduce the background (at the expense of a 80% loss of efficiency), with almost no consequences on the minimum luminosity needed for the discovery or the exclusion.

Shown in Fig.28 are the mass distributions obtained in the same configurations as in Fig.27, when a tight b-tagging criterion is applied. At 192 GeV, and for $m_h = 90$ GeV/c^2, the numbers of signal and background events expected are 7.7 and 4.9 respectively, assuming a 100% branching fraction into invisible final states.

3.3.2 Search in Associated Pair-production $e^+e^- \rightarrow Ah$

The $e^+e^- \rightarrow hA$ associated production leads to two main final states, $b\bar{b}b\bar{b}$ in 83% of the cases and $\tau^+\tau^- q\bar{q}$ in 16% of the cases, if supersymmetric decays are absent.

a) The $b\bar{b}b\bar{b}$ Topology

This four-jet final state is similar to the four-jet topology arising from the Higgs-strahlung process, and a similar selection procedure can therefore be applied. Here, the Z mass constraint cannot be used, and the requirement of incompatibility with a WW final state must be removed to retain a sizeable efficiency for the case $m_h = m_A \sim 80$ GeV/c^2. However, since the b-quark content is much higher in this four-b-jet topology than in the Higgs-strahlung process, a much tighter b-tagging criterion can be applied. In terms of background rejection, this may even over-compensate the removal of the two previous requirements while keeping a high efficiency, varying between 10 and 35%.

The four-jet energies and directions can then be fitted to satisfy the total energy-momentum conservation constraint in order to achieve a good mass resolution. Shown in Fig.29a are the distributions of the sum of the fitted m_h and m_A values as obtained in the ALEPH detector with an integrated luminosity of 500 pb^{-1} at 175 GeV, for $\tan\beta = 10$ and $m_A = 65$ and 75 GeV/c^2.

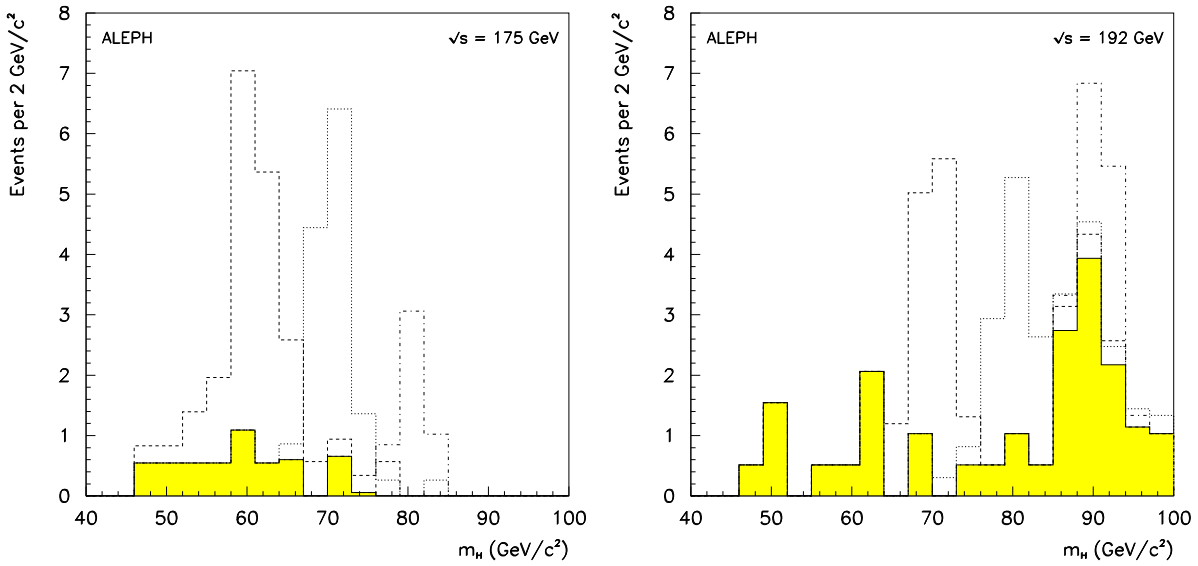

Figure 27: *Distribution of the missing mass recoiling against the e^+e^- or $\mu^+\mu^-$ pair, in the acoplanar lepton pair topology, as obtained from the ALEPH simulation at 175 GeV (left) and 192 GeV (right), with an integrated luminosity of 500 pb^{-1}. The signal (in white) is shown on top of the background (shaded histogram), with Higgs boson masses of 60 (dashed), 70 (dotted) and 80 (dash-dotted) GeV/c^2 at 175 GeV, and 70 (dashed), 80 (dotted) and 90 (dash-dotted) GeV/c^2 at 192 GeV.*

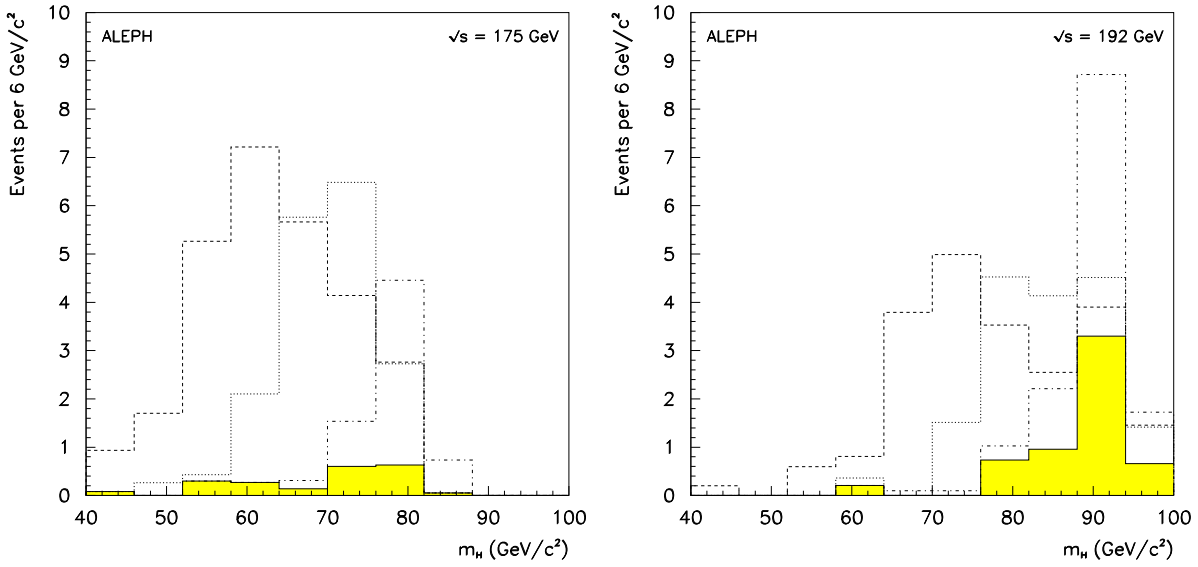

Figure 28: *Same as in Fig.27, for the acoplanar jet topology, after a tight b-tagging (optional) requirement is applied.*

The same distributions as seen by OPAL are shown in Fig.29b with 500 pb^{-1} taken at 192 GeV, for $m_{\mathrm{h}} = m_{\mathrm{A}} = 70$ GeV/c^2. Since for large $\tan\beta$ values the h and A masses are expected to be close to each other, the mass resolution is expected to improve by imposing this mass equality in the fit procedure. This was done by DELPHI for $m_{\mathrm{h}} = m_{\mathrm{A}} = 79$ GeV/c^2 at 192 GeV, and the result is shown in Fig.30a for an integrated luminosity of 300 pb^{-1}. Finally, the distribution of m_{h} *vs* m_{A} that would be obtained in L3 in the mass configuration (60 GeV/c^2, 80 GeV/c^2) if the signal cross-section amounted to 0.5 pb is shown in Fig.30b at 190 GeV, for an integrated luminosity of 1 fb^{-1}.

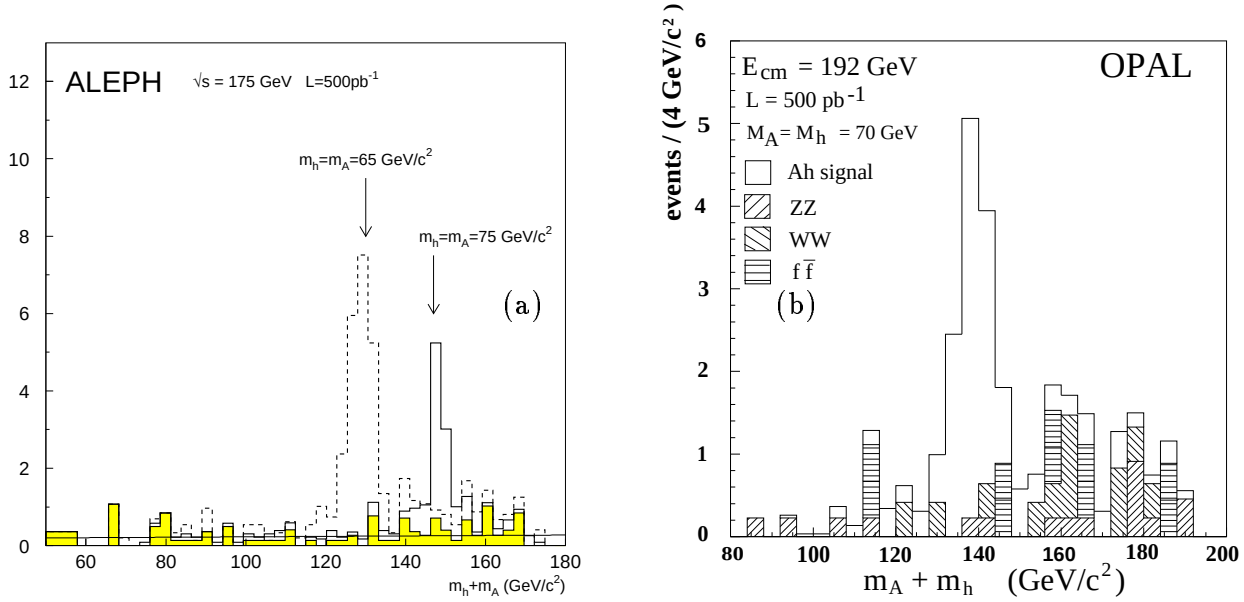

Figure 29: *Mass distributions obtained in the hA* $\rightarrow b\bar{b}b\bar{b}$ *topology. (a)* $m_{\mathrm{h}} + m_{\mathrm{A}}$ *from ALEPH (175 GeV, 500* pb^{-1}*); and (b)* $m_{\mathrm{h}} + m_{\mathrm{A}}$ *from OPAL (192 GeV, 500* pb^{-1}*).*

b) The $\tau^+\tau^-\mathrm{b}\bar{\mathrm{b}}$ Topology

For this topology, the same analysis as for the Higgs-strahlung process was used by ALEPH and DELPHI (with the exception that the very last fit intended to improve the $\tau^+\tau^-$ and hadronic mass resolution with the m_{Z} constraint does not apply). The background level is already very low, except when m_{h} and m_{A} are close to m_{Z} in which case the ZZ background can be reduced by tagging b-quarks. In this configuration, however, the signal is expected to have a very low cross-section except at the highest possible center-of-mass energy, $\sqrt{s} = 205$ GeV. Altogether, when added to the preceding one, this analysis increases the selection efficiency of the hA channel by about 20%.

c) The Case h or A $\rightarrow \chi\chi$

If either h or A decays predominantly into $\chi\chi$, the relevant topology becomes that of an acoplanar jet pair, as already described in Section 3.3.1b). However, the pair of jets is actually

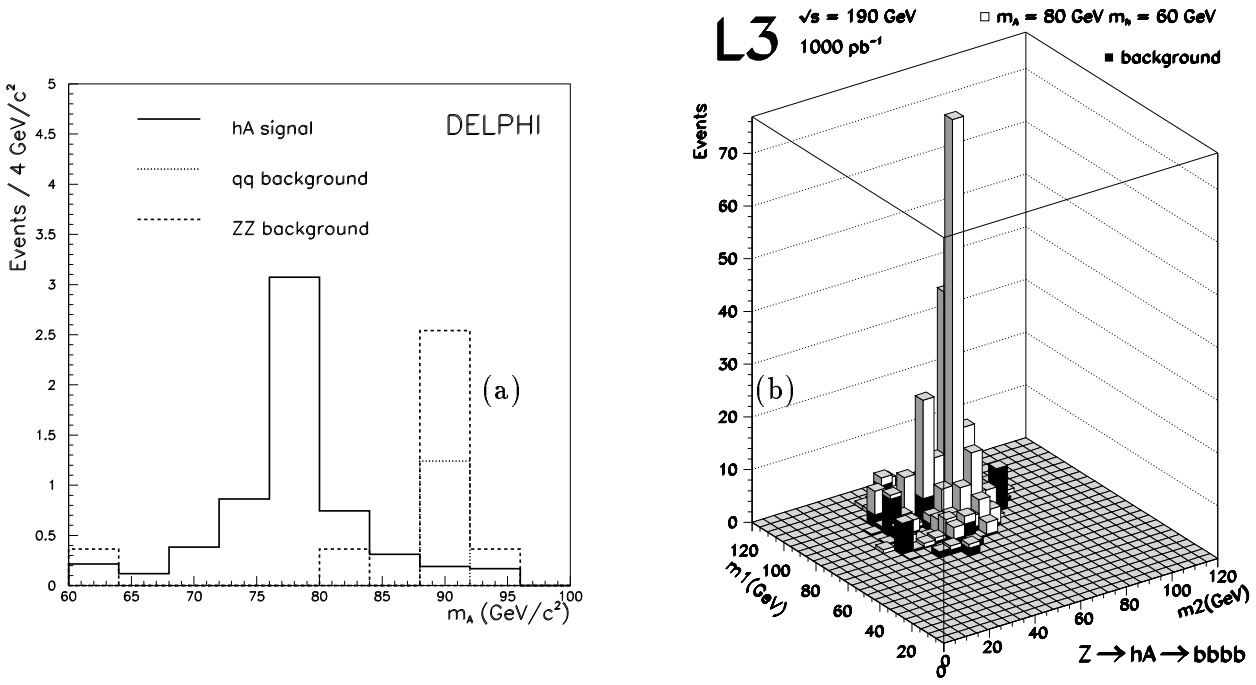

Figure 30: *Mass distribution obtained in the hA* $\rightarrow b\bar{b}b\bar{b}$ *topology, (a)* $m_{\mathrm{h}} = m_{\mathrm{A}}$ *from DELPHI (192 GeV, 300* pb^{-1}*); and (b)* m_{h} *vs* m_{A} *from L3, assuming a signal-cross-section of 0.5 pb (190 GeV, 1* fb^{-1}*).*

a pair of b-quarks in that case, therefore improving the selection efficiency of a b-tagging criterion with respect to the $e^+e^- \rightarrow$ hZ configuration.

In the unfortunate situation where both h and A predominantly decay into a pair of LSPs, the resulting final state becomes totally invisible and cannot be found at LEP2. However, in that case, there is a fair chance to discover the lightest supersymmetric particle *via* a direct neutralino search.

3.4 Discovery and Exclusion Limits

Using the definitions of Appendix 5.3, a minimum signal cross-section was inferred for the $e^+e^- \rightarrow$ hA process from the expected number of background events, both for the discovery and the exclusion. Since the background mass distribution is mostly uniform over the (m_{h},m_{A}) plane, it turns out that this minimum signal cross-section does not depend on m_{h} and m_{A}. For instance, at 192 GeV and with an integrated luminosity of 150 pb^{-1}, a cross-section in excess of 65 (30) fb can be discovered (excluded) in the $e^+e^- \rightarrow$ hA channel when supersymmetric decays are closed.

For the Higgs-strahlung process, the total cross-section is reduced with respect to the standard model expectation by a factor denoted $\sin^2(\beta - \alpha)$ in the MSSM. The number of events expected is also directly affected by the branching ratio of the h decay into $b\bar{b}$. For each m_{h},

a minimum value for $R^2 \equiv \sin^2(\beta-\alpha) \times BR(\mathrm{h} \to \mathrm{b\bar{b}})$ was inferred for the discovery and the exclusion. The result, which is model-independent, is shown in Fig.31 for the three center-of-mass energies 175, 192 and 205 GeV, with integrated luminosities of 150, 150 and 300 pb^{-1}, respectively [58]. The interpretation of the negative searches at LEP1 (from Ref.[117]) is also shown in this plot.

Since this limit becomes irrelevant when supersymmetric decays are dominant, it is supplemented by the 95% C.L. upper limit on $R^2 \equiv \sin^2(\beta-\alpha) \times BR(\mathrm{h} \to$ invisible final states), as shown in Fig.32.[2] At LEP2, this limit is worse by about a factor of two than in the case where h predominantly decays into $\mathrm{b\bar{b}}$, while it was better at LEP1. In order to make easier the use of these curves to test other models, such as non-minimal supersymmetric extensions of the standard model, the exclusion and discovery limits on $R^2 = \sin^2(\beta-\alpha) \times BR(\mathrm{h} \to \mathrm{b\bar{b}})$ are presented in Table 15, for the three center-of-mass energies, and when combining the results at 175 and 192 GeV, on the one hand, and with the 205 GeV results in addition, on the other.

To interpret these results in the MSSM framework, both the $\mathrm{e^+e^-} \to \mathrm{hA}$ cross-section and the $\sin^2(\beta-\alpha)$ value were computed and compared to the above minimum values in a systematic scan of the $(m_{\mathrm{A}}, \tan\beta)$ plane, for $M_t = 175 \pm 25$ GeV/c^2 and for the three different stop mixing configurations, *(i)* No mixing: $A_t = 0$ and $|\mu| \ll M_S$; *(ii)* Typical mixing: $A_t = M_S$ and $\mu = -M_S$ (these values of A_t and μ give a moderate impact of the stop mixing for large $\tan\beta$ but a mixing effect close to maximal if $\tan\beta$ is small); and *(iii)* Maximal mixing: $A_t = \sqrt{6}M_S$ and $|\mu| \ll M_S$, with $M_S = 1$ TeV.

The results of the above analysis are summarized in a series of figures (Figs.33 and 34), which display the areas in the $(m_{\mathrm{A}}, \tan\beta)$ and $(m_{\mathrm{h}}, \tan\beta)$ planes that can be covered for a given energy of LEP2, $\sqrt{s} = 175, 192$ and 205 GeV at the integrated luminosities 150, 150 and 300 pb^{-1}, respectively. The top-quark mass and the stop mixing parameters are varied as specified above. The figures are obtained by combining the four LEP experiments. At $\sqrt{s}$= 175 GeV, an increase in luminosity beyond 150 pb^{-1} does not improve the potential of the machine for the discovery of the light Higgs boson in any relevant way. The analogous conclusion was reached in the standard model case. At $\sqrt{s}$= 192 GeV, still 150 pb^{-1} of integrated luminosity per experiment are sufficient to make proper use of the discovery potential of the machine, and a larger luminosity of $\simeq$ 300 pb^{-1} gives only a slight improvement in the upper bound on the Higgs boson mass which can be discovered or excluded. Although for any center-of-mass energy the variation from 150–200 pb^{-1} to 300–400 pb^{-1} of integrated luminosity yields a gain of at most 2 to 3 GeV/c^2 in the maximal Higgs boson mass that can be reached, at $\sqrt{s} = 205$ GeV the results are presented for 300 pb^{-1} since for this energy value the increase in luminosity translates into a quite impressive coverage of $\tan\beta$.

Comparing the experimental limits for the center-of-mass energies 175 GeV and 192 GeV, Fig.33 a/b and c/d, it is clear that the higher energy value allows a remarkably larger part of the parameter space to be covered. For $M_t = 175$ GeV/c^2 and in particular for $\sqrt{s} = 175$ GeV,

[2] Since this analysis was done in ALEPH only, it was assumed that the other experiments would contribute in the same proportions as for the visible decays to perform the combination.

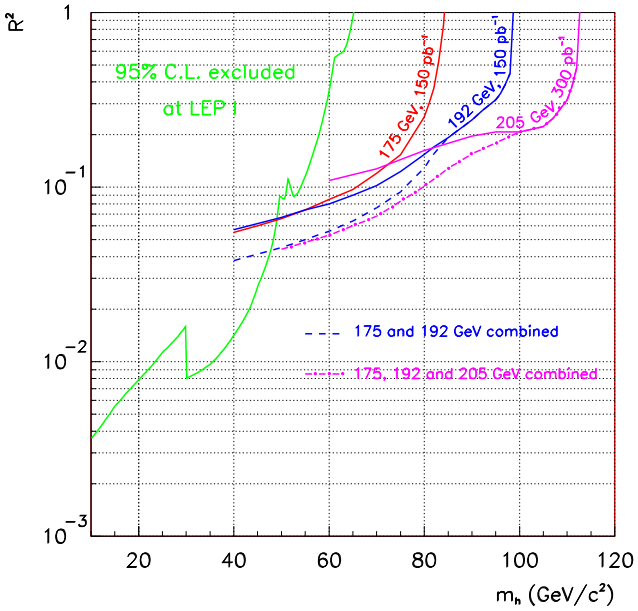

Figure 31: *95% C.L. upper limits on R^2, as a function of m_{h} for a visible Higgs boson, for the three center-of-mass energies: $R^2 = \sin^2(\beta-\alpha) \times BR(h \rightarrow$ any visible final state) for the LEP1 part of the curve and $R^2 = \sin^2(\beta-\alpha) \times BR(h \rightarrow b\bar{b})$ for the LEP2 part of the curve.*

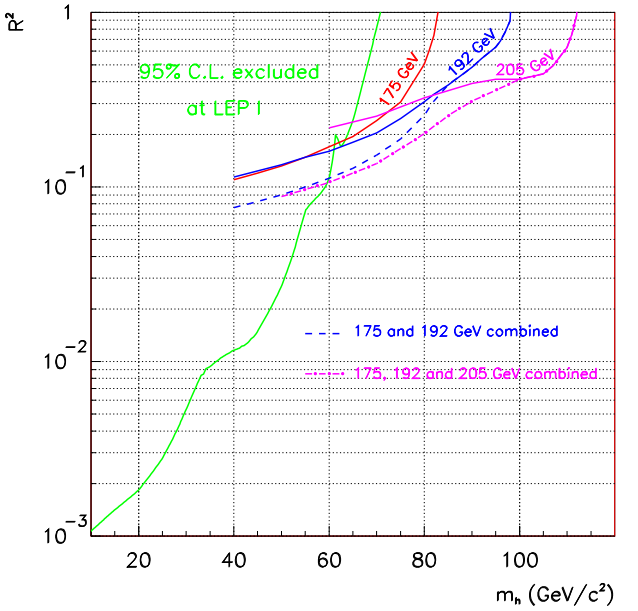

Figure 32: *95% C.L. upper limits on R^2, as a function of m_{h} for an invisible Higgs boson, for the three center-of-mass energies: $R^2 = \sin^2(\beta-\alpha) \times BR(h \rightarrow$ any invisible final state).*

Table 15: *Minimum value for* $R^2 = \sin^2(\beta-\alpha) \times BR(h \to b\bar{b})$ *at the three center-of-mass energies, with integrated luminosities of 150, 150 and 300* pb^{-1}*, respectively, and for various Higgs boson masses. Also shown is the combination of the 175 GeV and 192 GeV results, with an integrated luminosity of 150* pb^{-1} *taken at each energy, and the overall combination of the 175, 192 and 205 GeV results, assuming 300* pb^{-1} *at 205 GeV. The combination of several center-of-mass energies have not been used in Fig.33 and 34.*

$\sqrt{s}$ = 175 GeV

$m_{\mathrm{H}}(\mathrm{GeV}/c^2)$	40	50	60	70	75	80	82	83	84
Exclusion	0.055	0.066	0.085	0.120	0.153	0.252	0.369	0.525	0.842
Discovery	0.136	0.164	0.207	0.303	0.381	0.620	0.963	—	—

$\sqrt{s}$ = 192 GeV

$m_{\mathrm{H}}(\mathrm{GeV}/c^2)$	40	50	60	70	80	90	95	97	98
Exclusion	0.057	0.067	0.080	0.103	0.154	0.242	0.316	0.387	0.447
Discovery	0.142	0.163	0.197	0.249	0.385	0.584	0.781	—	—

Combination of 175 and 192 GeV

$m_{\mathrm{H}}(\mathrm{GeV}/c^2)$	40	50	60	70	80	90	95	97	98
Exclusion	0.038	0.045	0.056	0.076	0.129	0.242	0.316	0.387	0.447
Discovery	0.095	0.113	0.139	0.190	0.317	0.584	0.781	—	—

$\sqrt{s}$ = 205 GeV

$m_{\mathrm{H}}(\mathrm{GeV}/c^2)$	60	70	80	90	100	105	110	111	112
Exclusion	0.109	0.127	0.162	0.196	0.207	0.222	0.315	0.375	0.481
Discovery	0.270	0.315	0.404	0.490	0.510	0.539	0.785	—	—

Combination of 175, 192 and 205 GeV

$m_{\mathrm{H}}(\mathrm{GeV}/c^2)$	50	60	70	80	90	100	105	110	112
Exclusion	0.044	0.053	0.068	0.101	0.155	0.207	0.222	0.315	0.481
Discovery	0.111	0.132	0.168	0.252	0.370	0.510	0.539	0.785	—

(a)

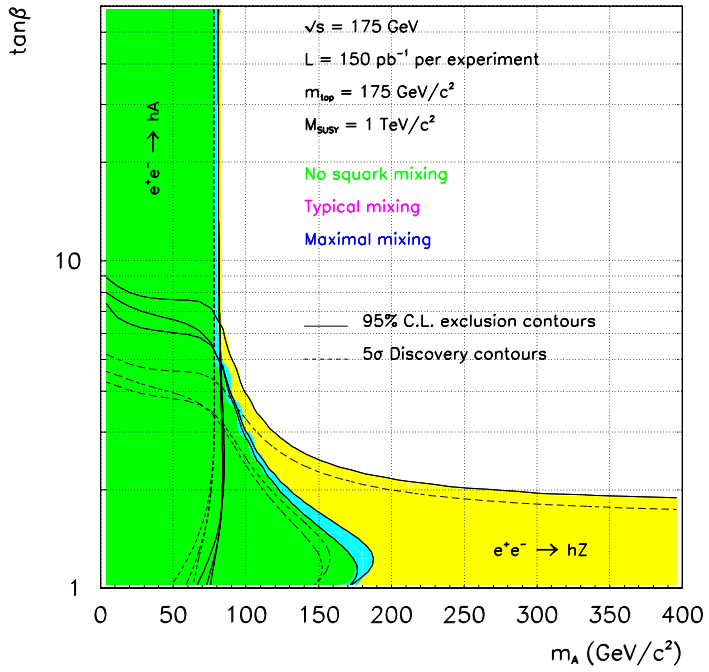

(b)

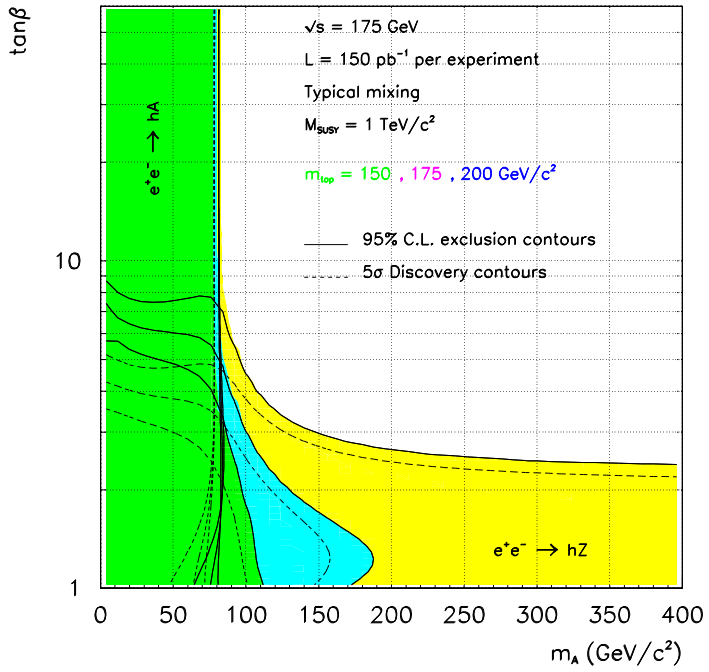

Figure 33: *Exclusion and discovery limits in the* $[m_A, \tan\beta]$ *plane for each of the center-of-mass energies, varying the values of the stop mixing parameters as specified in the text (a, c and e) and varying the values of* M_t*= 150, 175, 200 GeV/*c^2 *for* $A = -\mu = M_S = 1$ *TeV (b, d and f).*

(c)

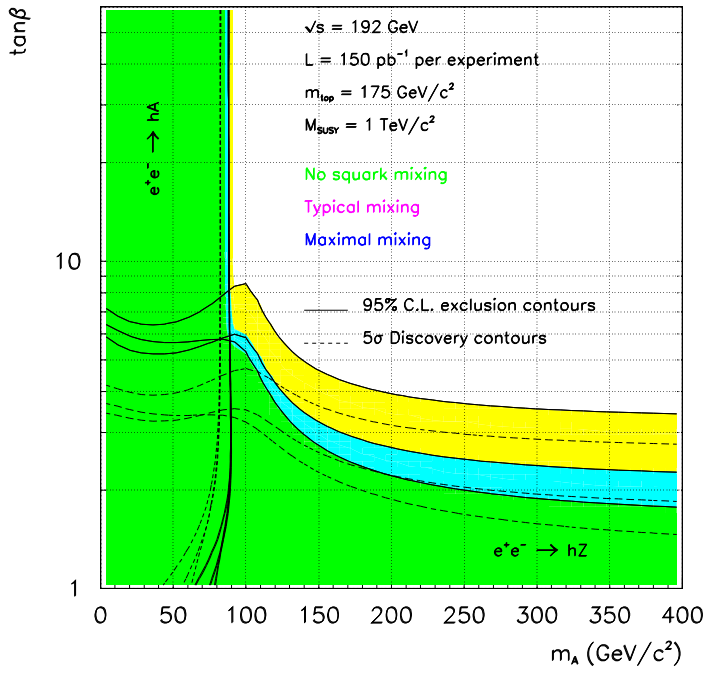

(d)

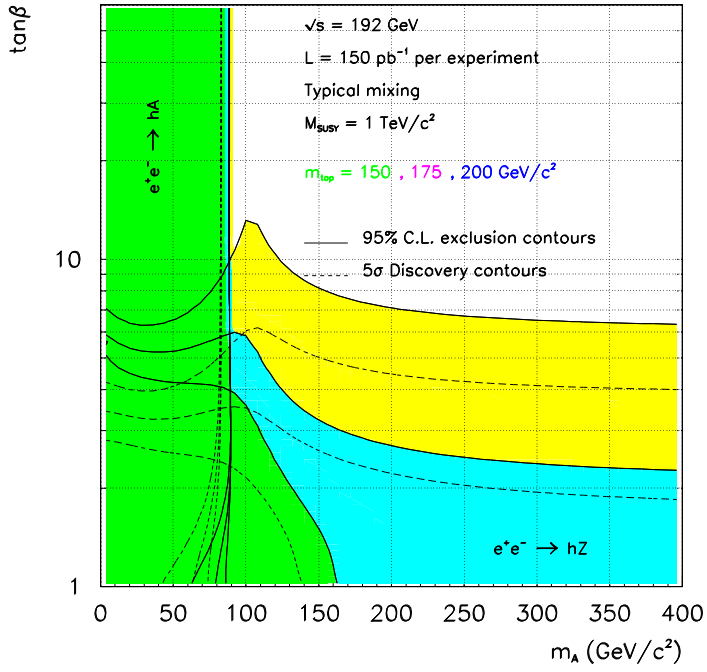

Figure 33: *(cont'd)*

(e)

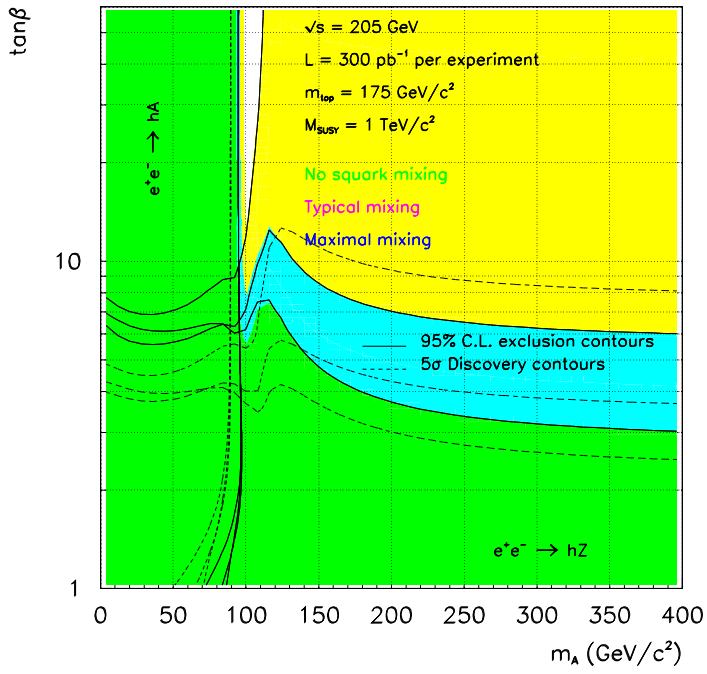

(f)

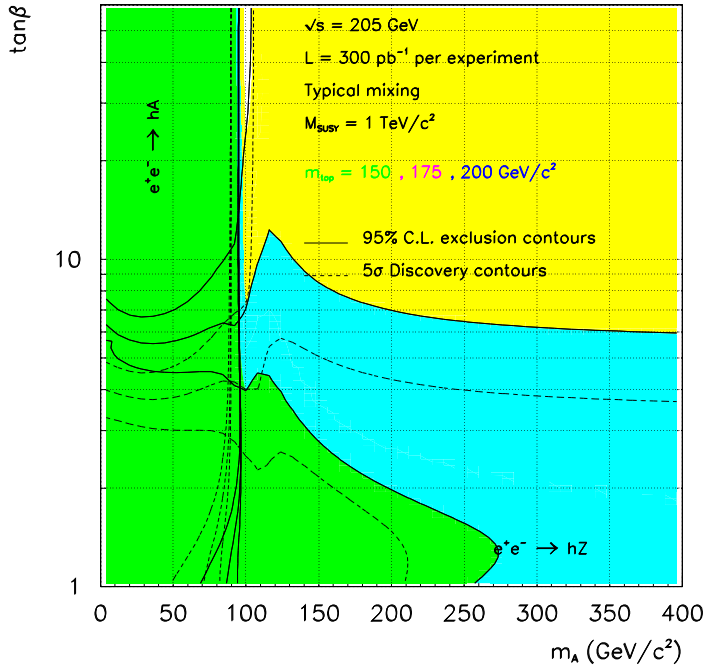

Figure 33: *(cont'd)*

(a)

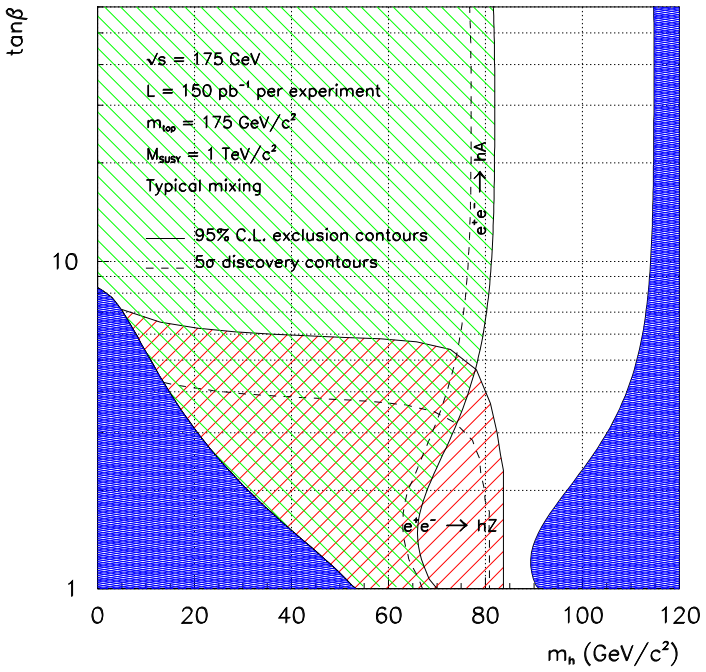

(b)

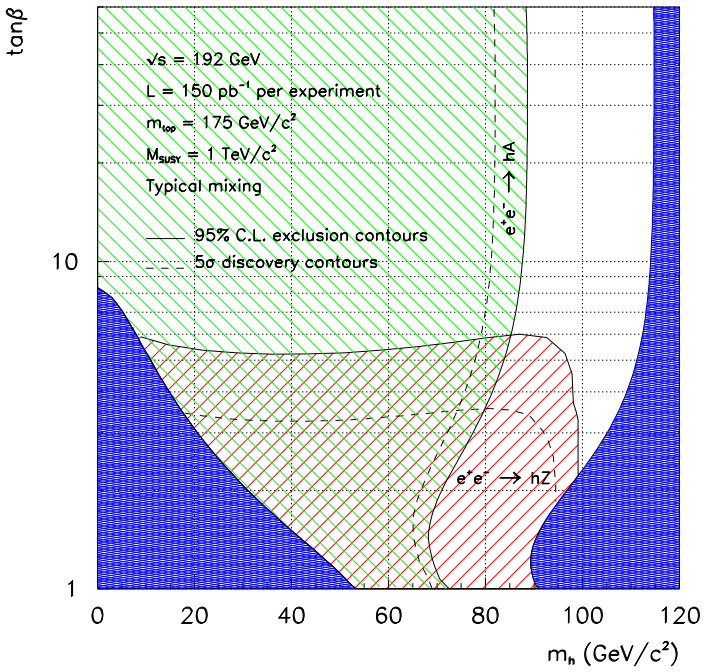

Figure 34: *Exclusion and discovery limits in the* $[m_{\mathrm{h}}, \tan\beta]$ *plane, for* $M_t = 175$ *GeV and* $A = -\mu = M_S = 1$ *TeV for each of the center-of-mass energies. The dark shaded areas are excluded theoretically.*

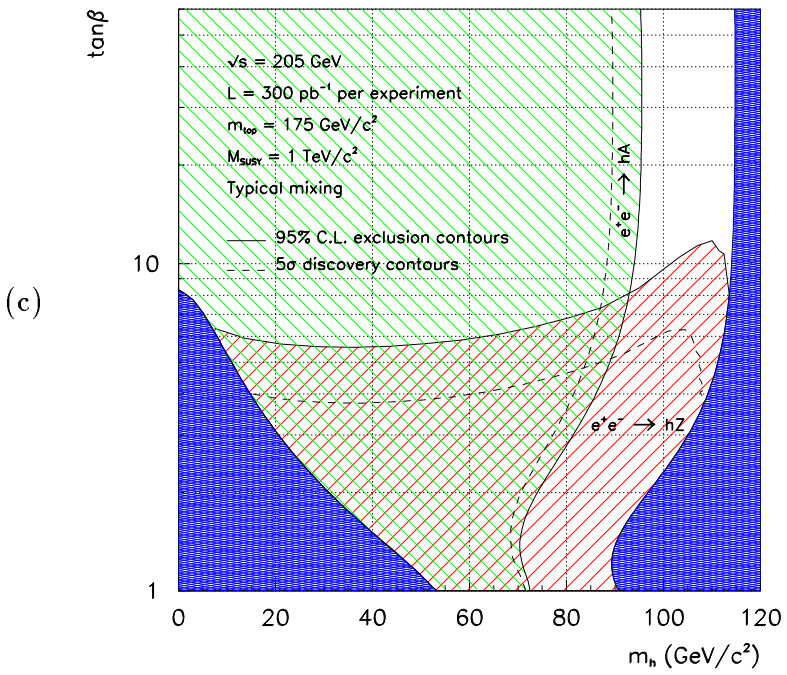

Figure 34: *(cont'd)*

the potential of LEP2 is rather limited at large $m_{\rm A}$, while for 192 GeV it is possible to cover the moderate and large m_A for small $\tan\beta$, $\tan\beta \leq 2-3$ (which is a difficult region for LHC). This is especially obvious if non-negligible mixing in the stop sector is considered. For large values of $m_{\rm A}$, the limit of the standard model Higgs boson is approached (light gaugino channels are not considered to be open) and the lightest CP-even Higgs boson acquires its maximal value. Since the maximal value of $m_{\rm h}$ increases with $\tan\beta$, the range in $\tan\beta$ covered by LEP2 directly reflects the range of standard model Higgs boson masses accessible to the experiments.

It is interesting to compare the upper limits on $m_{\rm h}$ which can be reached experimentally, Table 16 and Fig.34, with the maximal h masses expected in the MSSM. In particular, if the experimental limits are compared to the h mass range preferred by gauge and b-τ Yukawa coupling unification, for $M_t \simeq 175$ GeV/c^2 it can be seen that a large part of the SUSY Higgs mass range is covered in the 192 GeV version of LEP2, in contrast to the lower energy of 175 GeV. In fact, the infrared fixed point solution can be excluded at the 95 % C. L. at $\sqrt{s} =$ 192 GeV if $M_t \leq 175$ GeV/c^2. (For $M_t \simeq 185$ GeV/c^2 the infrared fixed point solution can be excluded only at $\sqrt{s}$ =205 GeV.)

3.5 MSSM *vs.* SM

No precise experimental analyses have yet been developed to cope with the situation in which a Higgs boson would be discovered and thus would need to be studied in detail. This can be

Table 16: *Maximal $m_{\rm h}$ (hZ and hA combined) and $m_{\rm A}$ (hA only), in GeV/c^2, that can be directly discovered and excluded in the MSSM for M_t = 175 GeV/c^2 and typical mixing at various LEP2 energies for two representative values of* $\tan\beta$ *(* These values of $m_{\rm h}$ are already excluded theoretically in the MSSM for typical mixing, M_S = 1 TeV and for the values of M_t and* $\tan\beta$ *considered here).*

$\sqrt{s}$	L_{min}	$\tan\beta = 2$		$\tan\beta = 30$		$\tan\beta = 2$		$\tan\beta = 30$	
(GeV)	($\rm pb^{-1}$)	$m_{\rm h}^{disc.}$	$m_{\rm A}^{disc.}$	$m_{\rm h}^{disc.}$	$m_{\rm A}^{disc.}$	$m_{\rm h}^{excl.}$	$m_{\rm A}^{excl.}$	$m_{\rm h}^{excl.}$	$m_{\rm A}^{excl.}$
175	150	80	75	77	77	84	82	83	83
192	150	95	78	82	82	98	87	88	88
205	300	108*	80	88	88	113*	93	95	95

partly explained by the relatively low luminosity currently expected at LEP2 which will not allow any accurate measurements to be performed in this field. It could however be imagined that if a new particle were discovered, a substantial extension of the LEP2 project could be decided upon with the purpose of identifying this particle.

The angular distribution of the Higgs boson produced in the Higgs-strahlung process is expected to be quite uniform at the LEP2 center-of-mass energies, and so is the angular distribution of the decay products in the Higgs boson rest frame. Even in the most difficult case $m_{\rm h} \sim m_{\rm Z}$, the numbers of events collected by the four experiments with 1 $\rm fb^{-1}$ taken at 192 GeV (323 events from the signal and 255 from the backgrounds, see Table 9) suffice to exhibit the flatness of these distributions, and to characterize unambiguously a $J^P = 0^+$ particle.

Such an excess of events after a b-tagging requirement is also sufficient to claim that this object often decays into $\rm b\bar{b}$, which also characterizes a Higgs particle. However, a precise measurement of the $\rm b\bar{b}$ branching fraction can only be done with a channel in which the evidence for a signal can be claimed without b-tagging, *i.e.* the $\rm H\ell^+\ell^-$ topology. This situation is particularly favourable if the Higgs boson mass is not degenerate with the Z mass, in which case the background is much reduced thanks to the excellent recoil mass resolution.

For instance, the cross-section for a 80 GeV/c^2 Higgs boson at $\sqrt{s}$ = 192 GeV in the $\rm H\ell^+\ell^-$ topology is 47 fb (after selection cuts, but with no b-tagging requirement), to be compared to 14 fb for the background. This already allows a measurement of the $\rm b\bar{b}$ branching fraction (if close to 100%) with a $\sim$ 20% statistical accuracy, if a luminosity of 1 $\rm fb^{-1}$ is given to each experiment. Similarly, the quantity $\sigma(\rm e^+e^- \rightarrow hZ) \times BR(h \rightarrow b\bar{b})$ can be determined with the same luminosity from the events collected in all the topologies with a statistical accuracy of $\sim$ 5% (resp. 10%) for a 80 GeV/c^2(resp. 90 GeV/c^2) Higgs boson.

Unfortunately, even if the systematics uncertainties were negligible (*e.g.* the errors related

to the b-tagging efficiency determination) this is not sufficient to distinguish the standard model and the MSSM in the region where only the Higgs-strahlung process plays a role. In this region, a statistical accuracy better than 1 or 2% is indeed required [118] to achieve this goal. The extension of the standard model would be manifested in this parameter range only if non-standard Higgs boson decays were observed. It is otherwise only in the region where the $e^+e^- \to hA$ process or, less likely, charged Higgs bosons (see Section 3.6) can be discovered, that this distinction is possible at LEP2.

3.6 Search for Charged Higgs Bosons

In the MSSM the mass of the charged Higgs bosons $H^\pm$ is expected to be larger than m_W. In general, for non-extreme stop mixing configuration, it is of the order of ${m_{H^\pm}}^2 = {m_A}^2 + {m_W}^2$, *i.e.* larger than ~ 90 GeV/c^2 within a few GeV/c^2, rendering rather difficult the discovery of such heavy objects at LEP2. However, this does not hold necessarily in other, e.g. non-minimal supersymmetric extensions of the Standard Model where light charged Higgs bosons – although heavier than 44 GeV/c^2 as shown by LEP1 data – cannot be ruled out. Their discovery would unambiguously signal the existence of an extended Higgs sector.

3.6.1 Production and Decays

Charged Higgs bosons are produced in pairs in the process $e^+e^- \to H^+H^-$ with a rate depending only on $m_{H^\pm}$ in the general two-doublet model. About 100 such events are expected to be produced with an integrated luminosity of 500 pb^{-1} for $m_{H^\pm} \sim 70$ GeV/c^2, irrespective of the center-of-mass energy from 175 to 205 GeV, and this rate decreases rapidly with increasing mass due to the β^3 kinematic suppression factor.

Furthermore, if it is assumed that the cascade decay modes [95] like $H^+ \to W^{+*}h$ are kinematically suppressed, the charged Higgs bosons are expected to decay predominantly into the heaviest kinematically accessible fermion pair provided it is not suppressed by a small CKM matrix element, *i.e.* $H^+ \to \tau^+\nu_\tau$ or $c\bar{s}$. Therefore the expected final states are $\tau^+\nu_\tau\tau^-\bar{\nu}_\tau$, $c\bar{s}\tau^-\bar{\nu}_\tau$ and $c\bar{s}\bar{c}s$, thus leading to an important irreducible background from $e^+e^- \to W^+W^-$ in addition to the low expected signal rate. This renders almost hopeless the discovery of charged Higgs bosons with mass around and above the W mass.

Searches for these final states have been developed by L3 [119] and DELPHI [64], using full detector simulation of signal and background processes for an integrated luminosity of 500 pb^{-1}. A search for the four-jet final state $c\bar{s}\bar{c}s$ has so far been developed by L3.

a) The $e^+e^- \to H^+H^- \to c\bar{s}\bar{c}s$ Channel

The process $e^+e^- \to H^+H^- \to c\bar{s}\bar{c}s$ leads to four-jet hadronic events. In order to distinguish a Higgs signal from the main background of $e^+e^- \to q\bar{q}$ and W^+W^-, use is made of the different

topological properties. The simulated hadronic energy deposits are clustered into four jets. For example at $\sqrt{s}$ = 175 GeV, for 60 and 70 GeV/c^2 Higgs signals, 75% and 69% selection efficiencies are expected respectively. The numbers of expected background events are: 3140 $q\bar{q}$, 4664 WW, and 90 ZZ for 500 pb^{-1}.

The four jets can be combined into two jet-pairs in three possible ways, and their energies and directions are fitted to the energy-momentum conservation and to the $m_{H^+} = m_{H^-}$ constraint. The combination with the smallest χ^2 is chosen, provided that the measured mass difference between the two jet-pairs is smaller than 5 GeV/c^2, and a mass resolution of about 1 GeV/c^2 is achieved. Unlike the hA $\rightarrow b\bar{b}b\bar{b}$ channel, no b-tagging requirement can be applied to reject the WW $\rightarrow$ four-jet background, but the signal-to-noise ratio is improved by removing events where one jet pair combination is consistent with a W pair, at the expense of a suppression of the signal efficiency when $m_{H^\pm} \simeq m_W$.

For $m_{H^\pm} \sim$ 60 GeV/c^2, the expected signal efficiency is about 7% and the number of background events is about 2 $q\bar{q}$ and 3 WW events, for an integrated luminosity of 500 pb^{-1} at $\sqrt{s}$ = 175 GeV.

b) The $e^+e^- \rightarrow H^+H^- \rightarrow c\bar{s}\tau^-\bar{\nu}_\tau$ Channel

The signature of an $e^+e^- \rightarrow H^+H^- \rightarrow c\bar{s}\tau^-\bar{\nu}_\tau$ signal is one isolated slim jet with missing energy coming from the τ decay recoiling against a hadronic system. In the DELPHI analysis, a preselection of hadronic final states is performed, and the events are clustered into three jets. The lowest multiplicity jet, *i.e.* the τ candidate, is required to have at most three charged particle tracks. Further cuts on the mass and on the angle between the two most energetic jets are applied to reject events without a clear 3-jet topology. A kinematic fit of the neutrino direction and the τ momentum (four unknowns) is performed by constraining the $\tau\nu$ and cs systems to have the same invariant mass and the total energy-momentum to be conserved (five equations). A χ^2 cut is applied to improve the signal-to-noise ratio. This retains from 16% to 29% of the signal events, depending on the $H^\pm$ mass and approximately 38 background events remain for 500 pb^{-1} at 175 GeV.

In the L3 analysis, the kinematic fit is replaced by the following approximate method:

(i) the missing momentum, $\vec{p}_{\rm miss}$, the missing energy, $E_{\rm miss}$, and the invariant mass of the two most energetic jets, $M_{\rm cs}$, are calculated. In order to improve the mass resolution, this mass is rescaled by the factor $E_{\rm beam}/(E_{\rm jet1} + E_{\rm jet2})$;

(ii) for the other hemisphere, the invariant mass $M^2_{\tau\nu} = (E_{\rm miss} + E_\tau)^2 - (\vec{p}_{\rm miss} + \vec{p}_\tau)^2$ is calculated, where $\vec{p}_\tau$ is the visible τ momentum.

The reconstructed masses of $M_{\rm cs}$ and $M_{\tau\nu}$ are shown in Fig.35. Cuts as given in the figure are applied. The expected signal efficiencies are about 5.6% and about 2 WW background events are expected for 500 pb^{-1} at 175 GeV.

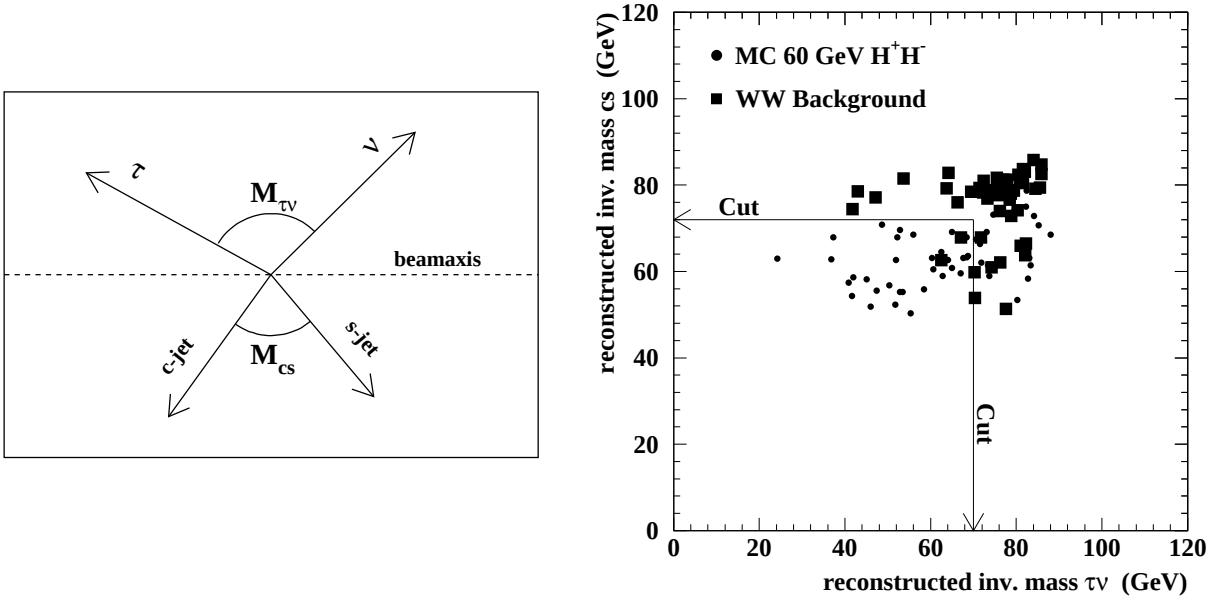

Figure 35: *Left: Schematic reconstruction of both invariant masses M_{cs} and $M_{\tau\nu}$ in the $cs\tau\nu$ channel. For details see text. Right: Reconstructed invariant masses of M_{cs} and $M_{\tau\nu}$ in the L3 analysis for a 60 GeV/c^2 Higgs signal and background events in the $cs\tau\nu$ channel for 500 pb^{-1} at 175 GeV.*

c) The $e^+e^- \to H^+H^- \to \tau^+\nu_\tau\tau^-\bar{\nu}_\tau$ Channel

The $e^+e^- \to H^+H^- \to \tau^+\nu_\tau\tau^-\bar{\nu}_\tau$ events are characterized by a low particle multiplicity and large missing energy. The background processes $e^+e^- \to \tau^+\tau^-(\gamma)$, $q\bar{q}$, WW and $\gamma\gamma \to f\bar{f}$ are relevant in this channel.

After applying selection criteria based on the acoplanarity, the total energy and the event thrust axis angle, the main remaining background comes from leptonic WW decays. Unlike the two other channels, a reconstruction of the Higgs boson masses is not possible because of too many unknowns due to the numerous missing energy sources. However, the energies of the decay products of the two taus can be measured, and part of the W decays into $e\nu_e$ and $\mu\nu_\mu$ can be removed by a cut on these two energies, which are expected to be larger in that case than for $\tau\nu_\tau$ final states due to the additional neutrinos from the τ decay.

The expected signal efficiencies are about 12% and about 1 WW background event is expected in the L3 analysis for 500 pb^{-1} at 175 GeV. For DELPHI, a 23% signal efficiency is achieved, for a total of 85 background events expected.

3.6.2 Results

In the framework of a general two Higgs doublet model, the results of this analysis can be expressed as a function of $Br(H^+ \to \tau^+\nu_\tau)$ (if it is assumed that off-shell decay modes are

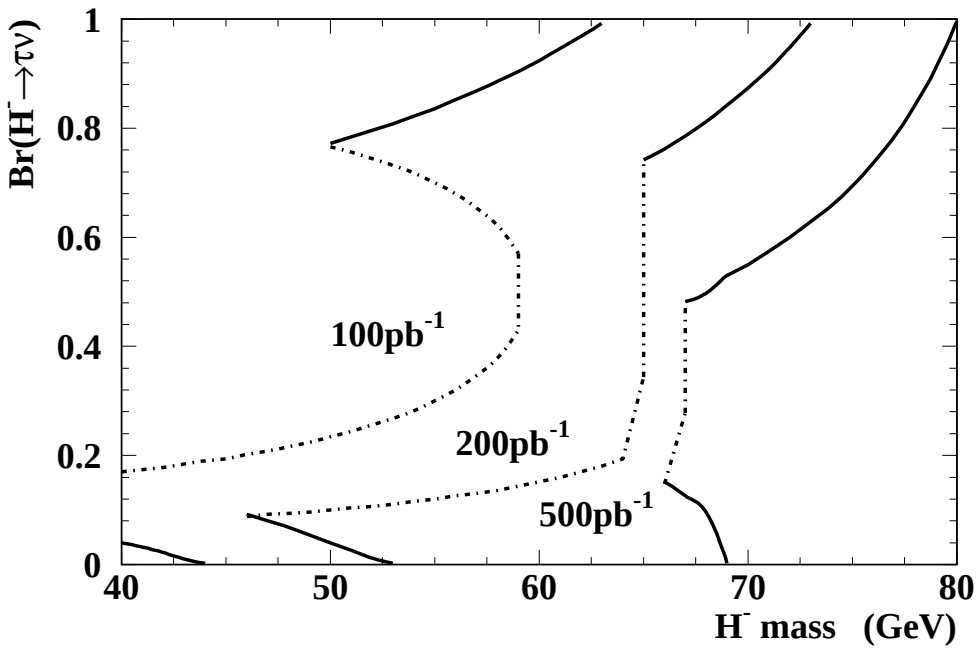

Figure 36: *3σ sensitivity regions as a function of the charged Higgs boson mass and its leptonic branching ratio at 175 GeV and for a total luminosity of 100, 200, and 500 pb^{-1}. The upper solid lines indicate the sensitivity limits from the $\tau\nu\tau\nu$ channel, the dashed lines come from the cs$\tau\nu$ channel, and the lower solid lines come from the cscs channel. (For simplicity, combined contour lines in overlapping sensitivity regions are not shown.)*

suppressed) and of $m_{\mathrm{H}^{\pm}}$. Combining the studies in the $\mathrm{c\bar{s}\bar{c}s}$, $\mathrm{c\bar{s}}\tau^{-}\bar{\nu}_{\tau}$, and $\tau^{+}\nu_{\tau}\tau^{-}\bar{\nu}_{\tau}$ channels described in the previous sections, the regions which can be explored with $\sqrt{s} = 175$ GeV are shown in Fig.36 for luminosities of 100, 200, and 500 pb^{-1} taken by one experiment. (These numbers would be roughly divided by four if the four LEP experiments were combined.)

Except for branching ratios into $\tau\nu_{\tau}$ near 0 or 1, all three channels contribute simultaneously which extends the sensitivity range by few GeV/c^2. Charged Higgs bosons with masses up to about 70 GeV/c^2 should be detectable independently of their decay branching ratios assuming a total luminosity of 500 pb^{-1} at 175 GeV. The region where a 99.73% CL (3σ) effect due to $\mathrm{H^{+}H^{-}}$ production can be detected is strongly dependent on the assumed luminosity. The boundary lines also depend strongly on the detection sensitivities due to the small change of the charged Higgs boson production cross-section with different $m_{\mathrm{H}^{\pm}}$. The expected variations of the number of background events for different Higgs masses is taken into account in the figure. The effect of increasing the center-of-mass energy to about 200 GeV is small since only a small change of the production cross section is expected.

The background at LEP2 from WW production with identical decay modes as for the

charged Higgs bosons can be controlled. Irreducible background only occurs if $m_{\rm H^\pm} \sim m_{\rm W}$. For leptonically decaying Higgs bosons, masses can however be explored up to about $m_{\rm W}$ due to the small branching fraction of the W boson into $\tau\nu_\tau$.

To summarize, LEP2 has a good potential for a charged Higgs boson discovery already in its first phase at 175 GeV [well beyond the current mass limit of LEP1 of 44 GeV/c^2] as soon as a sufficient luminosity of about 200 pb^{-1} is collected. Even with an increase of the machine energy to around 200 GeV, it is extremely difficult to explore the kinematic region around and above $m_{\rm W}$ because of the large irreducible background from WW production and the low production cross section.

3.7 Complementarity between LEP2 and LHC

As with the SM Higgs boson, it is an important task to compare the Higgs discovery potential of LEP2 with the potential of LHC for the minimal supersymmetric standard model MSSM [120]. The comparison will be based again on the LEP energy $\sqrt{s} = 192$ GeV with an integrated luminosity of $\int\mathcal{L} = 150$ pb^{-1} per experiment [yet all four experiments combined] and the presumably ultimate integrated luminosity $\int\mathcal{L} = 3\times10^5$ pb^{-1} of LHC, with the results from ATLAS and CMS combined.

The lightest of the neutral scalar Higgs bosons h can be produced at the LHC in gluon–gluon fusion [56, 72], and through Higgs–strahlung off W bosons [74] and top quarks [121]. This Higgs particle will be searched for in the $\gamma\gamma$ and $b\bar{b}$ decay channels. Tagging leptonic W/Z and t decays provides an experimental trigger for the $b\bar{b}$ search, but also reduces considerably the huge backgrounds from non–b jets. The area of the $[m_A, \tan\beta]$ parameter plane in which the light scalar Higgs boson h can be discovered in this way at the LHC is shown in Fig.37 by the shaded regions [122]. The boundary of the LEP2 discovery range is indicated by the full line. No method has yet been found which allows the discovery of h in the parameter range of large $\tan\beta > 5$ and m_A between ~ 90 and ~ 170 GeV at either of the two machines.

While the area in which the pseudoscalar Higgs boson A can be discovered at LEP is rather modest, a large domain is accessible at LHC, Fig.38. A clean signal of A comes from $\tau^+\tau^-$ decays; in addition, cascade decays $A \to Zh$ with subsequent leptonic Z decays provide promising search channels. The search for A in $t\bar{t}$ decays requires the theoretical control of the top background production at a level between 10 and 2% which is an extremely difficult problem. A similar picture applies to the search for the heavy scalar Higgs particle H at the LHC, cf. Fig.38. In particular, the classical four–lepton decay of H via ZZ intermediate states can be exploited. At LEP2 the heavy Higgs H might be produced only in a small region of the MSSM parameter range. The search for charged MSSM Higgs particles is frustrated in either machine. While the LEP2 energy is not sufficient to produce these particles pairwise outside a tiny domain of the MSSM parameter space, the search technique at the LHC is restricted so far to $t \to bH^+$ decays with a rather limited range in the charged Higgs mass.

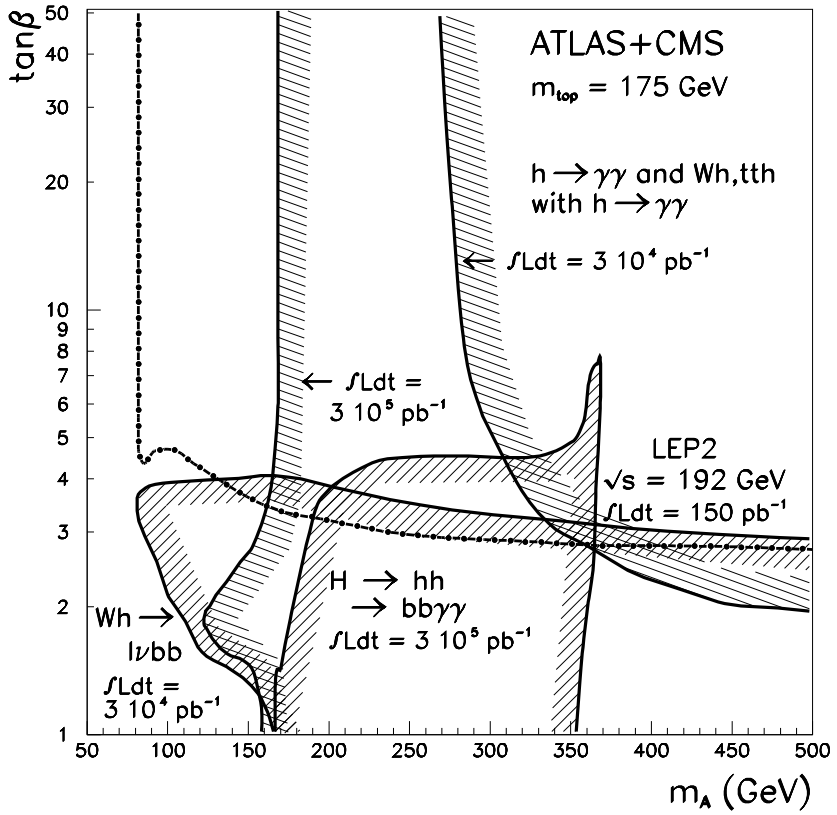

Figure 37: *The regions in the $[m_A, \tan\beta]$ parameter space in which the lightest CP-even Higgs boson h can be covered at LEP2 (Higgs–strahlung and associated production for 150 pb^{-1} at $\sqrt{s}$ = 192 GeV) and at LHC ($\gamma\gamma$ decay channel in direct production and associated $Wh, t\bar{t}h$ production for $3 \times 10^4 pb^{-1}$ and $3 \times 10^5 pb^{-1}$, $b\bar{b}$ decay channel in associated $Wh, t\bar{t}h$ production for $3 \times 10^4 pb^{-1}$, and $H \to hh \to b\bar{b}\gamma\gamma$ decay channel for $3 \times 10^5 pb^{-1}$). Parameters: M_t = 175 GeV, $A = 0$, $|\mu| \ll M_S$ = 1 TeV, but the masses of all supersymmetric particles are set to* 1 *TeV.* (Courtesy of D. Froidevaux and E. Richter-Was)

The predictions for the LHC have to be considered with some caution. The computation of the Higgs spectrum and couplings have been treated in analogy to the LEP2 simulations; however, the masses of all SUSY particles have been assumed heavy. Since the couplings in the gg fusion cross sections as well as in the $\gamma\gamma$ branching ratios for h decays are generated by loops, this channel could be affected strongly by light charginos and stop particles [123]. Depending on the point considered in the SUSY parameter space, the variation of $\sigma\times$BR through SUSY-loop effects can go either way, enhancing or spoiling the Higgs signal. The problem of SUSY loop corrections is much less severe in search channels which are based on reactions realized already at the Born level, as Wh at the LHC, and all the search channels in e^+e^- collisions. A problem of pp collisions are the QCD corrections. They are known for the signal in gg fusion [72], but not for all background processes; the assumption that significances are estimated in a conservative way by setting K factors to unity is expected to be fulfilled in large parts of the SUSY parameter space, but this is not guaranteed yet for large $\tan\beta$. Moreover,

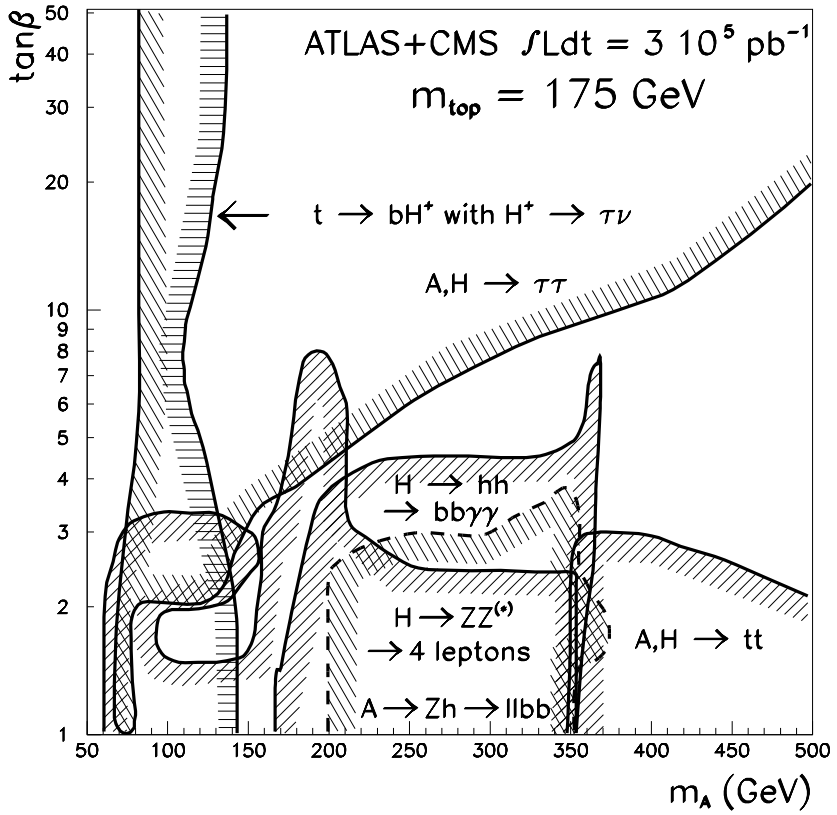

Figure 38: *The regions in the $[m_A, \tan\beta]$ parameter space which can be covered at LHC in all possible channels associated with the heavy scalar, the pseudoscalar and the charged Higgs bosons (parameters as in previous figure).* (Courtesy of D. Froidevaux and E. Richter-Was)

if the Higgs bosons do not only decay to SM particles but instead to invisible LSP and other neutralino/chargino states with potentially large branching ratios [41, 115], the analysis must be modified and the conclusions would eventually be altered rather dramatically.

Combining the discovery potentials of LEP2 at $\sqrt{s} = 192$ GeV and of LHC by summing up all Higgs production channels, the entire $[m_A, \tan\beta]$ parameter plane of the MSSM is predicted to be covered within the standard framework of non–SUSY Higgs decays [based on the parameter set $M_t = 175$ GeV, $M_S = 1$ TeV and $A, \mu \ll M_S$]. The discovery potential of LEP (LHC) in the search for h increases for smaller (larger) values of M_t, A, μ and M_S which are associated with smaller (larger) values of m_h. In the region of m_A values less than about 150 GeV, the search for h can be performed by LEP2 while the other heavy Higgs particles, H, A and $H^\pm$, can be searched for at the LHC. As discussed before, the observation of at least two different Higgs states, at LEP2 or LHC, is a crucial step in disentangling the supersymmetric theory from the Standard Model. Moreover, the channels exploited in the search for h are different at LEP2 and LHC. This implies that the couplings involved will be different and hence the physics tested in both cases will be complementary.

4 Non–Minimal Extensions

4.1 The Next–to–Minimal Supersymmetric Standard Model

In this section we shall augment the MSSM by introducing a single gauge singlet superfield N leading to a model which is referred to as the NMSSM[124].

The classic motivation for singlets is that they can solve the so-called μ-problem of the MSSM [125] by eliminating the μ-term and replacing its effect by the vacuum expectation value (vev) $< N >= x$, which may be naturally related to the usual Higgs vev's $< H_i >= v_i$. However such models in which the superpotential contains only trilinear terms, possess a $\mathbb{Z}_3$ symmetry which is spontaneously broken at the electroweak breaking scale. This results in cosmologically stable domain walls [126] which make the energy density of the universe too large. This cosmological catastrophe can be avoided by allowing explicit and non-renormalizable $\mathbb{Z}_3$ breaking terms suppressed by powers of the Planck mass which will ultimately dominate the wall evolution [127] without affecting the phenomenology of the model. However such terms induce a destabilisation of the gauge hierarchy [128] due to tadpole contributions to the N mass in supergravity models with supersymmetry breaking in the hidden sector.

Where does all this leave the NMSSM? This depends on one's point of view. If there might be some [yet unknown] solution to the domain wall problem, then one can consider models with $\mathbb{Z}_3$ symmetry which is broken spontaneously. Another approach is to avoid the domain wall problem by considering more general NMSSM models *without* a $\mathbb{Z}_3$ symmetry. Note that $\mathbb{Z}_3$ violating terms, such as a μ term, large enough to avoid the domain wall problem, can still be sufficiently small as to have no impact on collider phenomenology. These more general models allow arbitrary renormalizable mass terms in the superpotential including the μ parameter, and linear and quadratic terms in N. The question of Planck scale tadpole contributions arises in this case. However, such contributions depend on supersymmetry breaking in a hidden sector of a supergravity theory, and are hence model dependent.

According to this discussion we shall consider two quite different versions of the NMSSM:

(i) The "General NMSSM" is defined by the following superpotential:

$$W = -\mu H_1 H_2 + \lambda N H_1 H_2 - \frac{k}{3} N^3 + \frac{1}{2}\mu' N^2 + \mu'' N + \ldots \tag{50}$$

This version of the model is essentially a generalization of the MSSM, and provides a more general realization of low-energy SUSY which is equally consistent with gauge coupling unification and high precision measurements. It reduces to the MSSM in the limit in which the N field is removed, and since it does not have a $\mathbb{Z}_3$ symmetry there is no domain wall problem.

(ii) The "Constrained NMSSM" is defined by the trilinear terms in eq.(50), i.e. $\mu = \mu' = \mu'' = 0$, plus the constraints of gauge coupling unification and universal soft SUSY-breaking parameters imposed at the unification scale $M_{GUT} \approx 10^{16}$ GeV [129, 130].

4.1.1 The General NMSSM

a) Masses and Couplings

The superfield N contains a singlet Majorana fermion, plus a singlet complex scalar. The real part of the complex scalar will be assumed to develop a vacuum expectation value. The singlet yields one additional CP-even state and one additional CP-odd state which are gauge singlets but can mix with the corresponding neutral Higgs states of the MSSM, leading to three CP-even Higgs bosons h_1, h_2, h_3 and two CP-odd Higgs bosons A_1, A_2. Although there are more neutral Higgs bosons than in the MSSM, they will have diluted couplings due to their singlet components, making their production cross-sections smaller.

The tree-level CP-odd mass matrix, after rotating away the Goldstone mode as usual, reduces to the 2×2 matrix in the basis (A, N) where A is the MSSM CP-odd field,

$$M_A^2 = \begin{pmatrix} m_A^2 & \cdot \\ \cdot & \cdot \end{pmatrix} \tag{51}$$

The entries represented by dots are complicated singlet terms. Unlike the MSSM, the parameter m_A^2 here is not a mass eigenvalue due to singlet mixing. The CP-odd matrix is diagonalized by rotating through an angle γ, leading to two CP-odd eigenstates A_1, A_2 of mass $m_{A_1} \leq m_{A_2}$.

The tree-level CP-even mass squared matrix in the basis (H_1, H_2, N) is

$$M^2 = \begin{pmatrix} m_Z^2 \cos^2\beta + m_A^2 \sin^2\beta & -(m_Z^2 + m_A^2 - 2\lambda^2 v^2)\sin\beta\cos\beta & \cdot \\ -(m_Z^2 + m_A^2 - 2\lambda^2 v^2)\sin\beta\cos\beta & m_Z^2 \sin^2\beta + m_A^2 \cos^2\beta & \cdot \\ \cdot & \cdot & \cdot \end{pmatrix} \tag{52}$$

where, as usual, $v = 174$ GeV, $\tan\beta = v_2/v_1$; again the dots correspond to singlet terms. Apart from the terms involving λ, the upper 2×2 block of this matrix is identical to the MSSM CP-even matrix. However, whereas the MSSM matrix is diagonalized by rotation through a single angle α, the matrix in eq.52 is diagonalized by a 3×3 unitary matrix V, leading to three mass eigenstates h_1, h_2, h_3 with masses ordered as $m_{h_1} \leq m_{h_2} \leq m_{h_3}$.

The singlets obviously cannot mix with charged scalars, and at tree-level the mass of the charged Higgs is

$$m_{H^\pm}^2 = m_A^2 + m_W^2 - \lambda^2 v^2 \tag{53}$$

Clearly a non-zero λ tends to reduce the charged scalar masses which can now be arbitrarily small, and – in contrast to the MSSM – *below the W mass.*

We shall define the relative couplings $R_i \equiv R_{ZZh_i}$ as the ZZh_i coupling in units of the standard model ZZH coupling, and similarly we shall define a Zh_iA_j coupling factor $R_{Zh_iA_j}$. For example R_{ZZh_1} is a generalization of $\sin(\beta-\alpha)$ and the $R_{Zh_1A_i}$ are generalizations of $\cos(\beta-\alpha)$ in the MSSM. The Zh_iA_j coupling factorises into a CP-even factor S_i and a CP-odd factor which depends only on the angle γ which controls singlet mixing in the CP-odd sector.

It can be shown that the CP-even Higgs bosons in this model respect the following relations [131, 132, 133]:

$$\begin{aligned} m_{h_1}^2 &\leq \Lambda^2 = m_Z^2 \cos^2 2\beta + \lambda^2 v^2 \sin^2 2\beta \\ m_{h_2}^2 &\leq \frac{\Lambda^2 - R_1^2 m_{h_1}^2}{1 - R_1^2} \\ m_{h_3}^2 &= \frac{\Lambda^2 - R_1^2 m_{h_1}^2 - R_2^2 m_{h_2}^2}{1 - R_1^2 - R_2^2} \end{aligned} \tag{54}$$

In the case $\lambda = 0$, Λ is equal to the lightest CP-even upper mass bound in the MSSM. The above results show that if $R_1 \approx 0$ we may simply ignore h_1 and concentrate on h_2 which then becomes the lightest physically coupled CP-even state and must satisfy $m_{h_2}^2 \leq \Lambda^2$. Similarly if both R_1 and R_2 are nearly zero, then $m_{h_3}^2 = \Lambda^2$.

It can also be shown that

$$\begin{aligned} m_{A_1}^2 &\leq m_A^2 \\ m_{A_2}^2 &= \frac{m_A^2 - m_{A_1}^2 \cos^2 \gamma}{1 - \cos^2 \gamma} \end{aligned} \tag{55}$$

If the lighter CP-odd state is weakly coupled ($\cos\gamma \approx 0$) then it is mainly singlet, and the heavier CP-odd state is then identified with the MSSM state of mass m_A.

b) Theoretical Upper Limit on Λ

According to eq.(54), Λ is clearly a function of $\tan\beta$ and λ, and to find the absolute upper bound on the mass of the lightest CP-even Higgs boson we must maximize this function (Λ_{max}). Radiative corrections, which drastically affect the bound [134], are included using recently proposed methods [89].

For a fixed $\tan\beta$, the maximum value of Λ is given by the maximum value of λ as derived from the triviality requirement that none of the Yukawa couplings becomes non-perturbative before the GUT scale of around 10^{16} GeV. Using the recently calculated two-loop RGEs [130], we find an upper limit on λ as a function of $\tan\beta$. The maximum value of λ is typically in the range 0.6-0.7 for a wide range of $\tan\beta$, depending on M_t and $\alpha_3(m_Z)$, and falls off to zero for $\tan\beta \rightarrow \approx 1.5$ or 60 because h_t or h_b, respectively, is very close to triviality. Having derived the maximum value of λ as a function of $\tan\beta$, we can use this information to obtain an M_t-dependent maximum value of Λ shown as the upper solid curve in Fig.39. The MSSM bound is also shown (lower solid curve) for comparison. The dashed line is the corresponding upper mass bound in the constrained NMSSM (see later).

As well as being the upper bound on the mass of the lightest CP-even Higgs boson, the parameter Λ plays an important role in constraining all the CP-even Higgs boson masses and couplings. Thus the value of Λ_{max}, corresponding to the upper solid line in Fig.39, also constrains h_2 and h_3 according to eq.(54).

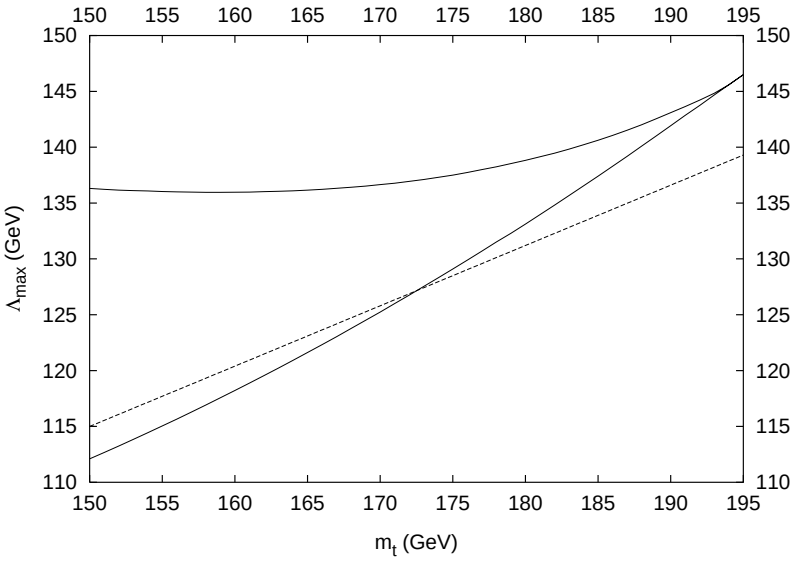

Figure 39: *Theoretical upper bound on the mass of the lightest CP-even Higgs boson as a function of M_t. We have used $\alpha_3(m_Z) = 0.12$, a mean squark mass of 1 TeV, and varied A_t and $\tan\beta$ in such a way as to maximize the upper bound. The upper solid line is for the NMSSM and the lower solid line is for the MSSM. As M_t becomes very large the two bounds become very close, since here h_t is always close to triviality and hence λ must be small. The dashed line refers to the constrained NMSSM.*

c) Experimental Lower Limits on Λ

Λ has a theoretical upper limit given by $\Lambda_{max} \approx 146$ GeV. Now we shall discuss how experiment may place a *lower* limit on Λ which we shall refer to as Λ_{min}. The meaning of Λ_{min} is as follows. For each value of Λ there are many possible sets of parameters (R_i, m_{h_i}) subject to the bounds in eq.(54). Each of the three (CP-even) Higgs bosons in each set may or may not be discovered at LEP, depending on how light it is and how strongly coupled to the Z it is. We can consider the present $R^2 - m_h$ 95% exclusion plots at LEP [119] and classify each of the three Higgs bosons in each set (for a fixed Λ) as excluded or not excluded. We may find, for some value of Λ, that for *all* the allowed sets at least one out of the three Higgs bosons is always excluded. In this case we classify this value of Λ as being excluded by experiment. We now define Λ_{min} as the largest value of Λ which may be excluded by the LEP data. There will be a different Λ_{min} for each of the expected LEP2 $R^2 - m_h$ 95% exclusion plots (see Fig. 31 and Table 15). If Λ_{min} exceeds Λ_{max} then the model is excluded.

Λ_{min} is approximately determined by the "worst case" of all three CP-even Higgs bosons having equal masses $m_{h_i} \approx \Lambda$, and equal couplings ${R_i}^2 \approx 1/3$. [3] Using this simple approximation, together with current $R^2 - m_h$ exclusion limits [119], LEP1 already places a limit on Λ of $\Lambda > \Lambda_{min} = 59$ GeV, which is just equal to the mass limit for a CP-even Higgs boson with its

[3] This approximate result is exact in the limit that 95% exclusion is equated to 50 produced events.

ZZh coupling suppressed by $R^2 = 1/3$.

The values of Λ_{min} which may be excluded by a future e^+e^- collider of a given energy and integrated luminosity [note that this is total luminosity of all four experiments pooled] are shown in Fig.40 where exclusion is approximately equated to 50 produced events.

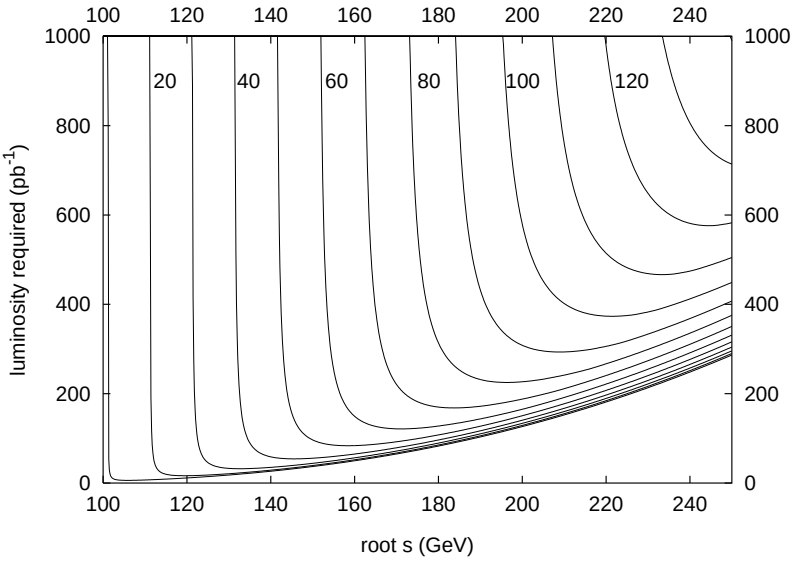

Figure 40: *Excluded values of* Λ *at* e^+e^- *colliders with energy* $\sqrt{s}$.

Focusing specifically on LEP2, we consider energies and integrated luminosities per experiment of $\sqrt{s}$ = 175, 192, 205 GeV and $\int \mathcal{L}$= 150, 150, 300 pb^{-1}, respectively. Using the $R^2 - m_h$ 95% exclusion plots [135], we find that LEP2 will yield the exclusion limits $\Lambda_{min} = 81, 93, 105$ GeV respectively, for the three sets of LEP2 machine parameters above. These excluded values of Λ (corresponding to $R^2 = 1/3$) are not far from the values of SM Higgs boson masses which may be excluded, due to the steep rise of the exclusion curves in the $R^2 - m_h$ plane.

d) Exclusion Limits in the $m_A - \tan\beta$ Plane

It is possible to obtain exclusion limits in this model in the $m_A - \tan\beta$ plane, rather similar to the familiar MSSM plots. The excluded regions are obtained from the following three searches:

(i) For the processes $Z \to Zh_i$, we exploit the fact that the upper 2×2 block of the CP-even mass squared matrix is completely specified (for fixed λ) in the m_A-$\tan\beta$ plane. However, unlike the MSSM, the CP-even spectrum is not completely specified since it depends on three remaining unknown real parameters associated with singlet mixing (i.e. the dots in eq.(52)). Nevertheless, since each choice of these parameters completely specifies the parameters m_{h_i} and R_i, we can scan over the unknown parameters; if the resulting spectrum is always excluded,

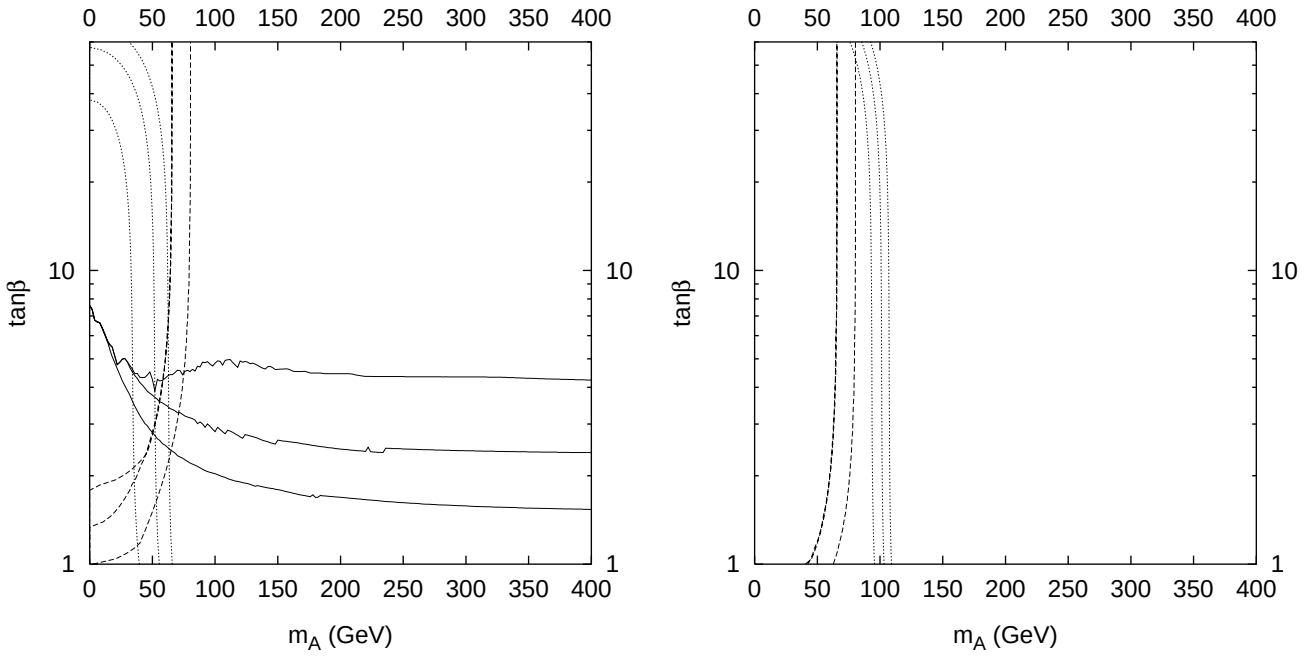

Figure 41: *Excluded regions of the General NMSSM with* $\lambda = 0$ *(left) and* $\lambda = 0.5$ *(right). We have included radiative corrections by assuming degenerate squarks at 1 TeV, with no squark mixing and* $M_t = 175$ *GeV. Note the influence of radiative corrections on the charged Higgs mass for large* $\tan\beta$ *since both* h_t *and* h_b *must be large for such corrections to be important.*

then we conclude that this point in the m_A-$\tan\beta$ plane (for fixed λ) is excluded. For these excluded regions we use the available LEP1 and LEP2 $R^2 - m_h$ 95% exclusion lines.

(ii) An excluded lower limit on m_A, as a function of $\tan\beta$ and λ in this model comes from the non-observation of $Z \to h_i A_j$. The excluded lower limit on m_A in this model is determined by the "worst-case" values of $m_{h_i}, m_{A_j}, S_i, \gamma$ consistent with this value of m_A. It turns out that the worst case experimentally is when the three CP-even Higgs bosons all have equal masses as heavy as possible

$$m_{h_i}{}^2 = m_A{}^2 + (m_Z{}^2 - \lambda^2 v^2)\sin^2 2\beta \tag{56}$$

and equal coupling factors, $S_i{}^2 \approx 1/3$, and the two CP-odd Higgs bosons both have masses equal to m_A and $\gamma = \pi/4$, leading to $R^2_{Zh_iA_j} = 1/6$. For these excluded regions we use the simple approximation that 50 events corresponds to 95% exclusion.

(iii) Finally we shall present excluded regions for charged Higgs production, assuming detection up to the kinematic limit. We note that the charged Higgs signal is the same as in the MSSM as considered in Section 3.

In Fig.41 we show the excluded regions of this model corresponding to the choice of pa-

rameter $\lambda = 0$ [4] for the three sets of LEP2 machine parameters $\sqrt{s} = 175$, 192, 205 GeV and $\int \mathcal{L} =$ 150, 150, 300 pb^{-1}, respectively, and using the LEP1 and LEP2 exclusion data, Fig. 31 and Table 15. In each case the solid lines correspond to exclusion limits from $Z \to Zh_i$ as obtained using procedure (i) above in the NMSSM, the dashed lines correspond to exclusion limits from $Z \to h_i A_j$ as obtained using procedure (ii) above in the NMSSM, and the dotted lines correspond to the exclusion limits from charged Higgs production using procedure (iii) above. These exclusion plots should be compared to similar exclusion plots in the MSSM for $M_t = 175$ GeV and degenerate squarks at 1 TeV, which are the parameters assumed in Fig.41.

In Fig.41 we also show a similar plot but with $\lambda = 0.5$. In this case the solid lines have disappeared beneath the $\tan\beta = 1$ horizon, because for larger λ the bound Λ may be larger, which allows a heavier CP-even spectrum which is consequently more difficult to exclude. The charged Higgs and $h_i A_j$ channels now give improved coverage, however, since larger λ decreases the charged Higgs mass, and also decreases the h_i masses for a fixed S_i coupling.

4.1.2 The Constrained NMSSM

As noted in the introduction, the constrained NMSSM is defined by eq.(50) with μ, μ', $\mu'' \to 0$ and the condition of universal SUSY-breaking gaugino masses $M_{1/2}$, scalar masses m_0 and trilinear couplings A_0 at M_{GUT}. In addition, the effective potential has to have the correct properties, i.e. the $SU(2) \times U(1)$ symmetry has to be broken by Higgs vev's, but the vev's of charged and/or colored fields as sleptons, squarks and charged Higgs scalars have to vanish. Finally, present lower limits on sparticle masses due to direct searches have to be satisfied, and for the top-quark mass M_t we require values between 150 GeV and 200 GeV.

A priori the constrained NMSSM has six parameters at M_{GUT}, three dimensionless couplings λ, k and h_t (the top-quark Yukawa coupling) and three dimensionful ones $M_{1/2}$, m_0 and A_0. The scale set by the known mass of the Z boson reduces the number of free parameters of the model to five. A scan of the parameter space of the model, which is consistent with all the above constraints, has been performed in [129] and [130]. Below we present results, relevant for the Higgs search at LEP2, which are based on the data obtained in [129]. We will discuss the allowed Higgs masses and couplings within the constrained NMSSM.

First note that neither a CP-odd Higgs boson A_j with sufficiently large coupling $R_{Zh_iA_j}$ nor a charged Higgs boson can be sufficiently light within the constrained NMSSM in order to be visible at LEP2. Thus we will concentrate on the neutral CP-even Higgs bosons in the following. Concerning their decays, it follows that neutralinos are too heavy to play a role, thus their branching ratios are close to the standard model ones (essentially $b\bar{b}$) and the same search criteria apply.

In general, the upper limit on the lightest Higgs mass as a function of the top-quark mass

[4] Strictly speaking if $\lambda = 0$ then there is no singlet mixing. However these curves apply to the case where λ is small (say less than 0.1) and singlet mixing is possible. Such small values of λ are always found in the constrained NMSSM.

depends on the magnitude of the SUSY-breaking parameters due to radiative corrections to the Higgs potential. For a gluino mass beyond 1 TeV more and more fine tuning is required between these parameters; thus Fig.39 shows the upper limit on the lightest Higgs boson within the constrained NMSSM as a dashed line, for gluinos lighter than 1 TeV.

As noted before, the lightest Higgs boson within the NMSSM can essentially be a gauge singlet state and thus couple very weakly to the Z boson. Fig.42 (left) shows the logarithm of the coupling R_1 as a function of the mass m_1 of the lightest Higgs boson. Two different regions exist within the constrained NMSSM: A densely populated region with $R_1 \sim 1$ and $m_1 > 50$ GeV, and a tail with $R_1 <$ (or $\ll$) 1 and m_1 as small as ~ 10 GeV. Within the tail, the lightest Higgs boson is essentially a gauge singlet state, which explains the small values of R_1.

The solid line in Fig.42 (left) indicates (for $m_1 > 60$ GeV) the boundary of the region which can be tested at LEP2 with a maximal c.m. energy of 192 GeV and a luminosity of 150 pb^{-1}; the dotted line corresponds to a maximal c.m. energy of 205 GeV and a luminosity of 300 pb^{-1} [both after combining all experiments [135]]. A large part of the region with $R_1 \sim 1$, but only a small part of the tail can be tested.

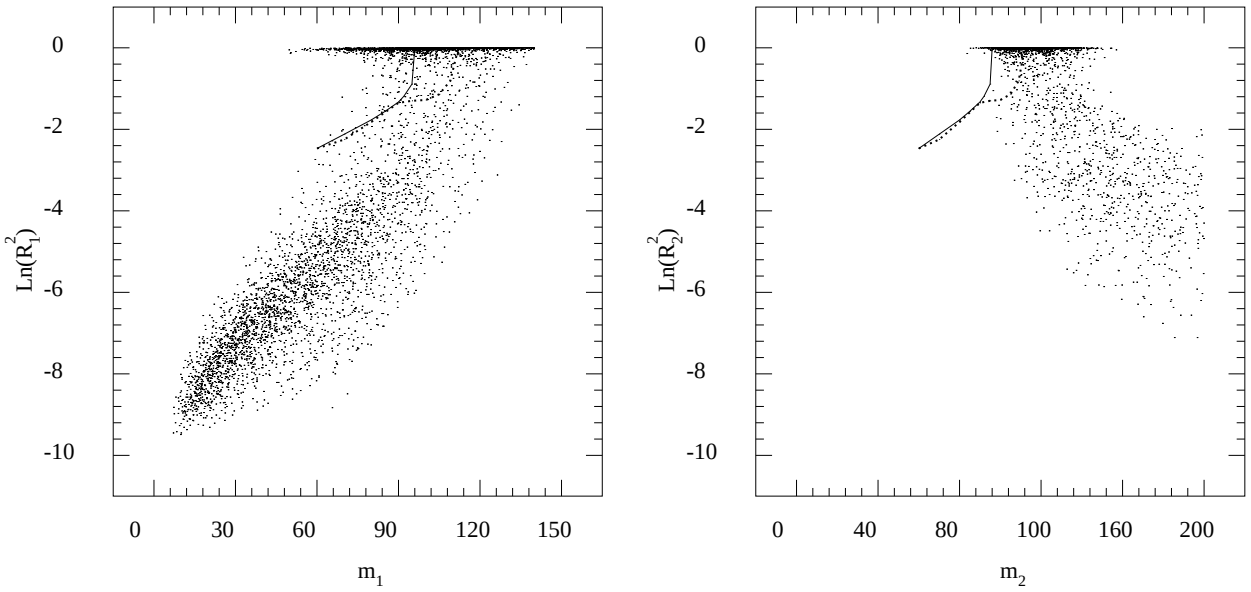

Figure 42: *The logarithm of the $ZZh_{1(2)}$ coupling $R_{1(2)}$ squared vs. the mass of the lightest CP-even state $h_{1(2)}$ in the constrained NMSSM.*

Fortunately, as noted above, the second lightest Higgs boson cannot be too heavy if the lightest Higgs boson is essentially a gauge singlet state [131], [132], [133]. In the region of the tail of Fig.42 (left), within the constrained NMSSM, the mass of the second Higgs boson h_2 varies between 80 GeV and the upper limit indicated in Fig.39 as a dashed line. Its coupling

to the Z boson R_2 is very close to 1 if $R_1 \ll 1$. Fig.42 (right) shows the logarithm of the coupling R_2 as a function of the mass m_2 of the second lightest Higgs. The tail of Fig.42 (left) corresponds to the region with $R_2 \sim 1$ in Fig.42 (right) and *vice versa*. Thus, a small part of the parameter space corresponding to the tail of Fig.42 (left) actually becomes visible at LEP2 through the observation of h_2, which behaves like the lightest Higgs boson of the MSSM in this case.

If a Higgs boson is observed, it will generally be very difficult, however, to distinguish the NMSSM from the MSSM [130]. This seems only possible if a Higgs boson happens to contain a sizeable amount of the singlet state (and hence a measurably reduced coupling to the Z boson), but couples still strongly enough in order to be visible. Finally, the constrained NMSSM could actually be ruled out at LEP2 if a neutral CP-odd Higgs particle, a charged Higgs particle, or an invisibly decaying Higgs particle would be observed.

4.2 Non-linear Supersymmetry

Most of the supersymmetric models investigated so far are models based on linearly realized supersymmetry. However, supersymmetry may as well be realized nonlinearly. Whereas the linear supersymmetric models require supersymmetric partners for all conventional particles in the standard model, the nonlinear models do not lead to SUSY partners. Most global nonlinear supersymmetric models require only one new particle: the Akulov-Volkov field [136], which is a Goldstone fermion. This Goldstino can be removed by going over to curved space, i.e. to supergravity, where it can be gauged away. In the flat space limit, the supergravity multiplet decouples from ordinary matter so that supersymmetry can manifest itself only in the Higgs sector.

The formalism for extending the standard model to a supersymmetric theory in a nonlinear way was developed in ref.[137]. Recently, the general form of the nonlinear supersymmetric standard model has been constructed and the Higgs potential in the flat space limit [138] has been derived.

The Higgs sector of the nonlinear SUSY models is evidently larger than that of the Standard Model. It contains at least two dynamical Higgs doublets and an auxiliary Higgs singlet. In the case that both the dynamical and the auxiliary singlet are included in the theory, the spectra of Higgs bosons in the nonlinear models resemble those of the linear model with two Higgs doublets and one singlet (NMSSM). Both models have three scalar, two pseudoscalar Higgs bosons and one charged Higgs boson pair. However, the structure of the Higgs potential is quite different between nonlinear models and the NMSSM. For the general nonlinear model, the complete potential in the flat space limit is given by [138]

$$\begin{aligned} V &= \tfrac{1}{8}(g_1^2+g_2^2)(|H^1|^2-|H^2|^2)^2+\tfrac{1}{2}g_2^2|H_1^+H_2|^2+|\mu_1+\lambda_1 N|^2\,|H^1|^2 \\ &\quad +|\mu_2+\lambda_2 N|^2\,|H^2|^2+|\lambda_0 H^{1T}\epsilon H^2+\mu_0 N+kN^2|^2 \end{aligned} \tag{57}$$

involving novel types of interactions between the Higgs fields. The two Higgs doublets H^1, H^2 and the singlet N develop the vev's v_1, v_2, and x respectively. The three scalar Higgs bosons are the eigenstates of the scalar-Higgs mass matrix. In a way similar to the NMSSM, an upper bound for the mass m_1 of the lightest scalar Higgs boson S_1 can be derived at the lowest order,[5]

$$m_1^2 \leq m_{1,max}^2 = m_Z^2(\cos^2 2\beta + 2\lambda_g^2 \sin^2 2\beta) \tag{58}$$

where $\lambda_g = \lambda_0^2/(g_1^2 + g_2^2)$. Hence, $m_1 \leq m_Z$ for $\lambda_0 \leq \sqrt{(g_1^2 + g_2^2)/2} \approx 0.52$ and $m_1 \leq 1.92\lambda_0 m_Z$ for $\lambda_0 > 0.52$. In the latter case, the upper bound of λ_0 determines the limit of m_1. For $M_t = 175$ GeV and with the GUT scale as cut-off scale, one obtains $m_1 \leq 130$ GeV. Even though at the c.m. energies of 175, 192, and 205 GeV for LEP2 the production of S_1 may be kinematically possible, the production rate is in general not large enough for S_1 to be detected. The main contributions to the production cross sections come from (i) the Higgs-strahlung process; (ii) the process where S_1 is radiated off leptons or quarks, and (iii) associated pair production $P_j S_1$, where P_j $(j = 1, 2)$ is a pseudoscalar Higgs boson.

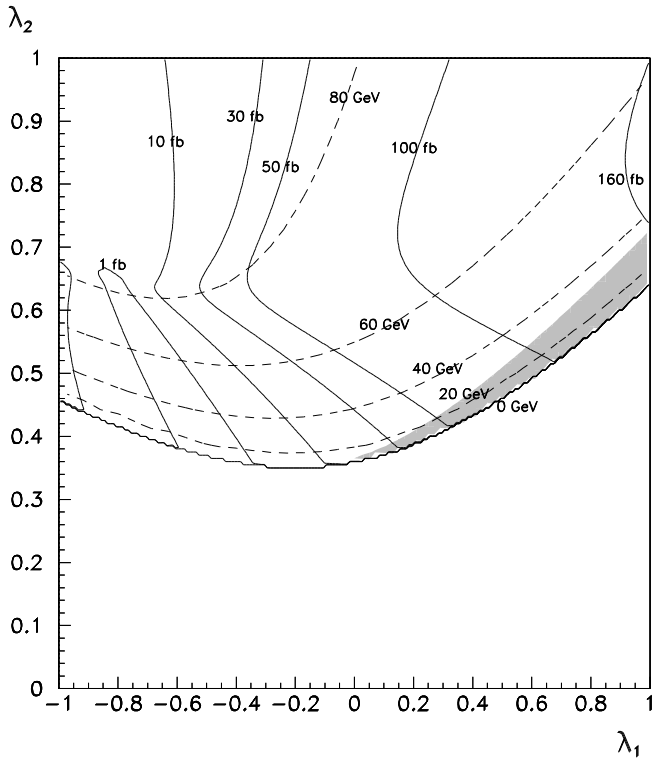

Figure 43: *Contour lines of the lightest scalar Higgs mass m_1 (dashed) and of the production cross section σ (full) at $\sqrt{s} = 175$ GeV, as functions of λ_1, λ_2 for $\tan\beta = 6$, $\lambda_0 = 0.3$, $k = -0.02$, $m_C = 400$ GeV. The shaded area marks the parameter region excluded by LEP1, defined as the region where the production cross section at the Z peak is greater than 1 pb.*

We have first searched for parameter regions where the experimental lower limit on m_1 given by the LEP1 data is minimal; it turned out that there are regions where even $m_1 = 0$ is still

[5] In the present exploratory analysis we have neglected the radiative corrections.

allowed. Fig.43 shows (dashed) the contour lines of m_1 and (full) the contour lines of the cross section σ for the production of S_1 in e^+e^- collisions at $\sqrt{s} = 175$ GeV, in the λ_1, λ_2 plane for a representative set of the parameters $\tan\beta$, λ_0, k and m_C (m_C being the charged-Higgs mass). In the shaded region, the cross section σ at $\sqrt{s} = m_Z$ is greater than 1 pb, which corresponds to the discovery limit of LEP1 for $m_1 \approx 65$ GeV [135]. This region is excluded by LEP1 since the discovery limit decreases with decreasing m_1. The discovery limit at $\sqrt{s} = 175$ GeV with a luminosity of 500 pb^{-1} is about 50 fb for $m_1 = 80$ GeV (about 30 fb for $m_1 = 40$ GeV) [135]. Thus the region accessible at LEP2 includes the area in Fig.43 where $m_1 < 80$ GeV and $\sigma > 50$ fb. As with LEP1, a massless S_1 could be undetectable.

For some parameter sets, the nonlinear SUSY model may be tested even if the lightest scalar is undetectable. If the production cross section of S_1 is smaller than the discovery limit, one can examine whether the production of the other Higgs bosons is kinematically possible and whether their production rates are large enough for discovery.

For the higher energies 192 and 205 GeV, the effects are similar to the 175 GeV case. Though the accessible region increases, an undetectable massless S_1 Higgs boson is still possible. Energies of 240 GeV and more are needed to test this nonlinear supersymmetric model conclusively.

4.3 Majoron Decays of Higgs Particles

There are a variety of well motivated extensions of the Standard Model (SM) with a spontaneously broken global symmetry. This symmetry could either be lepton number or a combination of family lepton numbers [139, 140]. These models are characterized by a more complex symmetry breaking sector which contains additional Higgs bosons. It is specially interesting for our purposes to consider models where such symmetry is broken at the electroweak scale [141, 142]. In general, these models contain a massless Goldstone boson, called majoron (J), which interacts very weakly with normal matter. In such models, the normal doublet Higgs boson is expected to have sizeable invisible decay modes to the majoron, due to the strong Higgs–majoron coupling. This can have a significant effect on the Higgs phenomenology at LEP2. In particular, the invisible decay could contribute to the signal of two acoplanar jets and missing momentum. This feature of majoron models allows one to strongly constrain the Higgs mass in spite of the occurrence of extra parameters compared to the SM. In particular, the LEP1 limit on the predominantly doublet Higgs mass is close to the SM limit irrespective of the decay mode of the Higgs boson [143, 144].

We consider a model containing two Higgs doublets ($\phi_{1,2}$) and a singlet (σ) under the $SU(2)_L \times U(1)_Y$ group. The singlet Higgs field carries a non-vanishing $U(1)_L$ charge, which could be lepton number. Here we only need to specify the scalar potential of the model:

$$\begin{aligned} V &= \mu_i^2 \phi_i^\dagger \phi_i + \mu_\sigma^2 \sigma^\dagger \sigma + \lambda_i (\phi_i^\dagger \phi_i)^2 + \lambda_3 (\sigma^\dagger \sigma)^2 + \\ &\quad \lambda_{12} (\phi_1^\dagger \phi_1)(\phi_2^\dagger \phi_2) + \lambda_{13} (\phi_1^\dagger \phi_1)(\sigma^\dagger \sigma) + \lambda_{23} (\phi_2^\dagger \phi_2)(\sigma^\dagger \sigma) \end{aligned}$$

$$+\delta(\phi_1^\dagger\phi_2)(\phi_2^\dagger\phi_1) + \tfrac{1}{2}\kappa[(\phi_1^\dagger\phi_2)^2 + \quad h.c.] \tag{59}$$

where the sum over repeated indices i=1,2 is assumed.

Minimization of the above potential leads to the spontaneous $SU(2)_L \times U(1)_Y \times U(1)_L$ symmetry breaking and allows us to identify a total of three massive CP even scalars H_i (i=1,2,3), plus a massive pseudoscalar A and the massless majoron J. We assume that at the LEP2 energies only three Higgs particles can be produced: the lightest CP-even scalar h, the CP-odd massive scalar A, and the massless majoron J. Notwithstanding, our analysis is also valid for the situation where the Higgs boson A is absent [145], which can be obtained by setting the couplings of this field to zero.

At LEP2, the main production mechanisms of invisible Higgs bosons are the Higgs-strahlung process ($e^+e^- \to hZ$) and the associated production of Higgs bosons pairs ($e^+e^- \to Ah$), which rely upon the couplings hZZ and hAZ respectively. The important feature of the above model is that, because of its singlet nature, the majoron is not sizeably coupled to the gauge bosons and cannot be produced directly, thereby evading strong LEP1 constraints. The hZZ and hAZ couplings depend on the model parameters via the appropriate mixing angles, but they can be effectively expressed in terms of the two parameters ϵ_A, ϵ_B:

$$\mathcal{L}_{hZZ} = \epsilon_B \left(\sqrt{2}G_F\right)^{1/2} m_Z^2 Z_\mu Z^\mu h \tag{60}$$

$$\mathcal{L}_{hAZ} = -\epsilon_A \frac{g}{\cos\theta_W} Z^\mu h \overleftrightarrow{\partial_\mu} A \tag{61}$$

The couplings $\epsilon_{A(B)}$ are model dependent. For instance, the SM Higgs sector has $\epsilon_A = 0$ and $\epsilon_B = 1$, while a majoron model with one doublet and one singlet leads to $\epsilon_A = 0$ and $\epsilon_B^2 \leq 1$.

The signatures of the Higgs-strahlung process and the associated production depend upon the allowed decay modes of the Higgs bosons h and A. For Higgs boson masses m_h accessible at LEP2 energies the main decay modes for the CP-even state h are $b\bar{b}$ and JJ. We treat the branching fraction $B = BR(h \to JJ)$ as a free parameter. In most models BR is basically unconstrained and can vary from 0 to 1. Moreover we also assume that, as it happens in the simplest models, the branching fraction for $A \to b\bar{b}$ is nearly one, and the invisible A decay modes $A \to hJ$, $A \to JJJ$ do not exist (although CP-allowed). Therefore our analysis depends upon five parameters: m_h, m_A, ϵ_A, ϵ_B, and B. This parameterization is quite general and very useful from the experimental point of view: limits on m_h, m_A, ϵ_A, ϵ_B, and B can be later translated into bounds on the parameter space of many specific models.

The parameters defining our general parameterization can be constrained by the LEP1 data. In fact Refs.[143, 146] analyze some signals for invisible decaying Higgs bosons, and conclude that LEP1 excludes m_h up to 60 GeV provided that $\epsilon_B > 0.4$. Similar results are obtained in fig.(32).

The $\bar{b}b + \not{p}_T$ topology is our main subject of investigation and we carefully evaluate signals and backgrounds, choosing the cuts that enhance the signal over the backgrounds. Our goal is to evaluate the limits on m_h, m_A, ϵ_A, ϵ_B, and B that can be obtained at LEP2 from this final

state. There are three sources of signal events with the topology $\not{p}_T$+ 2 b-jets: one due to the associated production and two due to the Higgs–strahlung.

$$e^+e^- \rightarrow (Z \rightarrow b\bar{b}) + (h \rightarrow JJ) \quad (62)$$
$$e^+e^- \rightarrow (Z \rightarrow \nu\bar{\nu}) + (h \rightarrow b\bar{b}) \quad (63)$$
$$e^+e^- \rightarrow (A \rightarrow b\bar{b}) + (h \rightarrow JJ) \quad (64)$$

The signature of this final state is the presence of two jets containing b quarks and missing momentum ($\not{p}_T$). It is interesting to notice that for light m_h and m_A, the associated production dominates over the Higgs–strahlung mechanism [146].

There are several sources of background for this topology:

$$e^+e^- \rightarrow Z/\gamma\ Z/\gamma \rightarrow q\bar{q}\ \nu\bar{\nu} \qquad e^+e^- \rightarrow (e^+e^-)\gamma\gamma \rightarrow [e^+e^-]q\bar{q}$$
$$e^+e^- \rightarrow Z^*/\gamma^* \rightarrow q\bar{q}[n\gamma] \qquad e^+e^- \rightarrow W^+W^- \rightarrow q\bar{q}'\ [\ell]\nu$$
$$e^+e^- \rightarrow W[e]\nu \rightarrow q\bar{q}'\ [e]\nu \qquad e^+e^- \rightarrow Z\nu\bar{\nu} \rightarrow q\bar{q}\ \nu\bar{\nu}$$

where the particles in square brackets escape undetected and the jet originating from the quark q is identified (misidentified) as being a b-jet.

At this point the simplest and most efficient way to improve the signal-over-background ratio is to use that the A and h decays lead to jets containing b-quarks. So we require that the events contain two b-tagged jets. Moreover, the background can be further reduced requiring a large $\not{p}_T$. We therefore have imposed a set of cuts which is based on the cuts used by the DELPHI collaboration for the SM Higgs boson search [63].

Depending on the h and A mass ranges, including or excluding an invariant mass cut $m \pm 10$ GeV [where m is the mass of the particle decaying visibly] gives better or weaker limits on the ZhA and ZZh couplings. Therefore, for each mass combination four limits are calculated (with or without invariant mass cut, with thrust cut or the cut on the minimal two-jet energy) and the best limit is kept.

We denote the number of signal events for the three production processes (62 – 64), after imposing all cuts, N_{JJ}, N_{SM}, and N_A respectively, assuming that $\epsilon_A = \epsilon_B = 1$. Then the expected number of signal events when we take into account couplings and branching ratios is

$$N_{exp} = \epsilon_B^2 [BN_{JJ} + (1-B)N_{SM}] + \epsilon_A^2 BN_A \quad (65)$$

In general, this topology is dominated by the associated production, provided it is not suppressed by small couplings ϵ_A or phase space. The most important background after the cuts is $Z/\gamma Z/\gamma$ production. The total numbers of background events summed over all relevant channels are 2.3, 2.8 and 5.9 for $\sqrt{s} = 175$, 190 and 205 GeV respectively.

In order to obtain the limits shown in Figs.44-45, we assumed that only the background events are observed, and we evaluated the 95 % CL region of the parameter space that can be excluded with this result. By taking the weakest bound, as we vary B, we obtained the

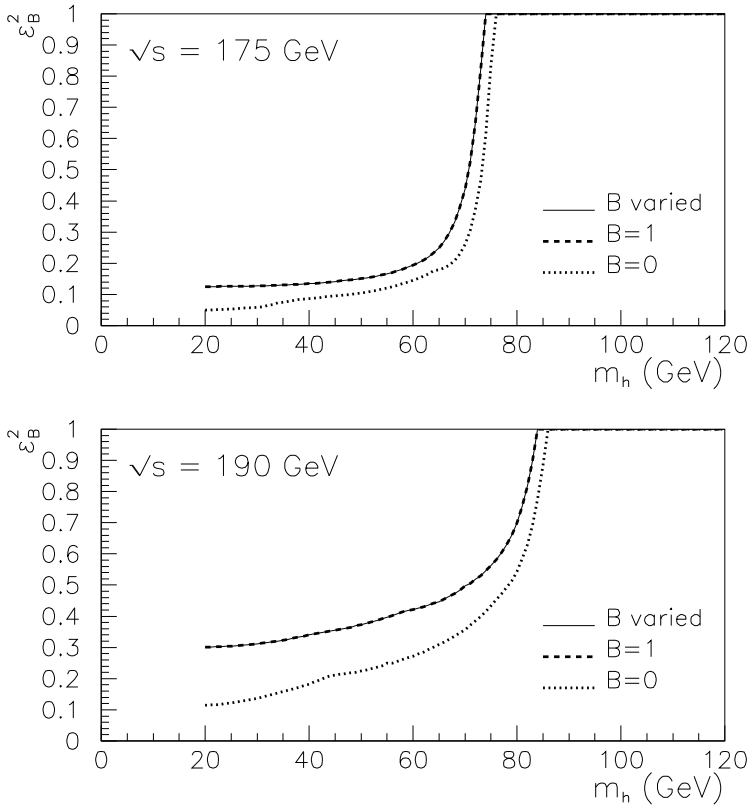

Figure 44: *Limits on ϵ_B^2 as a function of m_h for 500 pb^{-1} and $\sqrt{s}$ =175 GeV and for 300 pb^{-1} and $\sqrt{s}$ = 190 GeV; for different values of $B = Br(h \to JJ)$*

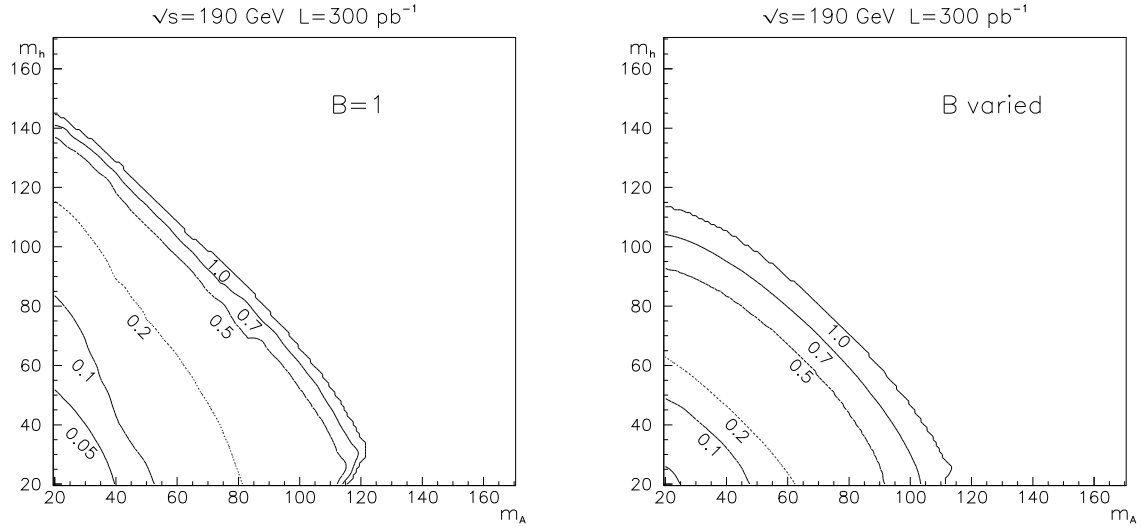

Figure 45: *Limits on ϵ_A^2 as a function of m_h, m_A for $\sqrt{s}$ = 190 GeV. The left plot shows the limits obtained for $B = Br(h \to JJ) = 1$, in the right plot B is varied from 0 to 1.*

absolute bound on ϵ_A, ϵ_B, and m_h independent of the h decay mode. The limits on ϵ_A obtained by searches for the $b\bar{b} + \not{p}_T$ final states are stronger than those obtained from the $b\bar{b}b\bar{b}$ topology. Moreover, the bounds in the limiting case $\epsilon_A = 0$ apply for the simplest model of invisibly decaying Higgs bosons, where just one singlet is added to the SM. A more complete presentation of these results will be given in Ref.[147].

4.4 Strongly Interacting Higgs Particle

The radiative corrections at LEP1 depend only logarithmically on the Higgs mass, and the measurements, although very precise, are not sufficient to determine the structure of the Higgs sector. It is therefore necessary to keep an open mind to the possibility that the Higgs sector is more complicated than in the Standard Model. Beyond the Standard Model various extensions have been suggested. One of the possibilities is supersymmetry which has been previously discussed. Another possibility is strong interactions in the form of technicolor, which at least in its simplest form is ruled out by the LEP1 data. Strong interactions in the Standard Model itself imply a heavy Higgs boson and can presumably be studied at the LHC.

However, the idea of strong interactions is more general. In particular it is possible that strong interactions are present in the singlet sector of the theory. In general the choice of representations in a gauge theory is arbitrary and presumably a clue to a deeper underlying theory. Singlets do not have quantum numbers under the gauge group of the Standard Model. They therefore do not feel the strong or electroweak forces, but they can couple to the Higgs particle. As a consequence, radiative corrections to weak processes are not sensitive to the presence of singlets in the theory, because no Feynman graphs containing singlets appear at the one–loop level. Because effects at the two–loop level are below the experimental precision, the presence of a singlet sector is not ruled out by any of the LEP1 precision data.

It is therefore not unreasonable to assume that there exists a hidden sector that affects Higgs physics only. Such an extension of the Standard Model involving singlet fields preserves the essential simplicity of the model, while at the same time acting as a realistic model for non–standard Higgs properties. Here we will study the coupling of a Higgs boson to an $O(N)$ symmetric set of scalars, which is one of the simplest possibilities introducing only a few extra parameters in the theory. The extra scalars may give rise to large invisible decay width of the Higgs particle. When the coupling is large enough, the Higgs resonance can become wide even for a light Higgs boson. This has led to the conclusion that this Higgs particle becomes undetectable at the LHC [148]. As one can measure missing energy more precisely at e^+e^- colliders than at a hadron machine, LEP2 can give important constraints on the parameters of the model. However, it is clear that there will be a range of parameters where this Higgs boson can be seen neither at LEP nor at the LHC.

a) The Model

The Higgs sector of the model is described by the following Lagrangian,

$$\begin{aligned}\mathcal{L} &= -\partial_\mu\phi^+\partial^\mu\phi - \lambda(\phi^+\phi - v^2/2)^2 \\ &- 1/2\,\partial_\mu\vec{\varphi}\partial^\mu\vec{\varphi} - 1/2\,m^2\,\vec{\varphi}^2 - \kappa/(8N)\,(\vec{\varphi}^2)^2 - \omega/(2\sqrt{N})\;\vec{\varphi}^2\,\phi^+\phi\end{aligned}$$

where ϕ is the normal Higgs doublet and the vector $\vec{\varphi}$ is an N–component real vector of scalar fields, which we call phions. Couplings to fermions and vector bosons are the same as in the Standard Model. The ordinary Higgs field acquires the vacuum expectation value $v/\sqrt{2}$. We assume that the $\vec{\varphi}$–field acquires no vacuum expectation value, which can be assured by taking ω positive. After the spontaneous symmetry breaking one is left with the ordinary Higgs boson, coupled to the phions into which it decays. Also the phions receive an induced mass from the spontaneous symmetry breaking. The factor N is taken to be large, so that the model can be analyzed in the $1/N$ expansion. By taking this limit, the phion mass stays small, but because there are many phions, the decay width of the Higgs boson can become large. Therefore the main effect of the presence of the phions is to give a large invisible decay rate to the Higgs boson. The invisible decay width is given by

$$\Gamma_H = \frac{\omega^2 v^2}{32\pi m_H} \tag{66}$$

The Higgs width is compared with the width in the Standard Model for various choices of the coupling ω in Fig.46. The model is different from Majoron models, since the width is not necessarily small. The model is similar to the technicolor–like model of Ref.[149].

Consistency of the model requires two conditions. One condition is the absence of a Landau pole below a certain scale Λ. The other follows from the stability of the vacuum up to a certain scale. An example of such limits is given in Fig.47, where $\kappa = 0$ was taken at the scale $2m_Z$, which allows for the widest range. For the model to be valid beyond a scale Λ one should be below the indicated upper lines in the figure. One should be to the right of the indicated lower lines to have stability of the vacuum.

For the search for the Higgs boson there are basically two channels; one is the standard decay, which is reduced in branching ratio due to the decay into phions. The other is the invisible decay, which rapidly becomes dominant, eventually making the Higgs resonance very wide, Fig.46. In order to find the bounds we neglect the coupling κ as this is a small effect. We also neglect the phion mass. For non–zero values of the phion mass the bounds can be found by rescaling the decay widths with the appropriate phase space factor. The present bounds, coming from LEP1 invisible search, are included as a dashed curve in Fig.48 below.

b) LEP2 Bounds

In the case of LEP2 the limits on the Higgs mass and couplings in the present model come essentially from the invisible decay, as the branching ratio into $\bar{b}b$ quarks drops rapidly with

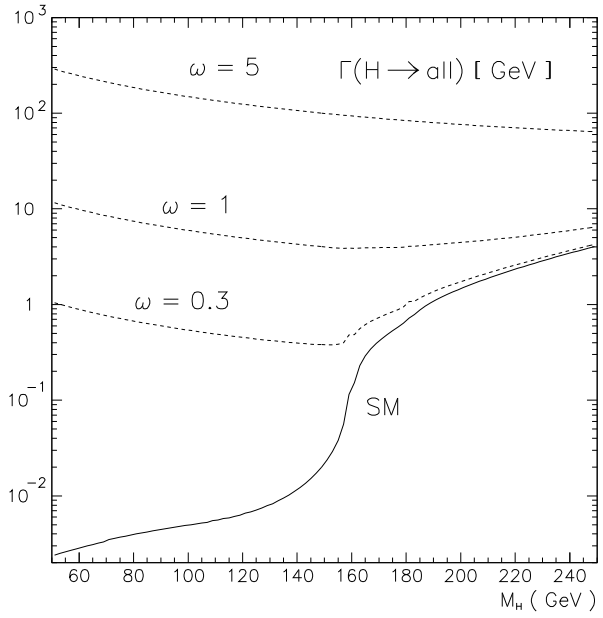

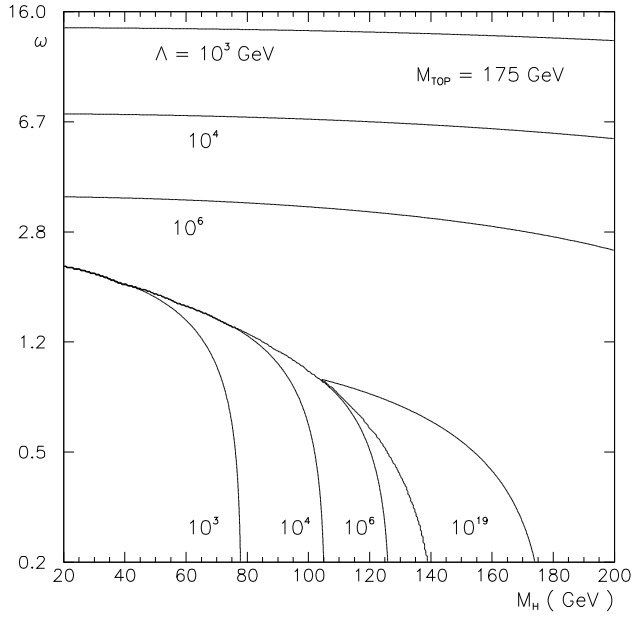

Figure 46: (left) *Higgs width in the phion model, in comparison with the Standard Model.*

Figure 47: (right) *Theoretical limits on the parameters of the model in the ω vs. M_H plane. For a given scale Λ, the physical region is below the upper lines and to the right of the lower lines.*

increasing φ–Higgs coupling. To define the signal we look at events around the maximum of the Higgs resonance, with an invariant mass $m_H \pm \Delta$ for $\Delta = 5$ GeV, which corresponds to a typical mass resolution. Exclusion limits are determined by Poisson statistics as defined in Appendix 5.3. The results are given by the full lines in Fig.48. One notices the somewhat reduced sensitivity for a Higgs mass near the Z boson mass and a looser bound for small Higgs masses because there the effect of the widening of the resonance prevails. The small ω region is covered by visible search. There is a somewhat better limit on the Higgs mass for moderate ω in comparison with the $\omega = 0$ case; this is due to events from the extended tail of the Higgs boson which is due to the increased width.

We conclude from the analysis that LEP2 can put significant limits on the parameter space of such a model. However there is a range where the Higgs boson will not be discovered, even if it does exist in this mass range. This also holds true when one considers the search at the LHC. Assuming moderate to large values of ω, i.e. in the already difficult intermediate mass range, it is unlikely that sufficient signal events are left at the LHC. In that case the only information can come directly from high–energy e^+e^- colliders or indirectly from higher precision experiments at LEP1.

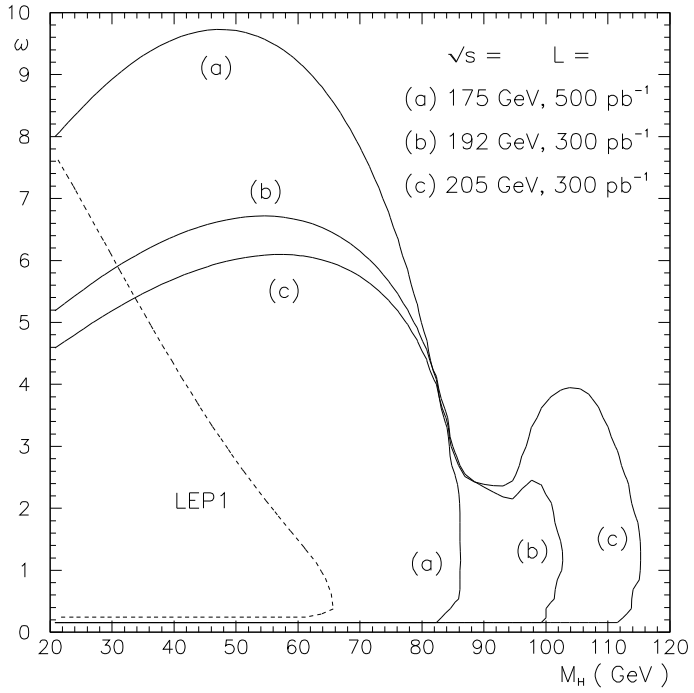

Figure 48: *Exclusion limits at LEP2 (full lines), and LEP1 (dashed). The region where ω is small can be covered by the search for visible Higgs decays.*

5 Appendices

5.1 Higgs-strahlung and WW Fusion

Compact forms can be derived for the cross section of the process [10, 11]

$$e^+e^- \to H + \bar{\nu}\nu \tag{67}$$

by choosing the energy E_H and the polar angle θ of the Higgs particle as the basic variables in the e^+e^- c.m. frame. The overall cross section that will be observed experimentally, receives contributions $3 \times \mathcal{G}_S$ from Higgs-strahlung with Z decays into three types of neutrinos, $\mathcal{G}_W$ from WW fusion, and $\mathcal{G}_I$ from the interference term between fusion and Higgs-strahlung for $\bar{\nu}_e\nu_e$ final states. We find:

$$\frac{d\sigma(H\bar{\nu}\nu)}{dE_H\, d\cos\theta} = \frac{G_F^3 m_Z^8 p}{\sqrt{2}\,\pi^3 s}\,(3\mathcal{G}_S + \mathcal{G}_I + \mathcal{G}_W) \tag{68}$$

with

$$\mathcal{G}_S = \frac{v_e^2 + a_e^2}{96}\,\frac{s s_\nu + s_1 s_2}{(s - m_Z^2)^2\,[(s_\nu - m_Z^2)^2 + m_Z^2\Gamma_Z^2]} \tag{69}$$

$$\mathcal{G}_I = \frac{(v_e + a_e)c_W^4}{8}\,\frac{s_\nu - m_Z^2}{(s - m_Z^2)\,[(s_\nu - m_Z^2)^2 + m_Z^2\Gamma_Z^2]} \times \left[2 - (h_1+1)\log\frac{h_1+1}{h_1-1} - (h_2+1)\log\frac{h_2+1}{h_2-1} + (h_1+1)(h_2+1)\frac{\mathcal{L}}{\sqrt{r}}\right] \tag{70}$$

$$\mathcal{G}_W = \frac{c_W^8}{s_1 s_2 r}\left\{(h_1+1)(h_2+1)\left[\frac{2}{h_1^2-1} + \frac{2}{h_2^2-1} - \frac{6s_\chi^2}{r} + \left(\frac{3t_1t_2}{r} - c_\chi\right)\frac{\mathcal{L}}{\sqrt{r}}\right] - \left[\frac{2t_1}{h_2-1} + \frac{2t_2}{h_1-1} + \left(t_1 + t_2 + s_\chi^2\right)\frac{\mathcal{L}}{\sqrt{r}}\right]\right\} \tag{71}$$

where $a_e = -1$ and $v_e = -1 + 4s_W^2$. The cross section is written explicitly in terms of the Higgs momentum $p = (E_H^2 - m_H^2)^{1/2}$, and the energy $\epsilon_\nu = \sqrt{s} - E_H$ and invariant mass squared $s_\nu = \epsilon_\nu^2 - p^2$ of the neutrino pair. The expression for $\mathcal{G}_W$ had first been obtained in Ref.[10]. The following abbreviations have been introduced:

$$s_{1,2} = \sqrt{s}(\epsilon_\nu \pm p\cos\theta) \qquad t_{1,2} = h_{1,2} + c_\chi h_{2,1}$$
$$h_{1,2} = 1 + 2m_W^2/s_{1,2} \qquad r = h_1^2 + h_2^2 + 2c_\chi h_1 h_2 - s_\chi^2$$
$$c_\chi = 1 - 2ss_\nu/(s_1 s_2) \qquad \mathcal{L} = \log\frac{h_1h_2 + c_\chi + \sqrt{r}}{h_1h_2 + c_\chi - \sqrt{r}}$$
$$s_\chi^2 = 1 - c_\chi^2$$

To derive the total cross section $\sigma(e^+e^- \to H\bar{\nu}\nu)$, the differential cross section must be integrated over the region $-1 < \cos\theta < 1$ and $m_H < E < \frac{1}{2}\sqrt{s}\,(1 + m_H^2/s)$.

5.2 Higgs Mass Computation: analytical approximation in the limit of a common scale M_S and restricted mixing parameters

In this appendix we present the results of the analytical approximation which reproduces the two–loop RG improved effective potential results in the case of two light Higgs doublets below M_S ($m_A \leq M_S$)

[89]. The two CP-even and the charged Higgs masses read

$$m^2_{h(H)} = \frac{TrM^2 \mp \sqrt{(TrM^2)^2 - 4\det M^2}}{2} \tag{72}$$

$$m^2_{H^\pm} = m^2_A + (\lambda_5 - \lambda_4)v^2, \tag{73}$$

where

$$TrM^2 = M^2_{11} + M^2_{22} \ ; \quad \det M^2 = M^2_{11}M^2_{22} - \left(M^2_{12}\right)^2, \tag{74}$$

with

$$\begin{aligned} M^2_{12} &= 2v^2[\sin\beta\cos\beta(\lambda_3+\lambda_4) + \lambda_6\cos^2\beta + \lambda_7\sin^2\beta] - m^2_A\sin\beta\cos\beta \\ M^2_{11} &= 2v^2[\lambda_1\cos^2\beta + 2\lambda_6\cos\beta\sin\beta + \lambda_5\sin^2\beta] + m^2_A\sin^2\beta \\ M^2_{22} &= 2v^2[\lambda_2\sin^2\beta + 2\lambda_7\cos\beta\sin\beta + \lambda_5\cos^2\beta] + m^2_A\cos^2\beta. \end{aligned} \tag{75}$$

The mixing angle α is equally determined by

$$\sin 2\alpha = \frac{2M^2_{12}}{\sqrt{(TrM^2)^2 - 4\det M^2}} \qquad \cos 2\alpha = \frac{M^2_{11} - M^2_{22}}{\sqrt{(TrM^2)^2 - 4\det M^2}} \tag{76}$$

The above quartic couplings are given by

$$\begin{aligned} \lambda_1 &= \frac{g_1^2+g_2^2}{4}\left(1 - \frac{3}{8\pi^2}\,h_b^2\,t\right) + \frac{3}{8\pi^2}\,h_b^4\left[t + \frac{X_b}{2} + \frac{1}{16\pi^2}\left(\frac{3}{2}\,h_b^2 + \frac{1}{2}\,h_t^2 - 8\,g_3^2\right)\left(X_b\,t + t^2\right)\right] \\ &\quad - \frac{3}{96\pi^2}\,h_t^4\,\frac{\mu^4}{M_S^4}\left[1 + \frac{1}{16\pi^2}\left(9\,h_t^2 - 5h_b^2 - 16g_3^2\right)t\right] \end{aligned} \tag{77}$$

$$\begin{aligned} \lambda_2 &= \frac{g_1^2+g_2^2}{4}\left(1 - \frac{3}{8\pi^2}\,h_t^2\,t\right) + \frac{3}{8\pi^2}\,h_t^4\left[t + \frac{X_t}{2} + \frac{1}{16\pi^2}\left(\frac{3\,h_t^2}{2} + \frac{h_b^2}{2} - 8\,g_3^2\right)\left(X_t\,t + t^2\right)\right] \\ &\quad - \frac{3}{96\pi^2}\,h_b^4\,\frac{\mu^4}{M_S^4}\left[1 + \frac{1}{16\pi^2}\left(9\,h_b^2 - 5h_t^2 - 16g_3^2\right)t\right] \end{aligned} \tag{78}$$

$$\begin{aligned} \lambda_3 &= \frac{g_2^2-g_1^2}{4}\left(1 - \frac{3}{16\pi^2}(h_t^2+h_b^2)\,t\right) + \frac{6}{16\pi^2}\,h_t^2\,h_b^2\left[t + \frac{A_{tb}}{2} + \frac{1}{16\pi^2}\left(h_t^2 + h_b^2 - 8\,g_3^2\right)\left(A_{tb}\,t + t^2\right)\right] \\ &\quad + \frac{3}{96\pi^2}\,h_t^4\left[\frac{3\mu^2}{M_S^2} - \frac{\mu^2 A_t^2}{M_S^4}\right]\left[1 + \frac{1}{16\pi^2}\left(6\,h_t^2 - 2h_b^2 - 16g_3^2\right)t\right] \\ &\quad + \frac{3}{96\pi^2}\,h_b^4\left[\frac{3\mu^2}{M_S^2} - \frac{\mu^2 A_b^2}{M_S^4}\right]\left[1 + \frac{1}{16\pi^2}\left(6\,h_b^2 - 2h_t^2 - 16g_3^2\right)t\right] \end{aligned} \tag{79}$$

$$\lambda_4 = -\frac{g_2^2}{2}\left(1-\frac{3}{16\pi^2}(h_t^2+h_b^2)\,t\right) - \frac{6}{16\pi^2}\,h_t^2\,h_b^2\,\left[t+\frac{A_{tb}}{2}+\frac{1}{16\pi^2}\left(h_t^2+h_b^2-8\,g_3^2\right)\left(A_{tb}\,t+t^2\right)\right]$$
$$+\frac{3}{96\pi^2}\,h_t^4\,\left[\frac{3\mu^2}{M_s^2}-\frac{\mu^2 A_t^2}{M_s^4}\right]\left[1+\frac{1}{16\pi^2}\left(6\,h_t^2-2h_b^2-16g_3^2\right)t\right]$$
$$+\frac{3}{96\pi^2}\,h_b^4\,\left[\frac{3\mu^2}{M_s^2}-\frac{\mu^2 A_b^2}{M_s^4}\right]\left[1+\frac{1}{16\pi^2}\left(6\,h_b^2-2h_t^2-16g_3^2\right)t\right] \tag{80}$$

$$\lambda_5 = -\frac{3}{96\pi^2}\,h_t^4\,\frac{\mu^2 A_t^2}{M_s^4}\left[1-\frac{1}{16\pi^2}\left(2h_b^2-6\,h_t^2+16g_3^2\right)t\right]$$
$$-\frac{3}{96\pi^2}\,h_b^4\,\frac{\mu^2 A_b^2}{M_s^4}\left[1-\frac{1}{16\pi^2}\left(2h_t^2-6\,h_b^2+16g_3^2\right)t\right] \tag{81}$$

$$\lambda_6 = \frac{3}{96\pi^2}\,h_t^4\,\frac{\mu^3 A_t}{M_s^4}\left[1-\frac{1}{16\pi^2}\left(\frac{7}{2}h_b^2-\frac{15}{2}h_t^2+16g_3^2\right)t\right] \tag{82}$$
$$+\frac{3}{96\pi^2}\,h_b^4\,\frac{\mu}{M_s}\left(\frac{A_b^3}{M_s^3}-\frac{6A_b}{M_s}\right)\left[1-\frac{1}{16\pi^2}\left(\frac{1}{2}h_t^2-\frac{9}{2}h_b^2+16g_3^2\right)t\right]$$

$$\lambda_7 = \frac{3}{96\pi^2}\,h_b^4\,\frac{\mu^3 A_b}{M_s^4}\left[1-\frac{1}{16\pi^2}\left(\frac{7}{2}h_t^2-\frac{15}{2}h_b^2+16g_3^2\right)t\right] \tag{83}$$
$$+\frac{3}{96\pi^2}\,h_t^4\,\frac{\mu}{M_s}\left(\frac{A_t^3}{M_s^3}-\frac{6A_t}{M_s}\right)\left[1-\frac{1}{16\pi^2}\left(\frac{1}{2}h_b^2-\frac{9}{2}h_t^2+16g_3^2\right)t\right]$$

They contain the same kind of corrections as eq.(26), including the leading D-term contributions, and we have defined,

$$X_{t(b)} = \frac{2A_{t(b)}^2}{M_s^2}\left(1-\frac{A_{t(b)}^2}{12M_s^2}\right); \qquad A_{tb} = \frac{1}{6}\left[-\frac{6\mu^2}{M_s^2}-\frac{(\mu^2-A_bA_t)^2}{M_s^4}+\frac{3(A_t+A_b)^2}{M_s^2}\right]. \tag{84}$$

All quantities in the approximate formulae are defined at the scale M_t. and $h_t = m_t(M_t)/(v\sin\beta)$ $h_b = m_b(M_t)/(v\cos\beta)$ are the top and bottom Yukawa couplings in the two-Higgs doublet model.

For $m_A \leq M_t$, $\tan\beta$ is fixed at the scale m_A, while for $m_A \geq M_t$, $\tan\beta$ is given by [79]

$$\tan\beta(M_t) = \tan\beta(m_A)\left[1+\frac{3}{32\pi^2}(h_t^2-h_b^2)\log\frac{m_A^2}{M_t^2}\right]. \tag{85}$$

For the case in which the CP-odd Higgs mass m_A is lower than M_s, but still larger than the top-quark mass scale, we decouple, in the numerical computations, the heavy Higgs doublet and define an

effective quartic coupling for the light Higgs, which is related to the running Higgs mass at the scale m_A through $\lambda(m_A) = (m_h(m_A)/2v^2)$. The low energy value of the quartic coupling is then obtained by running the SM renormalization-group equations from the scale m_A down to the scale M_t. In the analytical approximation, for simplicity the effect of decoupling of the heavy Higgs doublet at an intermediate scale is ignored but is partially compensated by relating the value of $\tan\beta$ at the scale M_t with its corresponding value at the scale m_A through its renormalization-group running, eq.(85). A subroutine implementing the above computations is available [93].

5.3 Deriving 5σ Discovery and 95% C.L. Exclusion Contours

The minimum luminosity needed to assess the discovery or to exclude the existence of a Higgs boson with mass $m_{\rm H}$ can directly be determined from the numbers of events expected from the signal and from the background processes at the three different center-of-mass energies. Given the rather small numbers of events involved in this process, it is preferable to use Poisson statistics to derive the result.

Several definitions for the "minimum luminosity needed" were proposed. For instance, the minimum luminosity needed for a 5σ discovery can be defined either *(i)* as the luminosity needed by the *typical* experiment, *i.e.* by an experiment that would actually observe the number of events expected; or *(ii)* as the luminosity for which 50% of the experiments would make the discovery at the requested 5σ level, where the *a priori* unknown numbers of events observed are properly generated according to a Poisson distribution around their expected values. Although both definitions lead to the same numerical result, a preference was given to the second one, which allows in addition the proportion of the experiments required to make the discovery to be varied.

In detail, let b and s be the numbers of background and signal events expected with a luminosity of 1 fb^{-1}, and α be the fraction needed for the discovery. The first definition corresponds to finding the smallest value of α that fulfills the condition

$$1 - \exp(-\alpha b) \sum_{i=0}^{N-1} \frac{(\alpha b)^i}{i!} \leq 5.7 \times 10^{-7}, \tag{1}$$

where $N = \alpha(s+b)$, *i.e.* that renders the probability of a background fluctuation smaller than the probability of a 5σ effect in the case of Gaussian distributions. The second requirement consists in finding the smallest value of α for which the number of events N_1 that would correspond to a 5σ (high) fluctuation of the background alone is smaller than the numbers of events N_2 that would correspond to a 50% probability (low) fluctuation of the total number of events (signal included). This amounts to finding a value of N which fulfills, in addition to (1), the following condition

$$\exp\left[-\alpha(s+b)\right] \sum_{i=0}^{N-1} \frac{[\alpha(s+b)]^i}{i!} \leq 0.5. \tag{2}$$

As to the exclusion of the existence of a signal at the 95% confidence level, the minimum luminosity needed has been similarly defined as the luminosity for which 50% of the experiments would actually exclude it in the case of the absence of signal. Again, this is equivalent to the luminosity needed by

the *typical* experiment, which is given by the value of α such that

$$\frac{\exp\left[-\alpha(s+b)\right]\sum_{i=0}^{N}\frac{\left[\alpha(s+b)\right]^{i}}{i!}}{\exp(-\alpha b)\sum_{i=0}^{N}\frac{(\alpha b)^{i}}{i!}} \leq 0.05,$$

where $N = \alpha b$.

In both instances, when deriving the result, b and s were conservatively increased (resp. reduced) by their systematic uncertainties, mainly coming from the yet limited Monte Carlo statistics. The numbers of events expected by each of the four experiments were then added together, and the individual uncertainties were added in quadrature.

However, one caveat should be mentioned. Even if it is legitimate to compute the minimum luminosity needed by each of the four individual experiments by requiring only 50% of the Gedanken-experiments to make the discovery/exclusion, this becomes unclear for the combined experiment: this minimum luminosity would not suffice in 50% of the cases, and this would not be "compensated" by having two (or four) such combined experiments. Since a choice for this fraction cannot be uniquely defined, the combined results have been presented with a fraction of 50% too.

References

[1] S. Glashow, *Nucl. Phys.* **20** (1961) 579; A. Salam, in *Elementary Particle Theory*, ed. N. Svartholm, (1968); S. Weinberg, *Phys. Rev. Lett.* **19** (1967) 1264.

[2] P.W. Higgs, *Phys. Rev. Lett.* **12** (1964) 132; and *Phys. Rev.* **145** (1966) 1156; F. Englert and R. Brout, *Phys. Rev. Lett.* **13** (1964) 321; G.S. Guralnik, C.R. Hagen, and T.W. Kibble, *Phys. Rev. Lett.* **13** (1964) 585.

[3] N. Cabibbo, L. Maiani, G. Parisi, and R. Petronzio, *Nucl. Phys.* **B158** (1979) 295; M. Lindner, *Z. Phys.* **C31** (1986) 295; M. Sher, *Phys. Rev.* **179** (1989) 273; M. Lindner, M. Sher, and H.W. Zaglauer, *Phys. Lett.* **228B** (1989) 139.

[4] M. Sher, *Phys. Lett.* **317B** (1993) 159; addendum *ibid.* **331B** (1994) 448; C. Ford, D.R.T. Jones, P.W. Stephenson, and M.B. Einhorn, *Nucl. Phys.* **B395** (1993) 17; G. Altarelli and I. Isidori, *Phys. Lett.* **337B** (1994) 141; J.A. Casas, J.R. Espinosa, and M. Quirós, *Phys. Lett.* **342B** (1995) 171.

[5] M. Veltman, *Nucl. Phys.* **B123** (1977) 89.

[6] D. Schaile *et al,* LEP Electroweak Working Group, Internal Note LEPEWWG/95–02; J. Ellis, G.L. Fogli, and E. Lisi, *Phys. Lett.* **333B** (1994) 118; and CERN-TH 95-202, *Z. Phys.* **C** in print; K. Hagiwara, S. Matsumoto, D. Haidt, and C.S. Kim, *Z. Phys.* **C64** (1994) 559; P. Chankowski and S. Pokorski, Report MPI-Ph/95-39.

[7] J.-F. Grivaz, Proc. International EPS Conference on High–Energy Physics, Brussels 1995.

[8] J. Ellis, M.K. Gaillard, and D.V. Nanopoulos, *Nucl. Phys.* **B106** (1976) 292; B.L. Ioffe and V.A. Khoze, *Sov. J. Part. Nucl.* **9** (1978) 50; B.W. Lee, C. Quigg, and H.B. Thacker, *Phys. Rev.* **D16** (1977) 1519; J.D. Bjorken, Proc. Summer Institute on Particle Physics, SLAC Report 198 (1976).

[9] D.R.T. Jones and S.T. Petcov, *Phys. Lett.* **84B** (1979) 440; R.N. Cahn and S. Dawson, *Phys. Lett.* **136B** (1984) 96.

[10] G. Altarelli, B. Mele and F. Pitolli, *Nucl. Phys.* **B287** (1987) 205.

[11] M. Krämer, W. Kilian, and P.M. Zerwas, DESY 95-216.

[12] A. Djouadi, M. Spira, and P.M. Zerwas, DESY 95-210, *Z. Phys.* **C** in print.

[13] J. Wess and B. Zumino, *Nucl. Phys.* **B70** (1974) 39.

[14] J. Wess and B. Zumino, *Phys. Lett.* **49B** (1974) 52; J. Iliopoulos and B. Zumino, *Nucl. Phys.* **B76** (1974) 310; S. Ferrara, J.Iliopoulos and B. Zumino, *Nucl. Phys.* **B77** (1974) 413; E. Witten, *Nucl. Phys.* **B188** (1981) 513.

[15] S. Dimopoulos and H. Georgi, *Nucl. Phys.* **B193** (1981) 150; S. Dimopoulos, S. Raby, and F. Wilczek, *Phys. Rev.* **D24** (1981) 1681; L. Ibañez and G.G. Ross, *Phys. Lett.* **105B** (1981) 439.

[16] J. Ellis, S. Kelley, and D.V. Nanopoulos,*Phys. Lett.* **260B** (1991) 131; P. Langacker and M.X. Luo *Phys. Rev.* **D44** (1991) 817; U. Amaldi, W. de Boer, and H. Fürstenau, *Phys. Lett.* **260B** (1991) 447; F. Anselmo, L. Cifarelli, A. Peterman, and A. Zichichi, *Nuovo Cimento* **104A** (1991) 1817.

[17] P. Langacker and N. Polonsky, *Phys. Rev.* **D47** (1993) 4028.

[18] M. Carena, S. Pokorski, and C.E.M. Wagner, *Nucl. Phys.* **B406** (1993) 59.

[19] A. Faraggi and B. Grinstein, *Nucl. Phys.* **B422** (1994) 3; J. Bagger, K. Matchev, and D. Pierce, *Phys. Lett.* **348B** (1995) 443; R. Barbieri, M. Ciafaloni, and A. Strumia, *Nucl. Phys.* **B442** (1995) 461; M. Bastero-Gil and J. Perez Mercader, *Nucl. Phys.* **B450** (1995) 21.

[20] P. Chankowski, Z. Pluciennik, and S. Pokorski, *Nucl. Phys.* **B439** (1995) 23; P. Chankowski, Z. Pluciennik, S. Pokorski, and C. Vayonakis, *Phys. Lett.* **358B** (1995) 264.

[21] P. Langacker and N. Polonsky, *Phys. Rev.* **D52** (1995) 3082; and private communication.

[22] P. Fayet, *Nucl. Phys.* **B90** (1975) 104.

[23] See, *e.g.*, J.F. Gunion, H.E. Haber, G.L. Kane, and S. Dawson, *The Higgs Hunter's Guide*, Addison-Wesley 1990.

[24] S.P. Li and M. Sher, *Phys. Lett.* **140B** (1984) 339.

[25] H.-P. Nilles and M. Nusbaumer, *Phys. Lett.* **145B** (1984) 73; J. Gunion and H. Haber, *Nucl. Phys.* **B272** (1986) 1.

[26] Y. Okada, M. Yamaguchi, and T. Yanagida, *Prog. Theor. Phys.* **85** (1991) 1; H.E. Haber and R. Hempfling, *Phys. Rev. Lett.* **66** (1991) 1815.

[27] J. Ellis, G. Ridolfi, and F. Zwirner, *Phys. Lett.* **257B** (1991) 83; and *Phys. Lett.* **262B** (1991) 477.

[28] K. Inoue, A. Kakuto, H. Komatsu, and S. Takeshita, *Prog. Theor. Phys.* **67** (1983) 1889.

[29] H. Arason, D.J. Castaño, B. Keszthelyi, S. Mikaelian, E.J. Piard, P. Ramond and B.D. Wright, *Phys. Rev. Lett.* **67** (1991) 2933; S. Kelley, J. Lopez, and D. Nanopoulos, *Phys. Lett.* **278B** (1992) 140; S. Dimopoulos, L. Hall, and S. Raby, *Phys. Rev. Lett.* **68** (1992) 1984; and *Phys. Rev.* **D45** (1992) 4192.

[30] V. Barger, M.S. Berger, and P. Ohmann, *Phys. Rev.* **D47** (1993) 1093.

[31] P. Langacker and N. Polonsky, *Phys. Rev.* **D49** (1994) 1454.

[32] W.A. Bardeen, M. Carena, S. Pokorski, and C.E.M. Wagner, *Phys. Lett.* **320B** (1994) 110.

[33] F. Abe et al., CDF Collaboration, *Phys. Rev.* **D50** (1994) 2966; and *Phys. Rev. Lett.* **74** (1995) 2626; S. Abachi et al., D0 Collaboration, *Phys. Rev. Lett.* **74** (1995) 2632.

[34] L. Alvarez Gaumé, J. Polchinski, and M.B. Wise, *Nucl. Phys.* **B221** (1983) 495; J. Bagger, S. Dimopoulos, and E. Masso, *Phys. Rev. Lett.* **55** (1985) 920; M. Carena, T.E. Clark, C.E.M. Wagner, W.A. Bardeen, and K. Sasaki, *Nucl. Phys.* **B369** (1992) 33;

[35] L.J. Hall, R. Rattazzi, and U. Sarid, *Phys. Rev.* **D50** (1994) 7048; R. Hempfling, *Phys. Rev.* **D49** (1994) 6168.

[36] M. Carena, M. Olechowski, S. Pokorski, and C.E.M. Wagner, *Nucl. Phys.* **B426** (1994) 269.

[37] G. Altarelli et al., *Interim Report on the Physics Motivations for an Energy Upgrade of LEP2*, CERN preprint CERN-TH/95-151, CERN-PPE/95-78, June 1995.

[38] H.E. Haber, Proc. *Electroweak Symmetry Breaking*, Budapest 1994.

[39] J. Gunion and H. Haber, *Nucl. Phys.* **B278** (1986) 449.

[40] J. Gunion and H. Haber, *Nucl. Phys.* **B307** (1988) 445.

[41] A. Djouadi, J. Kalinowski, and P.M. Zerwas, *Z. Phys.* **C57** (1993) 569.

[42] G. Anderson, *Phys. Lett.* **243B** (1990) 265; P. Arnold and S. Vokos, *Phys. Rev.* **D44** (1991) 3620; J.R. Espinosa and M. Quiros, *Phys. Lett.* **353B** (1995) 257.

[43] J. Fleischer and F. Jegerlehner, *Nucl. Phys.* **B216** (1983) 469; A. Denner, J. Küblbeck, R. Mertig, and M. Böhm, *Z. Phys.* **C56** (1992) 261; B.A. Kniehl, *Z. Phys.* **C55** (1992) 605.

[44] B.A. Kniehl, *Phys. Rep.* **240C** (1994) 211.

[45] F.A. Berends, W.L. van Neerven, and G.J.H. Burgers, *Nucl. Phys.* **B297** (1988) 429; erratum *ibid.* **B304** (1988) 921.

[46] E. Gross, B.A. Kniehl, and G. Wolf, *Z. Phys.* **C63** (1994) 417; erratum *ibid.* **C66** (1995) 32.

[47] V. Barger, K. Cheung, A. Djouadi, B. Kniehl, and P.M. Zerwas, *Phys. Rev.* **D49** (1994) 79.

[48] K. Hagiwara, R. Szalapski, and D. Zeppenfeld, *Phys. Lett.* **318B** (1993) 155; K. Hagiwara and M.L. Stong, *Z. Phys.* **C62** (1994) 99; B. Grzadkowski and J. Wudka, Report IFI-2-95; G.F. Gounaris, F.M. Renard, and N.D. Vlachos, Report PM-95-30; W. Kilian, M. Krämer, and P.M. Zerwas, DESY 95-217.

[49] A. Djouadi, D. Haidt, B.A. Kniehl, B. Mele, and P.M. Zerwas, Proc. e^+e^- *collisions at 500 GeV: The Physics Potential*, Munich–Annecy–Hamburg, ed. P.M. Zerwas, DESY 92-123A.

[50] E. Boos, M. Sachwitz, H. Schreiber, and S. Shichanin, *Int. J. Mod. Phys.* **A10** (1995) 2067.

[51] L. Resnick, M.K. Sundaresan, and P.J.S. Watson, *Phys. Rev.* **D8** (1973) 172; J. Ellis et al., in Ref.[8].

[52] E. Braaten and J.P. Leveille, *Phys. Rev.* **D22** (1980) 715; N. Sakai, *Phys. Rev.* **D22** (1980) 2220; T. Inami and T. Kubota, *Nucl. Phys.* **B179** (1981) 171; M. Drees and K. Hikasa, *Phys. Lett.* **240B** (1990) 455; S.G. Gorishny, A.L. Kataev, S.A. Larin, and L.R. Surguladze, *Mod. Phys. Lett.* **5** (1990) 2703; A.L. Kataev and V.T. Kim, *Mod. Phys. Lett.* **A9** (1994) 1309; L.R. Surguladze, *Phys. Lett.* **341B** (1994) 61.

[53] K.G. Chetyrkin, J.H. Kühn, and A. Kwiatkowski, Proc. *QCD at LEP*, Aachen 1994; K.G. Chetyrkin and A. Kwiatkowski, Report LBL-37269.

[54] S. Narison, *Phys. Lett.* **341B** (1994) 73.

[55] J. Fleischer and F. Jegerlehner, *Phys. Rev.* **D23** (1981) 2001; D.Y. Bardin, B.M. Vilenskij, and P.Kh. Khristova, *Sov. J. Part. Nucl.* **53** (1991) 152; B.A. Kniehl, *Nucl. Phys.* **B376** (1992) 3; A. Dabelstein and W. Hollik, *Z. Phys.* **C53** (1992) 507.

[56] H. Georgi, S.L. Glashow, M.E. Machacek, and D.V. Nanopoulos, *Phys. Rev. Lett.* **40** (1978) 692.

[57] T. Inami, T. Kubota, and T. Okada, *Z. Phys.* **C18** (1983) 69; A. Djouadi, M. Spira, and P.M. Zerwas, *Phys. Lett.* **264B** (1991) 440.

[58] The experimental sections have been coordinated by P. Janot.

[59] T. Sjöstrand, *The PYTHIA 5.7 and JETSET 7.4 Manual*, LU-TP.95/20, CERN-TH.7112/93; and *Comput. Phys. Commun.* **82** (1994) 74.

[60] S. Ambrosanio and B. Mele, *Nucl. Phys.* **B374** (1992) 3.

[61] D. Apostolakis, P. Distas, and S. Katsanevas, to be published in *Z. Phys.* **C** .

[62] P. Janot, in preparation; see also the part *"Generators for New Physics"* of this report.

[63] P. Bambade et al., *Higgs Boson Search at LEP2 with DELPHI*, DELPHI 95-57, PHYS 493 (1995).

[64] G. Burkart et al., *DELPHI Higgs Boson Studies in the LEP2 Physics Workshop*, DELPHI 95-161, PHYS 579 (1995).

[65] P. Bagnaia et al., *Higgs Search with the L3 Experiment at LEP2*, L3 Note 1842 (1995).

[66] E. Duchovni et al., *The OPAL LEP2 Workshop Report*, OPAL Technical Note, in preparation.

[67] P. Janot, *Will a Higgs Boson be Found at Future e^+e^- Colliders?*, LAL 92-27 (1992) and Proc. of the XXVIIth Rencontres de Moriond.

[68] See for instance D. Brown and M. Frank, *Tagging b Hadrons Using Track Impact Parameter*, ALEPH 92-135, PHYSIC 92-124 (1992).

[69] See for instance T. Mattisson, `QVSRCH`*: A Tool for Inclusive Secondary Vertex Finding*, ALEPH 92-173, PHYSIC 92-155 (1992).

[70] P. Lutz, *Higgs Boson(s) Search at LEP2: The $\tau^+\tau^- q\bar{q}$ Channel*, DELPHI 95-155 PHYS 576 (1995).

[71] H. Georgi, S.L. Glashow, M. Machacek, and D.V. Nanopoulos, *Phys. Rev. Lett.* **40** (1978) 692.

[72] M. Spira, A. Djouadi, D. Graudenz, and P.M. Zerwas, *Nucl. Phys.* **B453** (1995) 17.

[73] S.L. Glashow, D.V. Nanopoulos, and A. Yildiz, *Phys. Rev.* **D18** (1978) 1724.

[74] D. Froidevaux and E. Richter–Was, *Z. Phys.* **C67** (1995) 213.

[75] ATLAS Technical Proposal CERN/LHCC/94–43; CMS Technical Proposal CERN/ LHCC/94–38.

[76] F. Gianotti, Proceedings of the International EPS Conference on High Energy Physics, Brussels 1995; E. Richter–Was et al., ATLAS Internal Note PHYS–048.

[77] R. Barbieri, M. Frigeni, and F. Caravaglios, *Phys. Lett.* **258B** (1991) 167; Y. Okada, M. Yamaguchi, and T. Yanagida, *Phys. Lett.* **262B** (1991) 54.

[78] A. Brignole, J. Ellis, G. Ridolfi, and F. Zwirner, *Phys. Lett.* **271B** (1991) 123; M. Dress and M. Noijiri, *Phys. Rev.* **D45** (1992) 2482.

[79] A. Brignole, *Phys. Lett.* **277B** (1992) 313; and *Phys. Lett.* **281B** (1992) 284.

[80] P.H. Chankowski, S. Pokorski, and J. Rosiek, *Phys. Lett.* **274B** (1992) 191; and *Nucl. Phys.* **B423** (1994) 437; A. Dabelstein, *Z. Phys.* **C67** (1995) 495; J. Rosiek, A. Sopczak *Phys. Lett.* **341B** (1994) 419.

[81] www address at http://itpaxp1.physik.uni-karlsruhe.de/~rosiek/neutral_higgs.html

[82] R. Hempfling and A.H. Hoang, *Phys. Lett.* **331B** (1994) 99.

[83] J.R. Espinosa and M. Quirós, *Phys. Lett.* **266B** (1991) 389.

[84] J. Kodaira, Y. Yasui, and K. Sasaki, *Phys. Rev.* **D50** (1994) 7035.

[85] J.A. Casas, J.R. Espinosa, M. Quirós and A. Riotto, *Nucl. Phys.* **B436** (1995) 3.

[86] M. Carena, K. Sasaki, and C.E.M. Wagner, *Nucl. Phys.* **B381** (1992) 66; P. Chankowski, S. Pokorski, and J. Rosiek, *Phys. Lett.* **274B** (1992) 191.

[87] H.E. Haber and R. Hempfling, *Phys. Rev.* **D48** (1993) 4280.

[88] H.E. Haber, R. Hempfling, and Y. Nir, *Phys. Rev.* **D46** (1992) 2907.

[89] M. Carena, J.R. Espinosa, M. Quiros, and C.E.M. Wagner, *Phys. Lett.* **355B** (1995) 209.

[90] A. Donini, preprint CERN-TH/95-287, November 1995.

[91] M. Carena, M. Quiros and C.E.M. Wagner, CERN preprint CERN-TH/95-157, August 1995, to appear in *Nucl. Phys.* **B** .

[92] H.E. Haber, R. Hempfling, and A.H. Hoang, CERN-TH/95-216, and TTP95-09 (1995).

[93] www address at http://surya11.cern.ch/users/mcarena, filename: subh.f

[94] www address at http://surya11.cern.ch/users/mcarena, filename: subhpole.f

[95] A. Djouadi, J. Kalinowski, and P. Zerwas, DESY 95-211.

[96] M. Diaz and H. Haber, *Phys. Rev.* **D46** (1992) 3086.

[97] V. Barger, M.S. Berger, P. Ohmann, and R.J.N. Phillips, *Phys. Lett.* **314B** (1993) 351.

[98] M. Carena, M. Olechowski, S. Pokorski, and C.E.M. Wagner, *Nucl. Phys.* **B419** (1994) 213.

[99] C. Kounnas, I. Pavel, and F. Zwirner, *Phys. Lett.* **335B** (1994) 403.

[100] M. Carena and C.E.M. Wagner, *Nucl. Phys.* **B452** (1995) 45.

[101] A. Djouadi. G. Girardi, C. Verzegnassi, W. Hollik, and F. Renard, *Nucl. Phys.* **B349** (1991) 48; M. Boulware and D. Finnel, *Phys. Rev.* **D44** (1991) 2054.

[102] J.D. Wells, C. Kolda and G.L. Kane, *Phys. Lett.* **338B** (1994) 219; P. Chankowski and S. Pokorski, Warsaw University preprint, IFT-95/5, to appear in Proc. *Beyond the Standard Model IV*, Lake Tahoe, CA, December 1994, MPI-PhT/95-49 (1995); A. Dabelstein, W. Hollik and W. Mösle, Proc. *Perspectives for Electroweak Interactions in e^+e^- Collisions*, ed. B. Kniehl, Ringberg 1995.

[103] D. Garcia, R. Jimenez and J. Sola, *Phys. Lett.* **347B** (1995) 309; and 321; D. Garcia and J. Sola, *Phys. Lett.* **B354** (1995) 335; and **357** (1995) 349.

[104] For bounds taking the LEP1.5 results into account, see J. Ellis, J. Lopez, and D. Nanopoulos, CERN-TH.95/314.

[105] C. Kounnas, I. Pavel, G. Ridolfi and F. Zwirner, *Phys. Lett.* **354B** (1995) 322.

[106] B. Ananthanarayan, K.S. Babu, and Q. Shafi, *Nucl. Phys.* **B428** (1994) 19; G.L. Kane, C. Kolda, L. Roszkowski, and J.D. Wells, *Phys. Rev.* **D50** (1994) 3498; G.K. Leontaris and N.D. Tracas, *Phys. Lett.* **336B** (1994) 194; H. Baer, M. Drees, C. Kao, M. Nojiri and X. Tata, *Phys. Rev.* **D50** (1994) 2148; J. Gunion and H. Pois, *Phys. Lett.* **329B** (1994) 736. P. Nath and R. Arnowitt, CERN-TH.7288/94 (1994), presented at the 29^{th} Rencontres de Moriond, Meribel, March 1994.; W. de Boer, R. Ehret, and D.I. Kazakov, *Phys. Lett.* **334B** (1994) 220; and *Z. Phys.* **C67** (1995) 647; W. de Boer, B. Burkart, E. Ehret, W. Oberschulte-Beckmann, V. Bednyakov, and S. Kovalenko, IEKP-KA/95-07.

[107] B. Barish et al., CLEO Collaboration, preprint CLEO CONF 94-1, to appear in the Proc. of the ICHEP94 Conference, Glasgow, Scotland, July 1994.

[108] S. Bertolini, F. Borzumati, A. Masiero, and G. Ridolfi, *Nucl. Phys.* **B353** (1991) 591; R. Barbieri and G. Giudice, *Phys. Lett.* **309B** (1993) 86.

[109] For a more extensive discussion, see M. Carena, P. Chankowski, M. Olechowski, S. Pokorski, and C.E.M. Wagner, CERN-TH.95/302.

[110] J.F. Gunion and H.E. Haber, *Nucl. Phys.* **B272** (1986) 1; *Nucl. Phys.* **B278** (1986) 449; and *Nucl. Phys.* **B307** (1988) 445; erratum *ibid.* **B402** (1993) 567.

[111] V. Driesen and W. Hollik, *Z. Phys.* **C68** (1995) 485.

[112] S. Komamiya, *Phys. Rev.* **D38** (1988) 2158.

[113] A. Dabelstein, *Nucl. Phys.* **B456** (1995) 25.

[114] S. Moretti and W.J. Stirling, *Phys. Lett.* **347B** (1995) 291, and erratum.

[115] A. Djouadi, P. Janot, J. Kalinowski, and P.M. Zerwas, DESY 95-212.

[116] V. Barger, M.S. Berger, and P. Ohmann, *Phys. Rev.* **D49** (1994) 4908.

[117] J.R. Espinosa, H.E. Haber, R. Hempfling, P. Janot, and M. Quirós, *Higgs Bosons in Low Energy Supersymmetry*, to be submitted to *Phys. Rep.*.

[118] See for instance P. Janot, *Higgs Boson Search at a 500 GeV e^+e^- Collider*, LAL 93-38 (1993) and Proc. *Physics and Experiments with Linear e^+e^- Collider.*

[119] See for instance A. Sopczak, *Status of Higgs Hunting at LEP: Five Years of Progress*, CERN-PPE/95-046 (*Phys. Rep.* in preparation); and references therein.

[120] Z. Kunszt and F. Zwirner, *Nucl. Phys.* **B385** (1992) 3.

[121] Z. Kunszt, *Nucl. Phys.* **B247** (1984) 339.

[122] E. Richter–Was, D. Froidevaux, F. Gianotti, L. Poggioli, D. Cavalli, and S. Resconi, ATLAS Internal Note, PHYS–074, December 1995; D. Froidevaux, private communication; see also [76].

[123] B. Kileng, *Z. Phys.* **C63** (1994) 87; B. Kileng, P. Osland and N.P. Pandita, NORDITA 95–48–P and *Z. Phys.* **C** in print.

[124] P. Fayet, *Nucl. Phys.* **B90** (1975) 104; H.-P. Nilles, M. Srednicki, and D. Wyler, *Phys. Lett.* **120B** (1983) 346; J.-P. Derendinger and C.A. Savoy, *Nucl. Phys.* **B237** (1984) 307; J. Ellis, J.F. Gunion, H.E. Haber, L. Roszkowski, and F. Zwirner, *Phys. Rev.* **D39** (1989) 844; L. Durand and J.L. Lopez, *Phys. Lett.* **217B** (1989) 463; M. Drees, *Int. J. Mod. Phys.* **A4** (1989) 3635.

[125] L. Hall and J. Lykken, and S. Weinberg, *Phys. Rev.* **D27** (1983) 2359; J.E. Kim and H.P. Nilles, *Phys. Lett.* **138B** (1984) 150; K. Inoue and A. Kakuto, T. Takano, *Prog. Theor. Phys.* **75** (1986) 664; A. A. Ansel'm and A.A. Johansen, *Phys. Lett.* **200B** (1988) 331; G. Giudice and A. Masiero, *Phys. Lett.* **206B** (1988) 480.

[126] A. Vilenkin, *Phys. Rep.* **121C** (1985) 263.

[127] S.A. Abel, S. Sarkar, and P.L. White, OUTP-95-22P, and *Nucl. Phys.* **B** to appear.

[128] U. Ellwanger, *Phys. Lett.* **133B** (1983) 187; J. Bagger and E. Poppitz, *Phys. Rev. Lett.* **71** (1993) 2380; J. Bagger, E. Poppitz, and L. Randall, EFI-95-21.

[129] U. Ellwanger, M. Rausch de Traubenberg, and C.A. Savoy, *Phys. Lett.* **315B** (1993) 331; and LPTHE 95-04, *Z. Phys.* **C** (to appear).

[130] T. Elliott, S.F. King, and P.L. White, *Phys. Lett.* **351B** (1995) 213; S.F. King and P.L. White, *Phys. Rev.* **D52** (1995) 4183.

[131] J.R. Espinosa and M. Quiros, *Phys. Lett.* **279B** (1992) 92; G. Kane, C. Kolda, and J. Wells, *Phys. Rev. Lett.* **70** (1993) 2686; J.R. Espinosa and M. Quiros, *Phys. Lett.* **302B** (1993) 51.

[132] J. Kamoshita, Y. Okada, and M. Tanaka, *Phys. Lett.* **328B** (1994) 67.

[133] S.F. King and P.L. White, SHEP 95-27, OUTP-95-31P, to appear in *Phys. Rev.* **D** .

[134] U. Ellwanger and M. Rausch de Traubenberg, *Z. Phys.* **C53** (1992) 521; U. Ellwanger and M. Lindner, *Phys. Lett.* **301B** (1993) 365; U. Ellwanger, *Phys. Lett.* **303B** (1993) 271; W. ter Veldhuis, PURD-TH-92-11; T. Elliott, S.F. King, and P.L. White, *Phys. Lett.* **305B** (1993) 71; T. Elliott, S.F. King, and P.L. White, *Phys. Lett.* **314B** (1993) 56; T. Elliott, S.F. King, and P.L. White, *Phys. Rev.* **D49** (1994) 2435.

[135] P. Janot, private communication.

[136] D.V. Volkov, V.P. Akulov, JETP Lett. 16 (1972) 438; *Phys. Lett.* **46B** (1973) 109.

[137] S. Samuel and J. Wess, *Nucl. Phys.* **B221** (1983) 153; *Nucl. Phys.* **B223** (1984) 488.

[138] B.R. Kim, *Z. Phys.* **C67** (1995) 337.

[139] Y. Chikashige, R. Mohapatra, and R. Peccei, *Phys. Lett.* **98B** (1980) 265.

[140] For a review see J.W.F. Valle, *Nucl. Phys.* **B26** (1991) 91; and references therein.

[141] A. Joshipura and J.W.F. Valle, *Nucl. Phys.* **B397** (1993) 105; A.S. Joshipura and S. Rindani, *Phys. Rev. Lett.* **69** (1992) 3269.

[142] A. Masiero and J.W.F. Valle, *Phys. Lett.* **251B** (1990) 273; J.C. Romao, C.A. Santos, and J.W.F. Valle, *Phys. Lett.* **288B** (1992) 311.

[143] A. Lopez-Fernandez et al., *Phys. Lett.* **312B** (1993) 240.

[144] B Brahmachari et al., *Phys. Rev.* **D48** (1993) 4224; ALEPH Collab., *Phys. Lett.* **313B** (1993) 312; and *Phys. Lett.* **313B** (1993) 299.

[145] O.J.P. Éboli, et al., *Nucl. Phys.* **B421** (1994) 65; F. de Campos et al., Proc. e^+e^- *Collision at 500 GeV: The Physics Potential*, ed. P. Zerwas, DESY 93-123C.

[146] F. de Campos et al., *Phys. Lett.* **336B** (1994) 446.

[147] O.J.P. Éboli, F. de Campos, J. Rosiek, and J.W.F. Valle, in preparation.

[148] T. Binoth, J.J. van der Bij, *Quarks 94*, Vladimir, Report Freiburg-THEP-94/26.

[149] R.S. Chivukula and M. Golden, *Phys. Lett.* **267B** (1991) 233.

[150] LEP2 Interim Report, CERN-TH/95-151.